POLITECNICO DI TORINO

Master Degree course in Environmental and Land Engineering

Master Degree Thesis

Geotechnical Analysis and Digital Ground Modeling for the Evaluation of Urban Underpass Alternatives: The Avenida Pérez Galdós Case Study (Valencia)

Supervisors
Prof. Marco Barla
Prof. Víctor Martínez Ibáñez

Candidate
Marco Berri

Academic Year 2025-2026

Abstract

The present work investigates the existing underpass of Avenida Pérez Galdós in Valencia, a central urban infrastructure built between the late 1960s and early 1970s within one of the city's most important traffic corridors. Despite its strategic role, very limited information is available regarding its original geometry and structural configuration. The absence of original design drawings, structural calculations and as-built documentation makes the assessment of its current behaviour highly uncertain.

The objective of this work is to reconstruct and interpret the geomechanical behaviour of the underpass by integrating the technical information currently available with the data collected during recent investigation campaigns. Geological, geophysical and topographic data were combined to define the stratigraphic model, interpret the geometry of the retaining walls and underlying collector, and identify the main uncertainties affecting the structure.

A representative transverse section was implemented in RS2 in order to analyse the soil–structure interaction under the adopted assumptions. Two geometrical scenarios were considered, with and without a possible footing-like base enlargement at the wall base. The numerical results do not indicate a global instability mechanism under the analysed operational conditions, although local stress concentrations and plastic strain zones, observed in both geometrical scenarios, highlight the need for further structural verification.

Possible intervention alternatives were then evaluated at a preliminary level, considering both the numerical results and the uncertainties affecting the existing structure. The study indicates that future decisions should be supported by additional inspection, monitoring and targeted structural assessment, especially in the areas where the numerical model suggests higher stress concentration or where deterioration has already been identified.

Contents

List of Figures 5

List of Tables 8

1 Introduction 9
- 1.1 Urban and demographic evolution of Valencia . . . 9
- 1.2 The Pérez Galdós–Giorgeta corridor . . . 12
- 1.3 Recent urban transformation of Avenida Pérez Galdós . . . 15
- 1.4 Problem statement . . . 17
- 1.5 Objectives and scope . . . 17
- 1.6 Methodological approach . . . 18
- 1.7 Research motivation . . . 19
- 1.8 Available sources and data framework . . . 19

2 Geological and geotechnical framework 23
- 2.1 Geological setting of Valencia . . . 23
  - 2.1.1 Regional geological framework . . . 23
  - 2.1.2 Geological evolution and stratigraphy . . . 24
  - 2.1.3 Quaternary framework and urban subsoil . . . 26
  - 2.1.4 Urban hydrogeology and groundwater conditions in Valencia . . . 26
- 2.2 Available geotechnical documentation . . . 29
- 2.3 Borehole investigation campaign . . . 29
  - 2.3.1 Introduction to the borehole dataset . . . 29
- 2.4 Definition of the stratigraphic model . . . 32
- 2.5 Geotechnical characterisation and selection of numerical parameters . . . 33
  - 2.5.1 Processing and statistical treatment of geotechnical data . . . 35
  - 2.5.2 Derivation of numerical parameters for FEM analysis . . . 36
- 2.6 Three-dimensional stratigraphic model in Civil 3D . . . 39
  - 2.6.1 Civil 3D Geotechnical Modeler workflow . . . 39
  - 2.6.2 Generation of the three-dimensional stratigraphic surfaces . . . 41
  - 2.6.3 Selection of representative layers and integration with the topographic model . . . 42
- 2.7 MASW survey and supporting geophysical interpretation . . . 44

3 Geometric and structural reconstruction of the existing underpass 47
3.1 Introduction and available documentation . . . 47
3.2 Ground penetrating radar investigations and survey reference system . . . 48
3.2.1 GPR method . . . 48
3.2.2 Survey reference axes . . . 49
3.3 Retaining wall geometry and reinforcement interpretation . . . 51
3.4 Axis-by-axis interpretation of the retaining wall . . . 52
3.5 Collector geometry and structural interaction . . . 53
3.6 Methodological reconstruction approach . . . 55
3.7 Geometric uncertainties and competing interpretations . . . 58
3.8 Adopted geometric assumptions and reconstruction scenarios . . . 59
3.9 Selection of the representative section for numerical modelling . . . 62
3.10 Summary of identified knowledge gaps . . . 63

4 Finite element analysis 65
4.1 Introduction and objectives of the numerical analysis . . . 65
4.2 Overview of the RS2 modelling environment . . . 66
4.3 Preparation of the geometrical model for RS2 . . . 66
4.3.1 Selection of the representative section . . . 66
4.3.2 CAD processing and DXF preparation . . . 67
4.4 Geometry of the numerical model . . . 69
4.5 Material properties . . . 70
4.5.1 Soil materials . . . 70
4.5.2 Concrete and structural materials . . . 71
4.5.3 Joints and contact conditions . . . 72
4.6 Boundary conditions and initial stress state . . . 73
4.7 Construction stages and loading sequence . . . 74
4.7.1 General approach . . . 74
4.7.2 Main stages . . . 75
4.7.3 Equivalent temporary support pressures . . . 75
4.7.4 Hydrostatic pressure inside the collector . . . 76
4.8 Mesh generation and numerical settings . . . 77
4.9 Analysis cases . . . 78
4.9.1 Scenario 1: wall with footing-like base enlargement . . . 78
4.9.2 Scenario 2: wall without footing-like base enlargement . . . 78
4.10 Results of Scenario 1: wall with footing-like base enlargement . . . 79
4.11 Results of Scenario 2: wall without footing-like base enlargement . . . 81
4.12 Comparison and interpretation of the analysed scenarios . . . 83
4.13 Limitations of the numerical model . . . 87
4.14 Summary of the finite element analysis . . . 87

5 Evaluation of intervention alternatives 89
5.1 Introduction . . . 89
5.2 Common requirement: inspection and monitoring . . . 90
5.3 Common light urban interventions . . . 90

5.3.1 Noise barriers . . . 90
5.3.2 Partial covering of open trench sections . . . 91
5.4 Alternative 0: preservation of the existing underpass in service . . . 92
5.5 Alternative 1: structural rehabilitation or replacement of the floor beams 93
5.5.1 General description . . . 93
5.5.2 Numerical simulation of beam removal . . . 93
5.5.3 Construction implications and preliminary assessment . . . 95
5.6 Alternative 2: closure and controlled backfilling of the underpass . . . 96
5.6.1 General description . . . 96
5.6.2 Technical concept and numerical modelling . . . 97
5.6.3 Numerical results and interpretation . . . 98
5.6.4 Preliminary assessment . . . 101
5.7 Alternative 3: adaptive reuse of the abandoned underpass . . . 101
5.7.1 General concept . . . 101
5.7.2 Energy reuse as an underground storage system . . . 102
5.7.3 Stormwater retention and temporary water storage . . . 102
5.7.4 Preliminary assessment . . . 103
5.8 Comparative assessment of the alternatives . . . 103
5.9 Discussion . . . 104

6 Conclusions and future work 107
6.1 Main findings . . . 107
6.2 Geotechnical and geometrical interpretation . . . 107
6.3 Finite element modelling results . . . 108
6.4 Assessment of intervention alternatives . . . 109
6.5 Limitations of the study . . . 109
6.6 Engineering perspective and broader relevance . . . 110
6.7 Recommendations for future work . . . 110

Bibliography 113

List of Figures

1.1 Valencia before the diversion of the Turia River 10
1.2 2025 orthophoto of Valencia 11
1.3 Map of Valencia highlighting the main avenues 13
1.4 Construction works of the Avenida Pérez Galdós underpass, January 1973 14
1.5 Traffic conditions along Avenida Pérez Galdós 15
1.6 Initial winning proposal ("Raíces") for the reurbanization of Avenida Pérez Galdós and Giorgeta. The project included the suppression of the existing tunnel infrastructure. 16

2.1 Regional geological framework of the Valencia area showing the distribution of Triassic, Jurassic, Cretaceous, Neogene and Quaternary formations. . . 24
2.2 Stratigraphic column and legend of the Valencia Sheet (722), showing Cretaceous, Neogene and Quaternary units. 25
2.3 Detail of the Geological Map of Spain, Sheet 722 – Valencia, showing the Quaternary deposits underlying the urban area. 26
2.4 Flood of the Turia River in October 1957, which led to the implementation of the Plan Sur diversion project 27
2.5 Graphic illustration of *Plan Sur*, showing the diversion of the Turia River constructed after the 1957 flood to prevent future inundations in the urban area 28
2.6 Location of the four boreholes along the Pérez Galdós–Giorgeta corridor. 30
2.7 Drilling equipment operating on site during the geotechnical investigation campaign. 34
2.8 Recovered material from borehole SR-04, showing the stratigraphic core boxes corresponding to the depth interval between 18.4 and 21.3 m. . . . 35
2.9 Generation of the three-dimensional stratigraphic model in Civil 3D using the Geotechnical Modeler environment. 43
2.10 Final three-dimensional stratigraphic model generated in Civil 3D using the Geotechnical Modeler environment. 44
2.11 2D shear wave velocity profiles obtained from MASW surveys performed along Avenida Pérez Galdós 45

3.1 Instrument used for the GPR survey, Proceq GS8000, and representative acquisition setup adopted in the underpass. 49

3.2 Indicative location of investigation GPR axes along the underpass and collector alignment. 50
3.3 View of the collector recorded during the 2024 inspection, showing the internal geometry of the structure. 54
3.4 Geometry summary of the collector reported after GPR investigations. . . 55
3.5 Geometric reconstruction criterion adopted for the retaining wall and collector. The figure shows the minimum and maximum GPR-based thickness limits and the red median line selected as representative geometry. 57
3.6 Geometric criterion adopted for the footing-like base enlargement. The adopted extension was defined as an intermediate value between the borehole that detected structural concrete at 1.55 m from the wall and the borehole that did not detect concrete at 2.51 m from the wall. 60
3.7 Reconstructed transverse section of the underpass and collector system considering the presence of a footing-like base enlargement. 61
3.8 Reconstructed transverse section of the underpass and collector system considering a vertical wall configuration without footing-like base enlargement. 61
3.9 Representative transverse section selected for numerical modelling, showing the reconstructed underpass and collector geometry superimposed onto the local stratigraphic profile. 62

4.1 Location of the representative section selected for the RS2 numerical analysis. 67
4.2 Preparation of the DXF geometry for Scenario 1, including the footing-like base enlargement. 68
4.3 Preparation of the DXF geometry for Scenario 2, without the footing-like base enlargement. 68
4.4 Numerical model geometry for Scenario 1, considering the presence of a footing-like base enlargement at the base of the retaining wall. 69
4.5 Numerical model geometry for Scenario 2, considering a continuous structural configuration without footing-like base enlargement. 70
4.6 Joint elements introduced to simulate simple contact between adjacent structural components in Scenario 1. 73
4.7 Boundary conditions, groundwater level and main loading scheme adopted in the RS2 model. 74
4.8 Equivalent temporary support pressures applied along the excavation boundaries during the staged analysis. 76
4.9 Finite element mesh adopted for Scenario 1, showing local refinement around the underpass and collector. 77
4.10 Finite element mesh adopted for Scenario 2, showing the refined discretization around the collector and excavation boundaries. 78
4.11 Absolute vertical displacement contours in the final operational stage of Scenario 1. 80
4.12 Major principal stress, σ_1, contours in the final operational stage of Scenario 1. 80
4.13 Absolute vertical displacement contours in the final operational stage of Scenario 2. 82
4.14 Major principal stress, σ_1, contours in the final operational stage of Scenario 2. 82

4.15 Comparison of minor principal stress σ_3 contours in the final operational stage. The same colour scale was adopted for both scenarios in order to improve the visual comparison. The results show that the tensile stress distribution is broadly comparable in the two scenarios, while the highest local tensile peak is obtained in Scenario 1. 85
4.16 Comparison of total displacement contours in the final operational stage. The same colour scale was adopted for both scenarios in order to improve the visual comparison. Scenario 1 shows slightly higher maximum total displacement, while both scenarios remain within the same order of magnitude. 86

5.1 Extract of the 2022 Strategic Noise Map of Valencia for road traffic noise, highlighting the acoustic exposure of the Pérez Galdós–Giorgeta corridor. 91
5.2 Absolute horizontal displacement contours after removal of the floor beam system. 94
5.3 Minor principal stress σ_3 after removal of the floor beam system. 95
5.4 Numerical configuration adopted for the controlled backfilling alternative. 98
5.5 Vertical displacement contours obtained for the controlled backfilling alternative after filling and surface loading. 99
5.6 Minor principal stress σ_3 contours for the controlled backfilling alternative. 100

List of Tables

2.1 Main information for the boreholes considered in the present study. 30
2.2 Summary of laboratory tests performed during the geotechnical investigation campaign. 31
2.3 Representative geotechnical layers adopted in the stratigraphic model. . . 33
2.4 Processed geotechnical parameters obtained from laboratory and in situ investigations. 36
2.5 Final geotechnical parameters adopted in the RS2 finite element analyses. 39
2.6 Coordinate input table used for the Civil 3D Geotechnical Modeler import, including real and virtual boreholes. 40
2.7 Stratigraphic input table used for the Civil 3D Geotechnical Modeler import. 41

3.1 Spacing between GPR investigation axes for the retaining wall. 50
3.2 Spacing between GPR investigation axes for the collector. 51

4.1 Final soil parameters adopted in the RS2 finite element analyses. 71
4.2 Concrete parameters adopted in the RS2 finite element analyses. 71
4.3 Joint parameters adopted to represent simple contact between structural elements. 72
4.4 Main interpreted construction stages adopted in the RS2 analysis. 75
4.5 Main results obtained for Scenario 1 in the final operational stage. 79
4.6 Main results obtained for Scenario 2 in the final operational stage. 81
4.7 Comparison between the final operational results of Scenario 1 and Scenario 2. 83

5.1 Preliminary assessment of Alternative 0. 92
5.2 Comparison between the operational stage and the beam-removal stage in the RS2 model without footing-like base enlargement. 96
5.3 Preliminary assessment of Alternative 1. 96
5.4 RS2 parameters adopted for the filling material. 97
5.5 Comparison between the operational stage and the backfilling stages in the RS2 model without footing-like base enlargement. 99
5.6 Preliminary assessment of Alternative 2. 101
5.7 Preliminary assessment of Alternative 3. 103
5.8 Comparative assessment of the intervention alternatives. 104

Chapter 1

Introduction

1.1 Urban and demographic evolution of Valencia

Valencia is located on the eastern coast of Spain, along the Mediterranean Sea, and serves as the capital of the *Comunitat Valenciana*. The city lies within a wide alluvial plain formed by the Turia River, which historically played a fundamental role in its foundation and development, providing water resources and enabling the creation of the extensive irrigated agricultural system known as the *Huerta de Valencia*. The geomorphological structure of the area, characterized by Quaternary alluvial deposits and a coastal sedimentary system, has strongly influenced both the spatial expansion and infrastructure development of the city [1].

The origins of Valencia date back to 138 BC, when it was founded as the Roman colony of *Valentia*. During the Islamic period, the city grew significantly and developed an advanced irrigation system, later consolidated after the Christian conquest by James I in 1238 [1]. However, the modern urban structure of Valencia began to take shape mainly in the 19th century, when the demolition of the medieval walls in 1865 enabled the expansion of the city and marked a decisive turning point in its spatial organisation.

The disappearance of the walled boundary created the conditions for the expansion of Valencia beyond its historical core. During the late nineteenth and early twentieth centuries, the city progressively developed new circulation systems and urban axes, while the surrounding rural paths were gradually incorporated into the expanding urban fabric. This process contributed to the formation of a radial and ring-based structure that would later influence the development of the main metropolitan corridors.

The development of railway infrastructure, beginning with the construction of the first station in 1851, further accelerated urban expansion and influenced the city's morphology [1]. At the same time, railway lines also acted as physical barriers to the continuity of several urban axes, delaying the consolidation of some peripheral corridors until their later dismantling or transformation.

A second major phase of growth occurred during the mid-20th century, particularly in the 1960s, when Valencia experienced rapid demographic and urban expansion. This period was characterized by a radial and later "oil stain" urban growth model, with the city spreading into surrounding agricultural land and incorporating nearby settlements

such as Russafa, Patraix, Campanar and Benimaclet [1].

The diversion of the Turia River, completed in 1969 as part of the *Plan Sur* after the catastrophic flood of 1957, represents one of the most significant urban transformations in Valencia's history. The former riverbed, initially intended to become a highway corridor, was instead converted into a continuous green space, the Turia Garden, thanks to strong social mobilisation [1]. This intervention redefined the city's environmental and spatial structure and remains a central element of its urban identity.

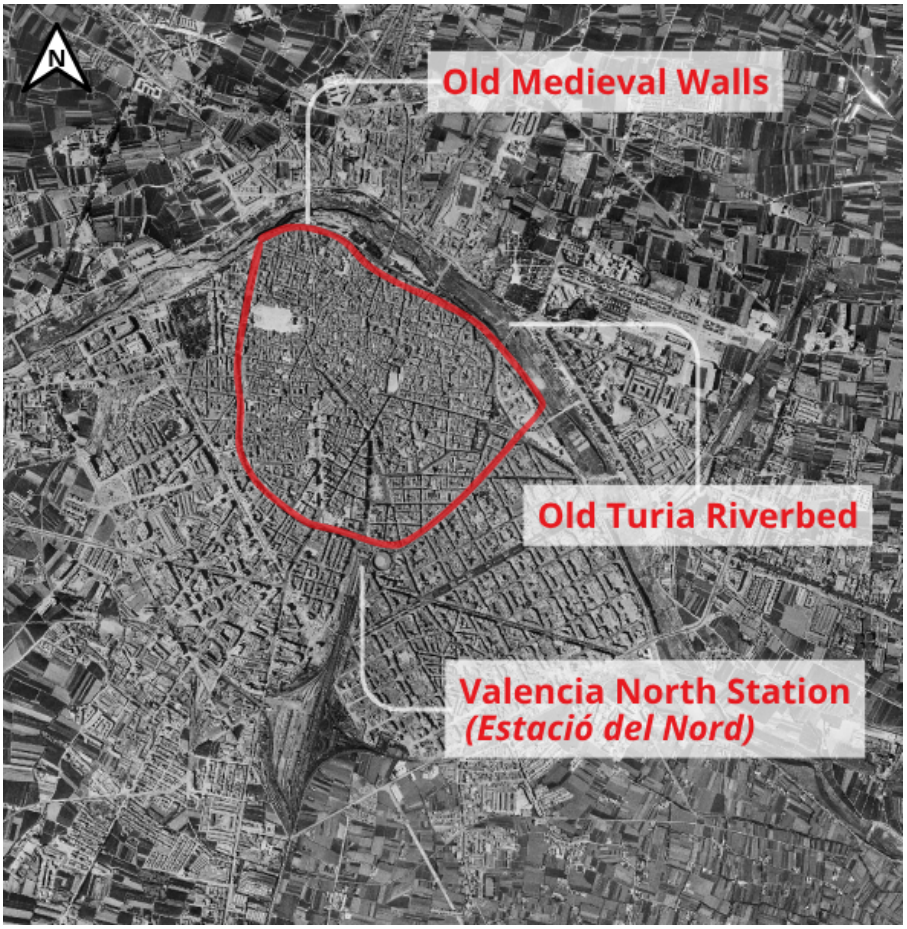

Figure 1.1. Valencia before the diversion of the Turia River [2].

By the late 20th century, urban planning policies shifted towards consolidation and sustainability. The 1988 General Urban Plan (PGOU) [3] introduced a model focused on limiting urban sprawl, protecting remaining agricultural land, improving public transport and regenerating peripheral neighbourhoods. Valencia has since evolved from a compact historical city into a metropolitan area exceeding 1.6 million inhabitants in its wider urban region [4], with increasing mobility demands and strong daily interactions between the urban core and its metropolitan hinterland.

Today, Valencia faces the challenge of balancing continued urban regeneration with

sustainable mobility and environmental resilience. Current planning strategies aim to reduce car dependency, enhance public transport and cycling infrastructure, and improve urban livability through the expansion of green spaces and the renaturalization of key urban corridors. These transformations, however, also generate tensions related to traffic congestion, accessibility and social acceptance, reflecting the complexity of contemporary urban development processes.

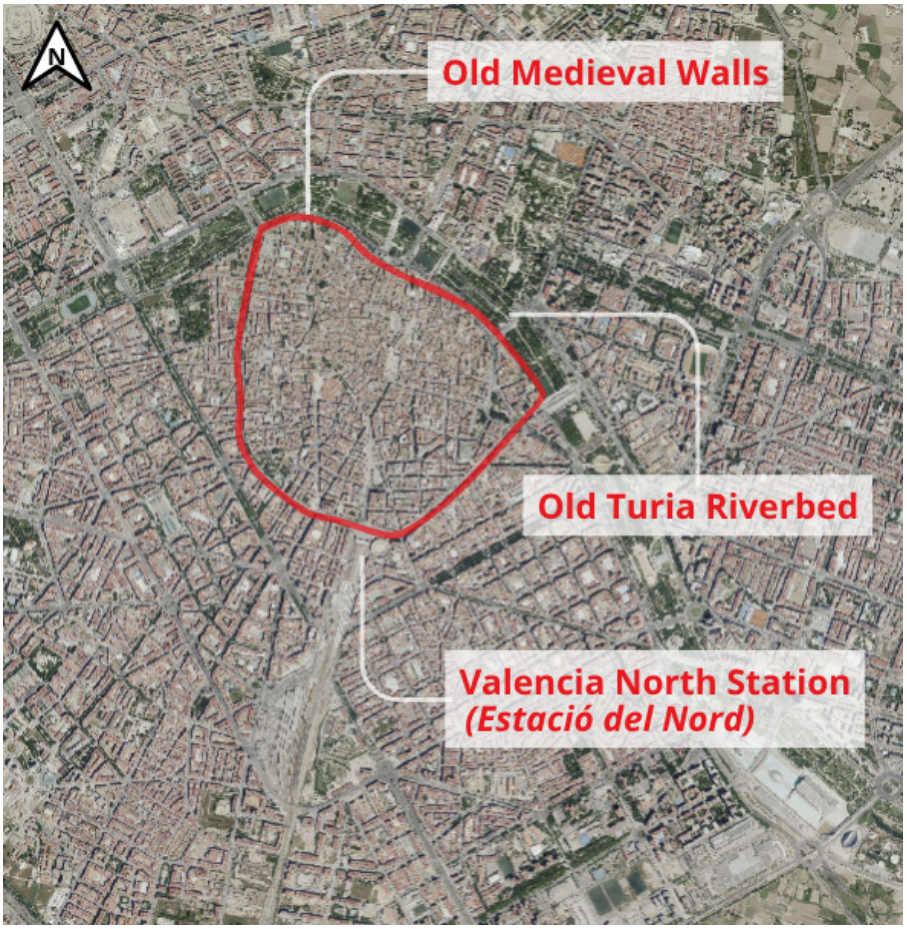

Figure 1.2. 2025 orthophoto of Valencia [2].

1.2 The Pérez Galdós–Giorgeta corridor

The Pérez Galdós–Giorgeta corridor must be understood within the broader historical framework of Valencia's *Camino de Tránsitos*. This road system was designed in the late nineteenth century by engineer Casimiro Meseguer as a set of urban links connecting the main entrances to the city. Although it had an important mobility function, its original conception also responded to fiscal and sanitary concerns, since it provided a new framework for controlling the inflow of goods after the demolition of the medieval walls [5].

The first phase of the *Camino de Tránsitos*, approved in 1891 along the right bank of the river, included the present-day avenues of Pérez Galdós, Giorgeta and Peris y Valero. Three years later, the complementary section along the left bank was projected, consolidating a new radial ring that strengthened the radiocentric structure of Valencia [5]. More specifically, the term *tránsitos* referred to traffic flows that did not necessarily have Valencia as their origin or destination, but passed through or around the city to connect routes located beyond the urban area. In this sense, the *Camino de Tránsitos* can be interpreted as an early circumferential infrastructure for organising through-traffic before the construction of the external bypass system that now allows long-distance traffic, including the AP-7 highway corridor (*Autopista del Mediterráneo*), to avoid the urban fabric [6].

In this sense, the present Pérez Galdós–Giorgeta axis was not originally conceived simply as a traffic artery, but as part of a strategic metropolitan-scale system combining circulation, urban control and territorial organisation. This historical origin explains both its generous width and its long-term infrastructural importance within the city.

The western section of this system was historically affected by major infrastructural discontinuities. In particular, the railway line to Utiel interrupted the corridor at the height of Calle Jesús, delaying its effective urban consolidation. Only in the 1960s and 1970s, after the dismantling of the railway line, were Pérez Galdós and Giorgeta finally connected as a continuous corridor, while underpasses and an overpass were constructed to ensure the link with Peris y Valero [5].

The historical naming of the avenue reflects this phased development. The first urbanised section, between Pechina and Jesús, received the name of Benito Pérez Galdós in 1923. The second section, between Jesús and the Camino Real de Madrid, was completed later and named Avenida Giorgeta in the 1930s [5].

Valencia underwent profound urban transformations throughout the second half of the 20th century, particularly following the diversion of the Turia River after the catastrophic flood of 1957. The *Plan Sur* redirected the river south of the city, freeing a vast central corridor that later became the *Jardín del Turia*, one of the most significant urban green infrastructures in Europe.

This transformation enabled the consolidation of a modern road network structured around large radial and ring avenues, designed to accommodate increasing car ownership and metropolitan expansion. Avenues such as Pérez Galdós, Giorgeta and the *Grandes Vías* became key elements of vehicular distribution, often functioning as urban highways rather than integrated public spaces. This evolution laid the groundwork for the introduction of grade-separated infrastructures, such as underpasses and tunnels.

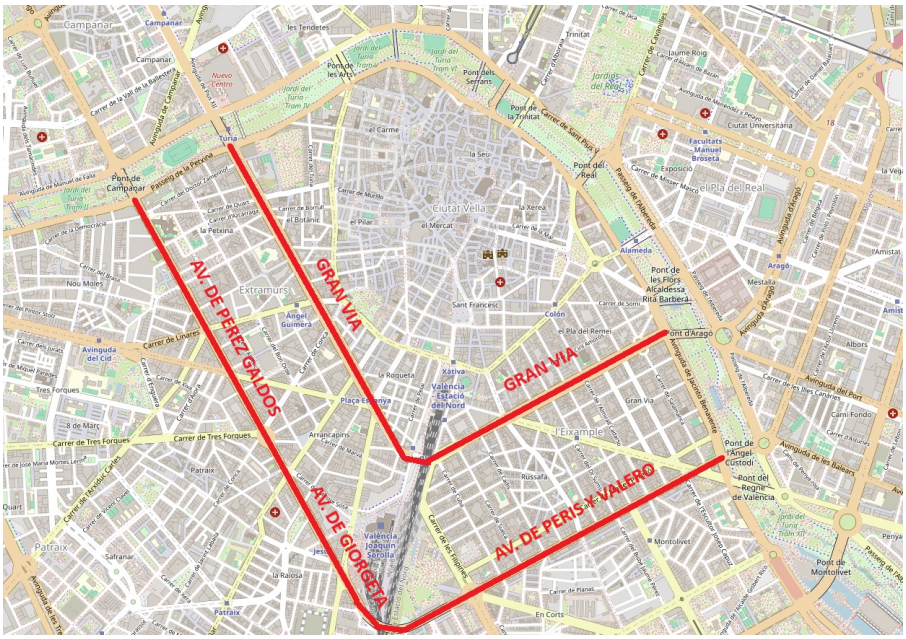

Figure 1.3. Map of Valencia highlighting the main avenues [7].

During the 1960s–1980s, this car-oriented model led to the construction of several grade-separated infrastructures aimed at improving traffic flow and reducing congestion. These interventions reflected a planning paradigm prioritizing vehicular mobility over pedestrian accessibility and urban cohesion [1]. Within this framework, the construction of the Pérez Galdós underpass became a solution to ensure traffic continuity along one of the most important nodes of the urban network.

Taking advantage of the reconstruction of the main sewer collector running beneath the roadway, the Pérez Galdós tunnel was constructed between 1968 and 1973. The redevelopment of the sewer system provided the technical opportunity for the construction of the underpass, enabling uninterrupted circulation along the main axis while maintaining surface-level accessibility.

Figure 1.4. Construction works of the Avenida Pérez Galdós underpass, January 1973 [8].

Since its completion in 1973, the tunnel has remained in continuous operation and continues to play a central role in Valencia's mobility system. Despite subsequent urban transformations, it still functions as a key element of traffic distribution, reflecting the long-lasting impact of late twentieth-century car-oriented planning.

In recent decades, urban planning policies in Valencia have increasingly focused on sustainability, climate adaptation and the rebalancing of public space. This shift is reflected in projects promoting pedestrianisation, cycling infrastructure and green corridors, often supported by European funding programs such as the *Next Generation EU*.

The Pérez Galdós–Giorgeta axis is one of the most important transport corridors in Valencia, extending approximately 2.2 km and historically accommodating up to 70,000 vehicles per day, later reduced to approximately 50,000–56,000 vehicles/day due to traffic management policies and external factors [9]. Originally conceived as a high-capacity urban artery, the avenue progressively became a physical and environmental barrier between adjacent neighbourhoods, generating high levels of noise and air pollution.

Figure 1.5. Traffic conditions along Avenida Pérez Galdós [10].

1.3 Recent urban transformation of Avenida Pérez Galdós

In recent years, Avenida Pérez Galdós has become the focus of an intense urban, political, and social debate within the city of Valencia. Historically conceived as a major traffic artery, the avenue has long been characterised by high vehicular density, elevated levels of air and noise pollution, and limited pedestrian accessibility. These conditions have progressively generated increasing concern among residents and local associations, ultimately leading to a rethinking of its urban role within the city as reported by local press [11, 12].

The first major wave of public criticism emerged from neighbourhood associations and civic groups, which denounced the avenue as one of the most problematic corridors in Valencia in terms of environmental quality and urban livability. Residents highlighted excessive traffic volumes, noise, and air pollution, as well as the barrier effect created by the central underpass, which limits pedestrian crossing and weakens the connection between neighbourhoods [13].

In response to these concerns, several preliminary proposals were developed over time. Among the most debated solutions was the potential removal of the existing underground tunnel, considered by many as an obsolete infrastructure inherited from a car-oriented planning paradigm. Some proposals envisioned its complete elimination or burial, with the aim of transforming the avenue into a green urban boulevard prioritizing pedestrians, cyclists, and public space, as shown in the municipal documentation [14].

However, these early proposals faced strong technical, economic, and political challenges. The tunnel was recognised as a key component of the city's traffic distribution system, and its removal raised concerns regarding severe congestion and the redistribution of traffic across the wider urban network.

As the planning process evolved, the initial radical proposals were progressively revised. The final design strategy shifted towards a more balanced and pragmatic approach, aiming to integrate environmental improvements while maintaining the functional role of the

avenue within Valencia's mobility system. Rather than removing the tunnel, the adopted solution preserves its function and concentrates the transformation on the surface level. The project therefore combines the reduction and reorganisation of surface traffic lanes with the expansion of pedestrian areas, the implementation of segregated cycling infrastructure, the introduction of new green areas and urban vegetation, and improvements to public transport efficiency. These measures are also intended to contribute to the mitigation of noise and air pollution, while increasing the quality and continuity of public space along the corridor.

Figure 1.6. Initial winning proposal ("Raíces") for the reurbanization of Avenida Pérez Galdós and Giorgeta. The project included the suppression of the existing tunnel infrastructure. [15]

This compromise reflects the necessity of reconciling sustainability goals with existing infrastructural constraints, as well as budget limitations and construction timelines linked to European funding requirements [16]. The implementation of the project was formalized through a public procurement procedure within the framework of the European Recovery and Resilience Plan (Next Generation EU). The intervention represents a major urban investment, initially estimated at over 32 million euros, and structured as an open tender process allowing multiple companies to submit proposals evaluated based on both economic and technical criteria [16].

A total of eleven bidders participated in the competition, highlighting the strategic importance and scale of the intervention within the urban transformation agenda of the city. The tender process was concluded in May 2025, with the contract awarded to the joint venture (UTE) formed by Pavasal and Grupo Bertolín, for a total value of approximately 24 million euros, significantly lower than the initial estimated budget [16].

Construction works officially started on June 30, 2025, marking the transition from planning to execution [17]. The intervention was scheduled to last approximately 14 months and to be carried out in successive phases, in order to maintain partial traffic circulation and minimise disruption.

Overall, the transformation of Avenida Pérez Galdós represents a paradigmatic case of contemporary urban regeneration, where environmental objectives, infrastructural constraints, political decisions, and social dynamics intersect in a complex and evolving process.

1.4 Problem statement

The transformation of the Pérez Galdós–Giorgeta corridor reflects a broader shift in contemporary urban planning, from car-oriented infrastructure toward more sustainable and multimodal urban environments. Within this process, the existing underpass has become a central yet unresolved element.

Although early redevelopment proposals considered its removal, the tunnel has been temporarily excluded from the current project. This decision does not resolve the issue, but rather postpones it, leaving an aging underground structure embedded within a rapidly changing urban system.

Constructed between the 1960s and 1970s, the underpass is now approaching the end of its nominal service life. However, its actual condition remains largely unknown. The main difficulty lies in the almost complete absence of original design documentation, construction records, and long-term monitoring data. This condition is typical of mid-20th century urban infrastructure, where documentation loss and lack of monitoring significantly complicate present-day evaluation.

As a result, key aspects such as geometry, material properties, and structural behaviour cannot be directly verified. This lack of information introduces a high level of uncertainty in any technical assessment. Consequently, the evaluation of the structure must rely on indirect reconstruction methods, combining limited available data with engineering interpretation.

The core problem addressed in this thesis is therefore the assessment of the current condition and structural reliability of the underpass, in order to support future decision-making regarding its maintenance, adaptation, or possible removal within the evolving urban framework.

1.5 Objectives and scope

The present work investigates the Pérez Galdós–Giorgeta corridor with a specific focus on the existing underpass and on its interaction with the surrounding ground and the underlying collector. The main objective is to develop a coherent technical interpretation of an infrastructure for which very limited original documentation is available, combining the information collected from historical sources, recent technical reports, geotechnical investigations, geophysical surveys and topographic data.

The study aims first to frame the underpass within the historical and urban development of the corridor, since its current role and the debate surrounding its future cannot be separated from the evolution of Avenida Pérez Galdós as one of the main infrastructural axes of Valencia. From an engineering point of view, the work then focuses on the reconstruction of the geological and geotechnical context of the site, the interpretation of the geometry of the retaining walls and collector, and the definition of representative structural and geotechnical assumptions suitable for numerical modelling.

A further objective is to assess the global geomechanical behaviour of the underpass–collector system through finite element modelling. The analysis is not intended to provide a definitive structural safety verification, but rather to evaluate the order of magnitude of displacements, stress redistribution and plastic zones under the adopted assumptions. Particular attention is given to the uncertainty associated with the possible presence of a footing-like base enlargement at the wall base, which represents one of the most relevant unresolved aspects of the structural reconstruction.

Finally, the thesis explores possible intervention strategies for the future management of the underpass. These alternatives are evaluated at a preliminary level, considering the numerical results, the existing uncertainties and the broader urban context. The scope of the work is therefore interpretative and comparative: it provides a technical basis for understanding the behaviour of the system and for supporting future decisions, but it does not replace detailed structural design, local reinforced concrete verification, or construction-level assessment.

The results should be interpreted within a framework of informed approximation rather than exact reconstruction. This limitation is a direct consequence of the absence of original drawings, the indirect nature of some investigation methods, and the simplified assumptions required for two-dimensional numerical modelling.

1.6 Methodological approach

The methodology adopted in this thesis is based on the progressive integration of heterogeneous sources of information. Since the original design documentation of the underpass is not available, the study could not rely on a conventional as-built reconstruction. Instead, the geometry, stratigraphy and mechanical behaviour of the system were interpreted by combining documentary analysis, field investigation data and numerical modelling.

The first phase consisted of analysing the historical and urban development of Avenida Pérez Galdós and Giorgeta, together with the recent planning documents related to the regeneration of the corridor. This step was necessary to understand the current role of the underpass and the reasons why its preservation, transformation or removal represents a relevant technical and urban issue.

The second phase focused on the geological and geotechnical characterization of the site. Borehole logs, laboratory tests, SPT results and groundwater observations were processed and organized in order to identify representative stratigraphic units. The MASW survey was used as a supporting geophysical tool to check the general consistency of the stratigraphic interpretation and to qualitatively confirm stiffness contrasts between the main soil layers. Based on this interpretation, a simplified geotechnical model was

developed and later used to define the material parameters adopted in RS2.

The third phase concerned the geometric and structural reconstruction of the underpass and of the collector located beneath it. Topographic data were used to define the external geometry and elevation relationships, while GPR results provided indirect information on wall thicknesses, reinforcement positions and collector dimensions. Since these data are affected by interpretation uncertainty, the reconstruction was developed through representative ranges and engineering assumptions rather than through a single deterministic as-built geometry.

The reconstructed section was then implemented in RS2 for the finite element analysis. Two main geometrical scenarios were analysed, respectively with and without a possible footing-like base enlargement at the base of the retaining wall. The numerical model was used to evaluate the global soil–structure interaction, the deformation pattern, the stress redistribution and the development of localized plastic zones. Additional analyses were then carried out to support the preliminary evaluation of possible intervention alternatives.

Throughout the work, each modelling assumption was checked against the available evidence and treated critically. The methodology therefore follows an iterative approach, in which geological interpretation, structural reconstruction and numerical modelling are not independent steps, but parts of the same process of progressive approximation of the real behaviour of the underpass–collector system.

1.7 Research motivation

This research originates from the need to address a real and unresolved engineering problem within a complex urban context. The case of Avenida Pérez Galdós is not an abstract academic exercise, but the analysis of an existing infrastructure whose technical characteristics are only partially known.

The coexistence of limited data, ageing infrastructure, and ongoing urban transformation creates a condition in which technical evaluation becomes both necessary and challenging. In this context, engineering judgement plays a crucial role in bridging the gap between incomplete information and the need for reliable assessments.

At the same time, the underpass has been at the center of a broader public and political debate, where technical aspects are often simplified or interpreted through non-engineering perspectives. This highlights the importance of rigorous and transparent analysis, capable of providing a solid technical basis for future decisions.

The motivation of this thesis is therefore to contribute to a clearer understanding of the structure, emphasizing the role of data quality, methodological rigor, and critical interpretation in the assessment of existing infrastructure.

1.8 Available sources and data framework

Unlike many structural assessment studies, the investigation of the Pérez Galdós underpass could not rely on original design documentation. Archival research confirmed that the original construction drawings, structural calculations, and detailed technical records are either lost or currently unavailable. Consequently, the present work is entirely based on

recent technical documentation produced within the framework of the urban regeneration project of Avenida Pérez Galdós and Giorgeta.

The initial technical basis of the study was provided by the official tender documentation (*pliegos*) issued during the public procurement process (2024). Among the available documents, three annexes were particularly relevant:

- **Anejo Nº3: "Trabajo Topográfico"**, containing the detailed topographic survey of the avenue and the digital cartographic material in CAD format provided by *Gecival S.L.* [18];
- **Anejo Nº6: "Estudio Geotécnico"**, which includes a preliminary geotechnical characterization based on two exploratory boreholes carried out by *C2C Servicios Técnicos de Inspección, S.L.* under commission from *Gecival S.L.* [19];
- **Anejo Nº27: "Evaluación estructural del paso inferior"**, representing the first formal structural assessment of the underpass and identifying the main uncertainties affecting its evaluation [20].

These documents constituted the starting point for the reconstruction of the geometry and for the definition of the investigation strategy adopted in this thesis. The evaluation process was developed with the involvement of the *Universitat Politècnica de València* (UPV), particularly Professors *Julián Alcalá González* and *Víctor Martínez Ibáñez*, who contributed to identifying the need for additional investigations.

In particular, Anejo Nº27 explicitly recommended further studies within the section *Propuesta de actuaciones*, including more extensive geotechnical characterisation and additional structural verification. Following these indications, a more comprehensive investigation programme was commissioned in 2025 by the UTE Bertolín–Pavasal. The geotechnical investigation campaign was carried out by *Intercontrol Levante S.A.*, while the complementary geophysical study was carried out by *Geozone Asesores S.L.* [21]. The available documentation included:

- four boreholes executed along the avenue axis;
- laboratory testing of soil samples;
- geophysical investigations, including MASW and GPR surveys.

The final results were progressively made available during the project development and formally delivered on March 5, 2026. This dataset represents the most detailed subsurface information currently available for the site and constitutes the primary basis for the geotechnical interpretation developed in this thesis.

Overall, the study is therefore based on the integration of:

- the tender-phase documentation produced in 2024, including topographic and preliminary geotechnical information [19];
- the structural assessment framework defined in Anejo Nº27 [20];

- the advanced geotechnical and geophysical investigations carried out in 2025 by *Intercontrol Levante S.A.* and *Geozone Asesores S.L.* [21].

Historical photographic material and secondary historical sources are extremely limited and provide only qualitative support to the analysis. As a result, the geometric and structural characterisation of the underpass had to be reconstructed indirectly through the interpretation and integration of recent technical sources, inherently affected by different levels of uncertainty.

As a preliminary step of the study, a broader geological and geomorphological characterisation of the Valencia area was also considered through independent scientific and technical references. This general framework supports the interpretation of the site-specific investigations, whose spatial extent remains necessarily limited.

Chapter 2

Geological and geotechnical framework

2.1 Geological setting of Valencia

2.1.1 Regional geological framework

The study area is located within the Gulf of Valencia along the western Mediterranean margin of Spain. Structurally, the Valencia coastal plain develops at the junction between the Iberian Chain and the Betic system. The region occupies a broad tectonic depression generated after the main Mesozoic Iberian compressive phase and subsequently affected by Alpine and post-Alpine tectonics.

Since the Miocene, the area has behaved predominantly as a distensive domain, characterised by progressive eastward stepping of structural blocks and significant subsidence toward the present coastline. This tectonic configuration explains the accumulation of thick Neogene and Quaternary sedimentary successions, locally reaching depths of approximately 200 m.

The regional distribution of lithological units and geological periods in the Valencia area is shown in Figure 2.1.

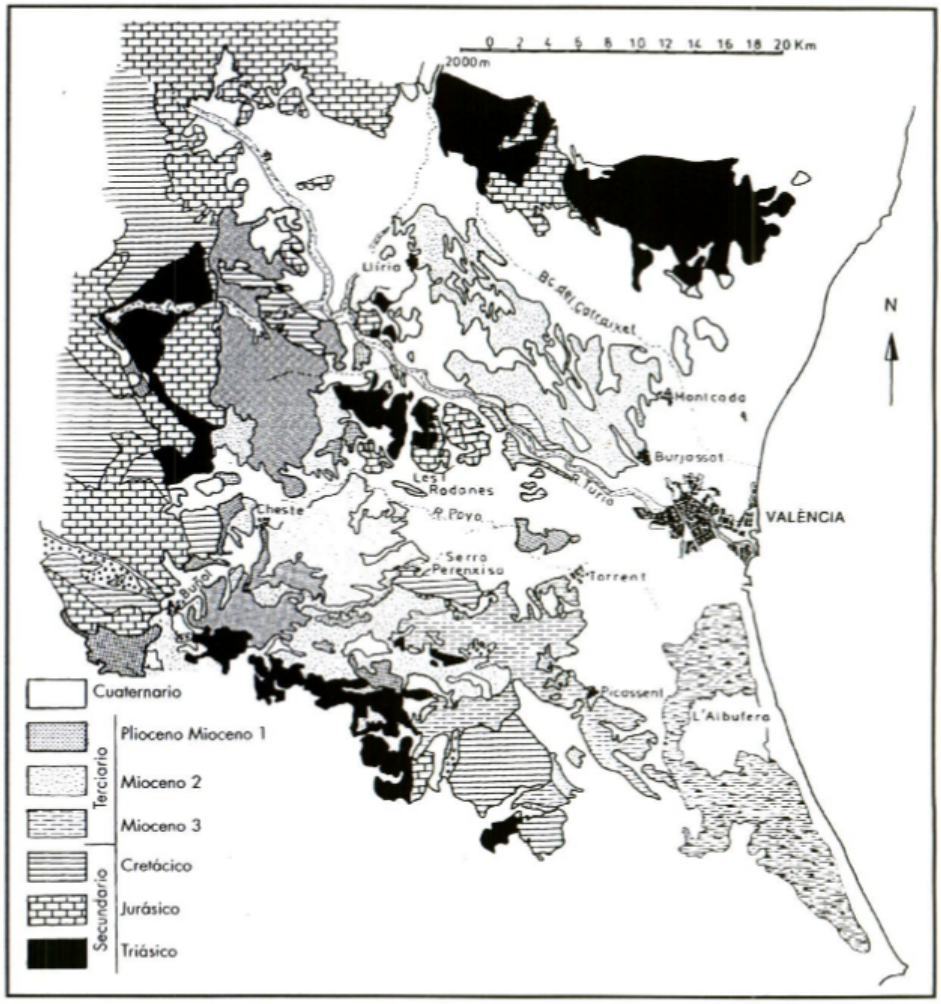

Figure 2.1. Regional geological framework of the Valencia area showing the distribution of Triassic, Jurassic, Cretaceous, Neogene and Quaternary formations (adapted from [22]).

2.1.2 Geological evolution and stratigraphy

According to the official report accompanying the Geological Map of Spain (MAGNA), Sheet 722 – Valencia [23], the geological evolution of the area can be summarised as follows:

- **Cretaceous**: deposition of marls, calcarenites and limestones in marine environments.
- **Neogene (Miocene)**: shallow marine sedimentation followed by progressive regression and lagoonal conditions, with deposition of marls and lacustrine limestones.

- **Quaternary**: development of an extensive continental–marine mixed depositional system linked to the Turia River delta, coastal processes and the evolution of the Albufera lagoon.

The stratigraphic succession and corresponding geological periods are illustrated in Figure 2.2, which is the legend of the Valencia Sheet (722), shown in Figure 2.3.

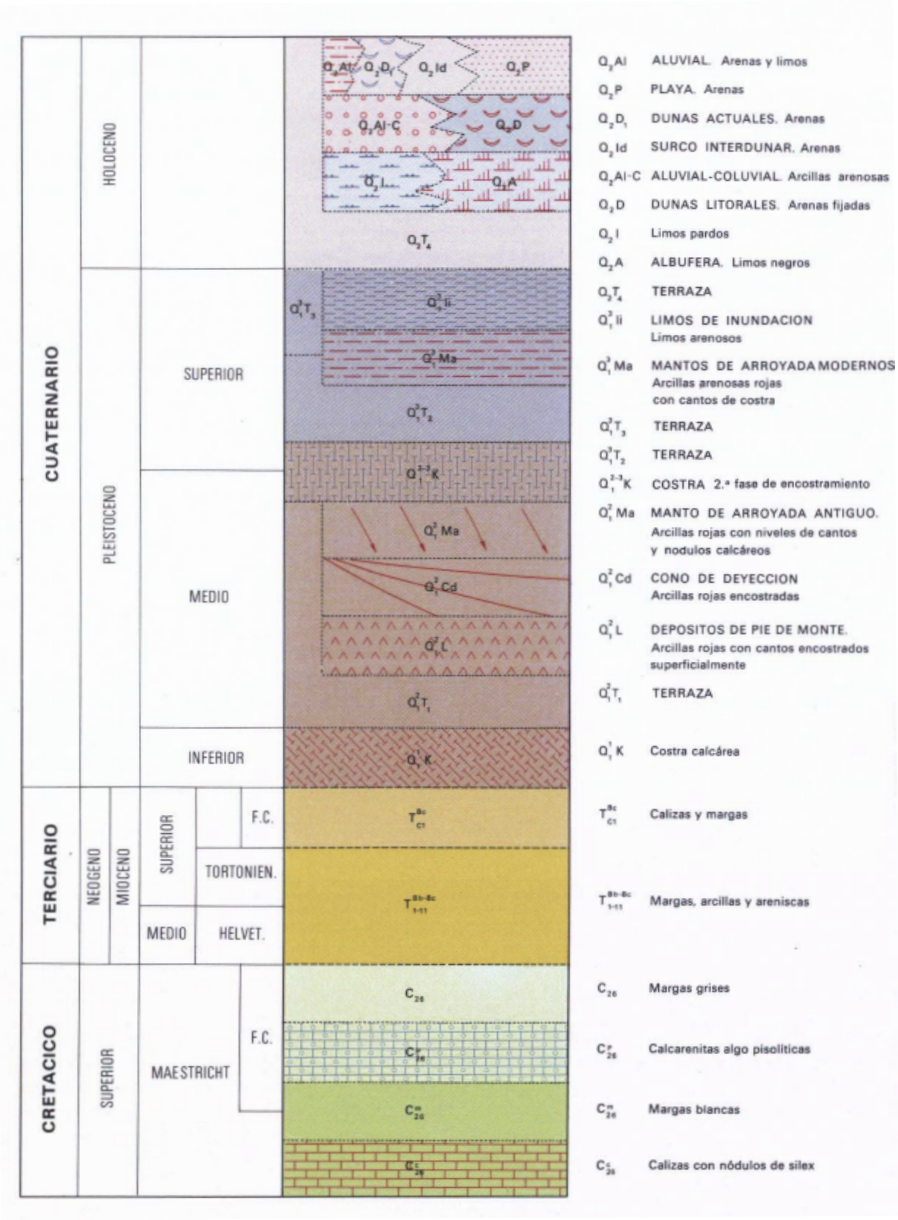

Figure 2.2. Stratigraphic column and legend of the Valencia Sheet (722), showing Cretaceous, Neogene and Quaternary units [22].

2.1.3 Quaternary framework and urban subsoil

The city of Valencia is almost entirely underlain by Quaternary deposits forming an extensive prelittoral plain. These deposits include floodplain silts, fluvial terraces, alluvial and colluvial materials, coastal dunes, beach sands and lagoonal deposits associated with the Albufera system.

They form a broad depositional cone corresponding to the superficial portion of the Turia delta. The deposits consist predominantly of grey to brown sandy silts, locally interbedded with clayey sands, gravels and sandy lenses. The Turia River has incised a system of terraces into these deposits, producing marked vertical and lateral heterogeneity within the urban subsoil.

A detailed view of the geological map (Sheet 722) in the urban area of Valencia is shown in Figure 2.3, highlighting the predominance of Quaternary floodplain deposits beneath the city.

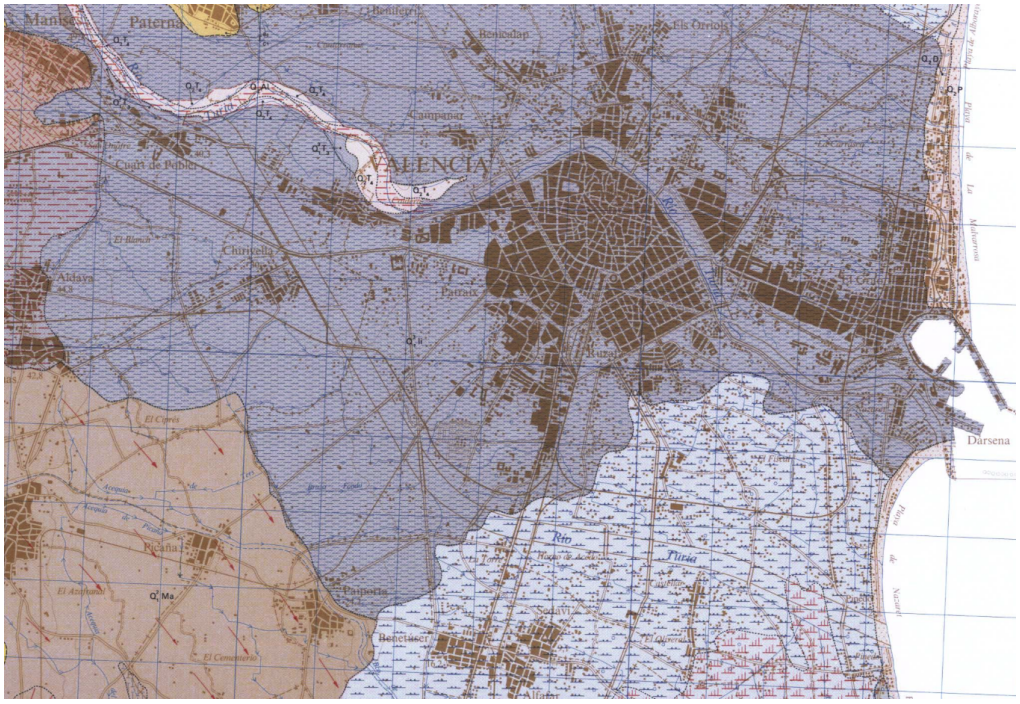

Figure 2.3. Detail of the Geological Map of Spain, Sheet 722 – Valencia, showing the Quaternary deposits underlying the urban area [22]. The legend of this map is shown in figure 2.2.

2.1.4 Urban hydrogeology and groundwater conditions in Valencia

The hydrogeological behaviour of the city is directly controlled by the Quaternary alluvial–deltaic framework described above. The heterogeneous alternation of sandy, gravelly and silty–clayey units hosts a shallow unconfined aquifer system hydraulically connected to the Turia River and influenced by coastal boundary conditions.

Regional hydrogeological investigations carried out by IGME [24] describe the Valencia plain as a coastal detrital aquifer system characterised by moderate to high permeability within coarse-grained horizons and lower permeability within fine-grained intercalations. Groundwater circulation in the urban area is therefore strongly conditioned by the geometry of palaeochannels and buried fluvial bodies. The catastrophic flood of the Turia River in October 1957 (Figure 2.4) represented a major turning point in the hydraulic and hydrogeological configuration of the city.

Figure 2.4. Flood of the Turia River in October 1957, which led to the implementation of the Plan Sur diversion project [25].

Following this event, the river was artificially diverted southwards through the so-called *Plan Sur*, while the former riverbed was converted into the present-day Turia Gardens (Figure 2.5). This intervention modified recharge conditions and altered local hydraulic gradients within the shallow aquifer system.

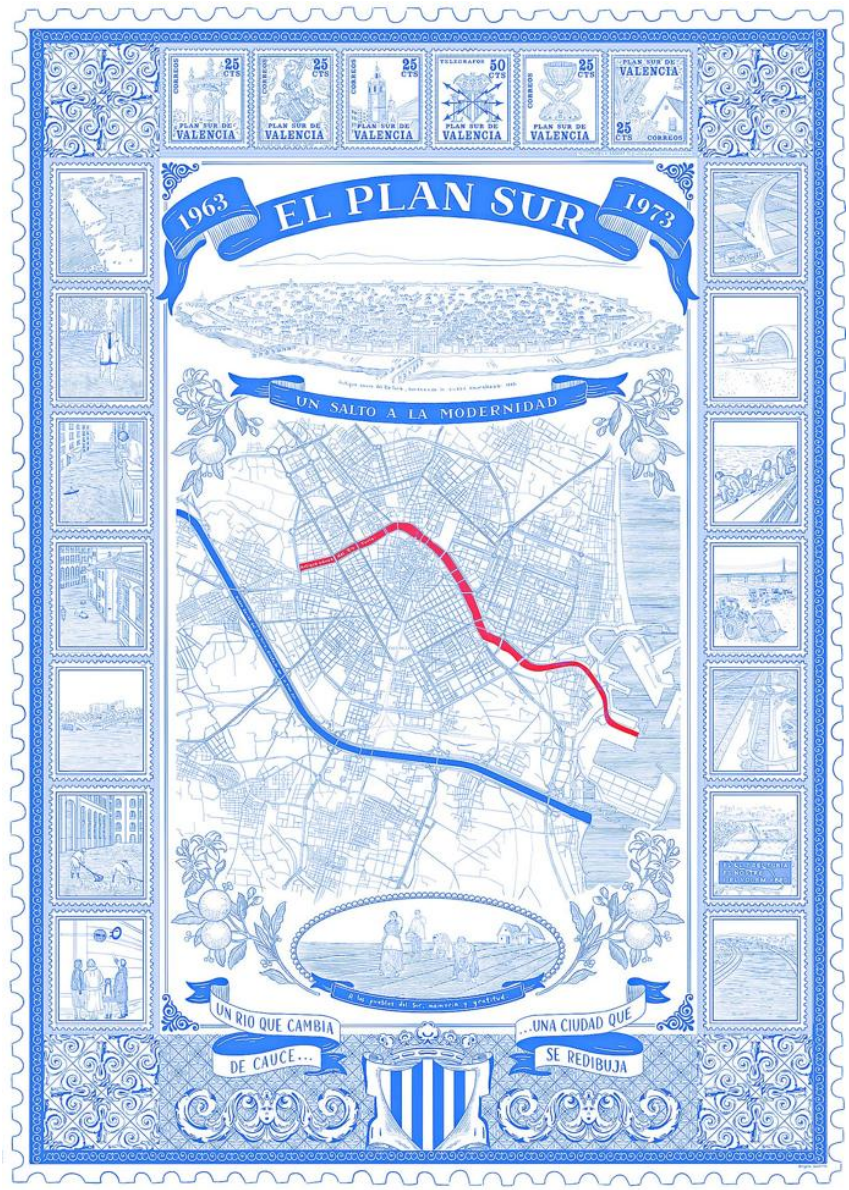

Figure 2.5. Graphic illustration of *Plan Sur*, showing the diversion of the Turia River constructed after the 1957 flood to prevent future inundations in the urban area [26].

Previous hydrogeological interpretations suggest the presence of buried palaeochannels beneath the urban fabric [27], which may locally act as preferential groundwater flow paths and partially explain the spatial variability of piezometric levels across the city.

Within the central urban area, the groundwater table is generally shallow, typically ranging between approximately 3 m and 10 m below ground level depending on topographic elevation and proximity to former fluvial branches. Shallower depths (3–5 m) are commonly observed in sectors closer to the historic floodplain, whereas slightly deeper levels (6–10 m) occur in relatively elevated areas.

Seasonal groundwater fluctuations are generally moderate, usually on the order of 0.5–1.5 m, although local variations may occur due to intense rainfall events or anthropogenic influences.

For the purposes of the present thesis, groundwater conditions are not inferred solely from regional hydrogeological interpretations. Direct measurements obtained from the available boreholes within the study area are used to define the reference phreatic surface adopted in the subsequent geomechanical characterisation and numerical modelling phases.

2.2 Available geotechnical documentation

The geotechnical characterisation adopted in this thesis is based on two complementary sources of subsurface information, developed within the framework of the project for the urban regeneration and renaturalisation of Avenida Pérez Galdós and Avenida Giorgeta.

The main geotechnical investigation campaign was carried out by *Intercontrol Levante S.A.*. This campaign included the borehole investigations, in situ tests and laboratory analyses used to define the stratigraphic and geotechnical framework of the study area. These data constitute the principal basis for the reconstruction of the subsoil conditions and for the definition of the representative geotechnical parameters adopted in the thesis.

In parallel, *Geozone Asesores S.L.* carried out the geophysical investigation titled *"Estudio geofísico mediante análisis multicanal de ondas superficiales 2D (MASW2D) para caracterización del subsuelo y auscultación con GPR3D en muro pantalla de paso inferior y colector en Av. Pérez Galdós (Valencia)"*. This study provided complementary information through MASW2D surveys and GPR3D inspections of the diaphragm wall of the underpass and of the underground collector. These data were mainly used to support the interpretation of the underground structures and to complement the geotechnical model derived from the borehole campaign.

Both sources were considered in relation to the recommendations formulated in Anejo Nº27 [20]. Together, they represent the most relevant documentation currently available for the geological, geotechnical and structural interpretation of the Avenida Pérez Galdós corridor. The resulting dataset constitutes the principal reference for the interpretation presented in this thesis and for the evaluation of the intervention strategies considered for the existing underpass.

2.3 Borehole investigation campaign

2.3.1 Introduction to the borehole dataset

The borehole dataset analysed in this thesis derives from the geotechnical investigation campaign carried out along Avenida Pérez Galdós as part of the broader subsurface investigation described in the previous section. This section focuses specifically on the four rotary boreholes used as direct control points for the stratigraphic interpretation and for the subsequent construction of the three-dimensional ground model.

The boreholes, identified as SR-01, SR-02 (PZ-01), SR-03 (PZ-02), and SR-04, were

distributed along the Pérez Galdós–Giorgeta corridor, as shown in Figure 2.6. Their location was selected to provide representative information on the stratigraphy, groundwater conditions, and mechanical properties of the soils affected by the renovation project.

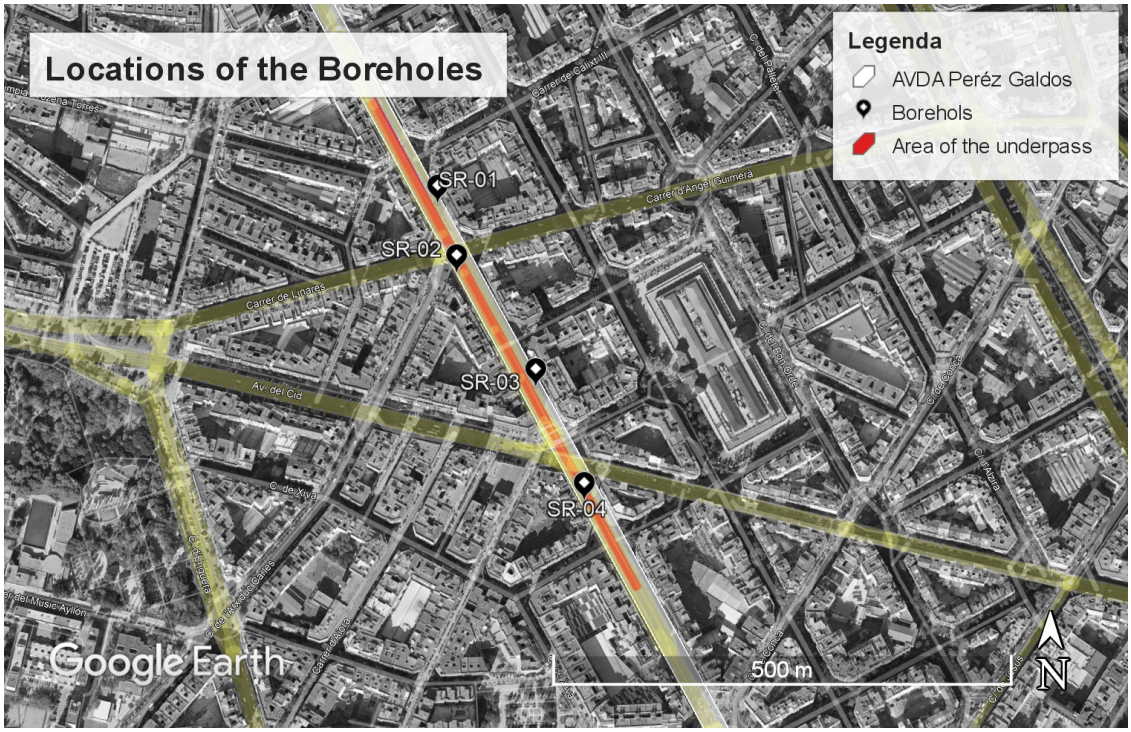

Figure 2.6. Location of the four boreholes along the Pérez Galdós–Giorgeta corridor.

Table 2.1. Main information for the boreholes considered in the present study.

Borehole	Execution date	UTM X	UTM Y	Ground level [m]	Depth [m]
SR-01	28/11/2025	724374.564	4372107.536	19.58	20.80
SR-02 (PZ-01)	20/10/2025	724382.830	4372049.251	19.56	23.60
SR-03 (PZ-02)	30/10/2025	724479.119	4371944.904	19.19	30.20
SR-04	28/10/2025	724530.299	4371813.518	18.36	22.40

According to the borehole logs, the campaign was commissioned by *GECIVAL Ingeniería*, while the drilling operations were carried out by *INTERCONTROL Servicios Técnicos*. The boreholes were executed within a relatively short time interval, as shown in Table 2.1, which allows the results to be compared under broadly consistent groundwater and seasonal conditions.

The laboratory programme associated with the boreholes included identification, strength, deformability, and chemical tests. In general terms, three undisturbed samples and five SPT tests were planned for each borehole. The complete set of laboratory tests

considered in the campaign is summarised in Table 2.2.

Table 2.2. Summary of laboratory tests performed during the geotechnical investigation campaign.

Test type	Number	Sample type
Identification tests		
Grain size analysis by sieving (UNE 103101/95)	32	SPT + UD
Atterberg limits determination (UNE 103103/94)	32	SPT + UD
Natural water content determination (UNE 103300/93)	32	SPT + UD
Soil density determination by hydrostatic balance method (UNE 103301/94)	12	UD
Specific gravity of soil particles (UNE 103302/94)	32	SPT + UD
Strength and deformability tests		
Direct shear test (UNE 103401/98)	4	UD
Unconfined compression test (UNE 103400/93)	4	UD
One-dimensional consolidation test (UNE 103405/94)	4	UD
Chemical tests		
Oxidisable organic matter content (UNE 103204:2019)	4	SPT/UD
Soil aggressiveness to concrete (UNE 83963/08, UNE 83962:2008)	2	SPT/UD
Sulphate content in solid materials (Código Estructural)	2	SPT/UD
Water aggressiveness to concrete (UNE 83952/08 and related standards)	2	Water

Note: SPT refers to samples obtained during Standard Penetration Tests, while UD refers to undisturbed soil samples.

The available information was initially fragmented, as borehole logs, field records and laboratory certificates became progressively available during the development of the investigation. As the documentation was released, the relevant data were extracted and organised into four dedicated Excel files, one for each borehole, in order to maintain a consistent structure for the interpretation process.

Each file included the main stratigraphic descriptions, sampling depths, laboratory results, SPT values, groundwater observations and references to the recovered samples. Both absolute elevations and depths below ground level were included, allowing the different boreholes to be compared consistently and facilitating the reconstruction of the geological profile along the corridor.

The structured database was used as an operational tool during both the geological interpretation and the numerical modelling phases. It allowed rapid consultation of the available information and made it easier to identify inconsistencies, anomalous values or possible transcription errors within the original documentation.

During the processing phase, some discrepancies were identified. In particular, certain elevation values required correction due to inconsistencies between borehole references, while some laboratory or field results appeared significantly different from the general behaviour observed in the surrounding soils. In these cases, the anomalous values were critically evaluated and, when considered non-representative, excluded from the subsequent interpretation and parameter selection.

From a preliminary inspection of the dataset, the subsoil immediately appeared highly heterogeneous and difficult to interpret through a simple stratigraphic subdivision. The borehole logs revealed the frequent presence of lenses and localised inclusions of material trapped between layers with completely different geological and geomechanical characteristics. Alternations between coarse granular deposits and fine cohesive soils were often abrupt, while the thickness and continuity of the layers varied significantly from one borehole to another.

The upper portion of the subsoil is generally composed of anthropogenic fills associated with the urban development of the area, including asphalt layers, construction debris, sandy gravels, and heterogeneous compacted materials. Below these fills, natural deposits were encountered, mainly consisting of silty-clayey soils with firm consistency alternating with sandy and gravelly horizons of variable compactness.

The borehole descriptions also highlighted the presence of gravel layers with sandy matrix and medium-to-high density, particularly in the deeper portions of SR-03 and SR-04, while cohesive fine-grained soils were more recurrent in intermediate depths. Several SPT values confirmed the strong variability of the deposits, ranging from relatively low resistance in fine materials to near-refusal conditions in dense gravelly horizons.

This pronounced heterogeneity made the interpretation process particularly complex and required a significant degree of approximation during the definition of the final stratigraphic model.

Once structured, the borehole dataset was interpreted in order to identify the geotechnically significant properties of the encountered horizons, compare the behaviour observed at the four investigation points, and define a coherent stratigraphic subdivision of the subsoil. The final objective was to establish representative soil layers based on both geological interpretation and mechanical behaviour, so that these layers could subsequently be implemented within the *Geotechnical Modeler* environment of Civil 3D.

In this context, the boreholes constitute the main direct source of information for the present thesis. While geophysical investigations provide continuity and indirect support between investigation points, borehole data remain the fundamental reference for identifying the sequence of fills, fine-grained deposits, and granular layers, as well as for assigning the physical and mechanical parameters required for the geotechnical model.

2.4 Definition of the stratigraphic model

The stratigraphic model was defined by simplifying the heterogeneous urban subsoil into a limited number of representative geotechnical units. The borehole logs showed frequent lateral variations and discontinuous lenses of material, so the objective was not to reproduce every local change, but to identify layers capable of representing the main

mechanical behaviour of the ground.

The interpretation was based on the comparison between borehole descriptions, laboratory tests, SPT results and geological observations. Through this process, five principal geotechnical layers were identified and adopted throughout the thesis:

Table 2.3. Representative geotechnical layers adopted in the stratigraphic model.

Layer	Spanish name	English meaning	From depth [m]	To depth [m]
R	Relleno antrópico	Anthropogenic fill	0.00	0.60–4.20
F1	Finos 1	Fine-grained soils 1, mainly sandy clays	0.60–4.20	8.00–9.40
G1	Gravas 1	Gravelly soils 1, mainly silty-sandy gravels	8.00–9.40	12.80–17.20
F2	Finos 2	Fine-grained soils 2, mainly clay	12.80–17.20	18.10–22.20
G2	Gravas 2	Gravelly soils 2, mainly gravel	18.10–22.20	22.40–30.20

Note: The reported depth intervals indicate the minimum and maximum depths at which each layer boundary was identified among the available boreholes. Layer G2 was identified only in SR-02, SR-03 and SR-04.

The depth ranges reported in Table 2.3 represent an approximated stratigraphic subdivision of the site for each borehole. The layer labelled as R corresponds to the superficial anthropogenic fill deposits associated with the urban history of the area. These materials are highly heterogeneous and include sandy gravels, silts, construction debris, and compacted artificial deposits.

The layers F1 and F2 represent predominantly fine-grained soils characterised by elevated fines content, moderate plasticity, and cohesive behaviour. These horizons mainly include silty-clayey materials with firm consistency and relatively low permeability.

Conversely, the layers G1 and G2 correspond to granular soils composed mainly of gravels and sandy gravels with medium-to-high compactness. These deposits generally exhibit higher stiffness, and significantly greater mechanical resistance compared to the fine-grained units.

Although the adopted subdivision inevitably simplifies the real geological complexity of the site, it provides a coherent and operational framework for the subsequent numerical analyses and geotechnical modelling activities.

2.5 Geotechnical characterisation and selection of numerical parameters

After defining the representative stratigraphic units, the available laboratory and in situ data were processed in order to assign physical and mechanical parameters to each layer. The objective of this phase was not to redefine the stratigraphic model, but to translate the interpreted geological units into a set of numerical parameters suitable for the subsequent Civil 3D and RS2 modelling stages.

The parameter selection was based on the grouped borehole data, laboratory test results, SPT values and engineering correlations. Particular attention was given to the distinction between fine-grained and granular units, since this distinction controls the selection of stiffness, strength and hydraulic parameters in the numerical model.

Figure 2.7 and Figure 2.8 show the drilling equipment employed during the site investigation campaign and an example of the recovered borehole core material, respectively.

Figure 2.7. Drilling equipment operating on site during the geotechnical investigation campaign.

Figure 2.8. Recovered material from borehole SR-04, showing the stratigraphic core boxes corresponding to the depth interval between 18.4 and 21.3 m.

2.5.1 Processing and statistical treatment of geotechnical data

For each identified layer, all the available laboratory and in situ test results were collected and grouped together. Average, minimum, and maximum values were calculated for each parameter in order to evaluate both the representative value and the variability of the dataset.

Particular attention was devoted to the identification of anomalous or non-representative values. Extremely scattered measurements, significantly inconsistent with the overall trend of the corresponding layer, were excluded from the calculation of representative parameters.

Regarding the Standard Penetration Test (SPT) results, values exceeding 50 blows were not directly considered in the correlations. In accordance with common geotechnical practice, all values greater than 50 were assumed equal to 50.

This limitation was introduced in order to avoid unrealistic overestimation of soil stiffness due to refusal or near-refusal conditions.

The complete set of processed geotechnical parameters is summarised in Table 2.4.

Table 2.4. Processed geotechnical parameters obtained from laboratory and in situ investigations.

Parameter	R	F1	G1	F2	G2
In situ test results					
SPT N-value	17	11	32.6	18.3	50
Grain size distribution					
Gravel (%)	49.25	4.53	51.51	3.08	42.85
Sand (%)	34.20	19.28	36.18	26.74	43.48
Fines (%)	16.55	76.19	12.31	70.19	13.67
Index and physical properties					
Water content (%)	7.30	15.14	4.53	17.05	5.48
Liquid limit, w_L (%)	–	23.58	–	23.93	–
Plastic limit, w_P (%)	–	15.49	–	16.28	–
Plasticity index, I_P (%)	–	8.10	–	7.65	–
Bulk unit weight, γ (kN/m^3)	22.40	20.83	21.30	21.33	–
Dry unit weight, γ_d (kN/m^3)	20.90	17.87	17.60	18.05	–
Specific gravity, G_s (-)	2.62	2.53	2.65	2.59	2.64
Void ratio, e_0 (-)	0.228	0.389	0.479	0.408	–
Strength parameters					
Undrained shear strength, S_u (kPa)	–	–	–	38.30	–
Effective cohesion, c' (kPa)	13	13	0	27.4	0
Effective friction angle, ϕ' (°)	27	27	–	34	–

Note: R, F1, G1, F2 and G2 indicate the representative geotechnical layers adopted for the interpretation of the investigation results. Missing values indicate parameters not applicable or not available for the corresponding layer.

2.5.2 Derivation of numerical parameters for FEM analysis

The definition of representative geotechnical parameters was required for the subsequent finite element analyses. After defining the stratigraphic model within the *Geotechnical Modeler* environment of Civil 3D, a representative section of the underpass and the corresponding soil stratigraphy were extracted and implemented in RS2. RS2, developed by *Rocscience*, is a two-dimensional finite element software commonly used for geotechnical and underground engineering analyses.

Each soil layer was associated with a set of mechanical and hydraulic parameters, including unit weight, stiffness, strength parameters, earth pressure coefficient at rest and permeability. The parameter selection therefore represents the transition between the geological interpretation of the ground and the numerical simulation of the underpass–collector system.

The parameters required for the finite element analyses were derived from the processed geotechnical dataset. Whenever possible, analytical formulations or empirical correlations available in the literature were adopted.

The void ratio was calculated from the dry unit weight and the specific gravity according to:

$$e_0 = \frac{G_s \gamma_w}{\gamma_d} - 1 \tag{2.1}$$

where G_s is the specific gravity of solids, γ_w is the unit weight of water, and γ_d is the dry unit weight of the soil.

The saturated unit weight was estimated as:

$$\gamma_{sat} = \frac{G_s + e_0}{1 + e_0} \gamma_w \tag{2.2}$$

while the unsaturated unit weight was directly taken from the measured bulk unit weight, when considered representative of the in situ condition.

The coefficient of earth pressure at rest, K_0, was initially estimated using Jaky's empirical expression [28]:

$$K_0 = 1 - \sin \phi' \tag{2.3}$$

This formulation is commonly adopted for normally consolidated soils and provides a first approximation of the in situ horizontal stress state. In the present case, the investigated ground includes anthropogenic fill materials, soils that may have experienced previous loading and unloading phases, and deposits located close to existing retaining structures. These conditions may have induced local stress redistribution or an overconsolidated stress state. For this reason, the calculated K_0 values were used as preliminary references, while a single representative value was later adopted in RS2 for the initial stress field, as discussed in the finite element analysis chapter.

The Young's modulus for the granular layers, namely R, G1 and G2, was estimated through empirical SPT-based correlations commonly adopted for coarse-grained soils. In particular, the adopted approach follows the general form of the correlations reported by Bowles [29], in which the deformation modulus is related to the corrected SPT blow count:

$$E = \alpha N_{SPT} \tag{2.4}$$

where E is expressed in MPa, N_{SPT} is the corrected SPT blow count, and α is an empirical coefficient selected within typical ranges for granular soils. The expression was used as a first-order stiffness estimate from penetration resistance.

For the fine-grained layers F1 and F2, the available unconfined compression test results were used as a reference for estimating stiffness. The undrained shear strength was obtained from the unconfined compressive strength according to the conventional relationship:

$$S_u = \frac{q_u}{2} \tag{2.5}$$

where q_u is the unconfined compressive strength and S_u is the corresponding undrained shear strength.

The Young's modulus was then estimated using the empirical relationship:

$$E = (150 \div 500)\, S_u \tag{2.6}$$

where E and S_u are expressed in MPa. This correlation was used to obtain an approximate stiffness estimate for the fine-grained layers from the available laboratory data.

For layer F1, which is located above the adopted groundwater level and was modelled as dry in RS2, the value of S_u derived as $q_u/2$ was used only as an intermediate empirical index for estimating Young's modulus. It was not adopted as an undrained strength parameter in the numerical model. The strength parameters assigned to F1 in RS2 were defined in effective stress terms, consistently with the drained Mohr–Coulomb formulation adopted for the analyses.

Layer F2 is located below the adopted phreatic level and is therefore more consistent with the use of an undrained shear strength derived from unconfined compression tests as a reference for stiffness estimation. Nevertheless, also for this layer, the final RS2 model adopted effective strength parameters within the Mohr–Coulomb framework, while the S_u-based correlation was used only to support the selection of the elastic stiffness.

Some stiffness values were subsequently refined during the numerical modelling phase in order to obtain operational parameters consistent with the adopted constitutive model and with the final RS2 simulations. This refinement was particularly relevant for the granular layers G1 and G2, whose stiffness and friction angles were increased with respect to the preliminary estimates. This adjustment was considered reasonable because these units are predominantly gravelly, show higher density and resistance in the investigation data, and represent the stiffer granular horizons of the stratigraphic profile.

In particular, the friction angle of G1 was increased from the preliminary value of approximately 34° to 36°, while the friction angle of G2 was increased from approximately 35° to 38°. This choice reflects the more granular and denser nature of these layers and provides a better representation of their expected drained shear strength in the RS2 model.

Poisson's ratio values were selected according to typical ranges reported in the literature for drained conditions, adopting lower values for granular soils and slightly higher values for cohesive fine-grained materials when appropriate.

The dilation angle, ψ, was conservatively assumed equal to 0° for all materials, in order to avoid overestimation of volumetric expansion during plastic yielding.

Finally, the tensile strength of the soils was assumed equal to zero. The final set of operational parameters adopted in the RS2 finite element analyses is summarised in Table 2.5.

Table 2.5. Final geotechnical parameters adopted in the RS2 finite element analyses.

Parameter	R	F1	G1	F2	G2
Stiffness parameters					
Young's modulus, E (MPa)	20.00	21.29	146.70	13.405	225.00
Poisson's ratio, ν (-)	0.30	0.35	0.28	0.28	0.35
Strength parameters					
Cohesion, c' (MPa)	0.0130	0.0130	0.0000	0.0274	0.0000
Friction angle, ϕ' (°)	27	27	36	34	38
Dilation angle, ψ (°)	0	0	0	0	0
Tensile strength (MPa)	0	0	0	0	0
Unit weight and hydraulic condition					
Unit weight, γ (MN/m^3)	0.02000	0.02080	0.02078	0.02090	0.02590
Water condition in RS2	Dry	Dry	Piezometric line	Piezometric line	Piezometric line

Note: The values reported in the table represent the final operational parameters adopted in the RS2 finite element analyses. Some parameters were refined to obtain a coherent representation of the soil behaviour within the Mohr–Coulomb model. For F1, the S_u value derived from unconfined compression tests was used only as an empirical reference for stiffness estimation and not as an undrained strength parameter in RS2.

2.6 Three-dimensional stratigraphic model in Civil 3D

2.6.1 Civil 3D Geotechnical Modeler workflow

Following the definition of the representative stratigraphic units, a three-dimensional ground model was developed in Autodesk Civil 3D v. 2025.2.4 using the integrated *Geotechnical Modeler* v. 2025 environment. This tool allows borehole information to be imported, visualised, and interpolated in three dimensions, providing a spatial representation of the subsurface stratigraphy.

The objective of this phase was not to assign mechanical properties to the soil layers or to perform a geotechnical numerical analysis within Civil 3D. Instead, the Civil 3D model was used as an intermediate geometrical and stratigraphic tool, aimed at reconstructing the spatial continuity of the soil layers and supporting the later extraction of representative sections for the RS2 finite element model.

The borehole information was imported through two separate input tables. The first table contained the borehole identification data, coordinates, ground elevations, total investigation depth, and final absolute elevation reached by each borehole. In addition to the four real boreholes, virtual lateral boreholes were included in the input table as interpolation aids, as discussed in the following subsection.

Table 2.6. Coordinate input table used for the Civil 3D Geotechnical Modeler import, including real and virtual boreholes.

Borehole ID	X [m]	Y [m]	Ground elev. [m]	Depth [m]	Final elev. [m]
Real boreholes					
SR-01	724374.564	4372107.536	19.58	20.80	-1.22
SR-02	724382.830	4372049.251	19.56	23.60	-4.04
SR-03	724479.119	4371914.901	19.19	30.20	-11.95
SR-04	724530.299	4371813.518	18.36	22.40	-4.11
Virtual boreholes on East side of the alignment					
SR-01-1	724123.000	4372132.000	19.58	20.80	-1.22
SR-02-1	724434.000	4372070.000	19.56	23.60	-4.04
SR-03-1	724535.000	4371917.000	19.19	30.20	-11.95
SR-04-1	724578.000	4371835.000	18.36	22.40	-4.11
Virtual boreholes on West side of the alignment					
SR-01-2	724323.000	4372092.000	19.58	20.80	-1.22
SR-02-2	724334.000	4372030.000	19.56	23.60	-4.04
SR-03-2	724435.000	4371907.000	19.19	30.20	-11.95
SR-04-2	724478.000	4371795.000	18.36	22.40	-4.11

Note: Virtual boreholes were introduced only to improve the geometric triangulation of the stratigraphic surfaces. They do not represent additional field investigations.

The second input table contained the simplified stratigraphic sequence assigned to each real borehole. The same sequence was later assigned to the corresponding virtual boreholes only for interpolation purposes.

Table 2.7. Stratigraphic input table used for the Civil 3D Geotechnical Modeler import.

Borehole ID	Layer	From [m]	To [m]	Description
SR-01				
SR-01	R	0.00	4.20	Anthropogenic fill
SR-01	F1	4.20	8.80	Sandy clays
SR-01	G1	8.80	14.60	Silty-sandy gravels
SR-01	F2	14.60	20.80	Clay
SR-02				
SR-02	R	0.00	1.60	Anthropogenic fill
SR-02	F1	1.60	8.60	Sandy clays
SR-02	G1	8.60	17.20	Silty-sandy gravels
SR-02	F2	17.20	22.00	Clay
SR-02	G2	22.00	23.60	Gravel
SR-03				
SR-03	R	0.00	0.60	Anthropogenic fill
SR-03	F1	0.60	9.40	Sandy clays
SR-03	G1	9.40	15.00	Silty-sandy gravels
SR-03	F2	15.00	22.20	Clay
SR-03	G2	22.20	30.20	Gravel
SR-04				
SR-04	R	0.00	0.80	Anthropogenic fill
SR-04	F1	0.80	8.00	Sandy clays
SR-04	G1	8.00	12.80	Silty-sandy gravels
SR-04	F2	12.80	18.10	Clay
SR-04	G2	18.10	22.40	Gravel

2.6.2 Generation of the three-dimensional stratigraphic surfaces

Once the borehole data were imported, the stratigraphic units were connected according to the adopted layer nomenclature: R, F1, G1, F2, and G2. The model could be visualised both through simplified two-dimensional borehole sticks and as interpolated three-dimensional surfaces.

A relevant limitation of the modelling process was related to the spatial arrangement of the four real boreholes, which were located approximately along the same road axis. This configuration is suitable for interpreting longitudinal variations along the avenue, but it is less favourable for generating stable three-dimensional triangulated surfaces. For this reason, virtual boreholes were introduced on both sides of the real alignment, at an approximate lateral distance of 30 m.

These virtual boreholes were assigned the same stratigraphic sequence as the corresponding real boreholes. This procedure does not introduce additional geological information and must therefore be interpreted only as a geometric interpolation aid. Its purpose was to stabilise the triangulation and to allow the construction of wider stratigraphic surfaces, avoiding the numerical and geometric instability that would have

resulted from using only four nearly aligned investigation points.

This assumption inevitably implies a simplified lateral continuation of the interpreted layers away from the borehole alignment. Therefore, the Civil 3D model should not be interpreted as a detailed reconstruction of transverse geological variability, but as a geometrical support for extracting representative stratigraphic sections for the subsequent finite element analysis.

2.6.3 Selection of representative layers and integration with the topographic model

During the interpretation phase, the possibility of defining a larger number of local stratigraphic units was initially considered. However, due to the limited number of boreholes and the strong heterogeneity of the subsoil, additional layers were only retained when they could be recognized consistently in more than one borehole and when their continuity was considered geologically reasonable.

This criterion was adopted to avoid the generation of unrealistic isolated lenses during the interpolation process within the Civil 3D environment. When a layer is identified only locally and cannot be correlated reliably with neighbouring boreholes, the triangulation algorithms implemented within the *Geotechnical Modeler* may generate artificial geometries that are not sufficiently supported by direct evidence. This issue becomes particularly relevant in the present case, where only four real boreholes were available and most of them were approximately aligned along the road axis.

The final subdivision into five representative units therefore represents a compromise between geological detail and modelling robustness. Although the adopted model inevitably simplifies the real complexity of the urban subsoil, it provides a sufficiently coherent framework for the subsequent extraction of representative geological sections and for the development of the finite element model in RS2.

After generating the first three-dimensional stratigraphic reconstruction, the model was superimposed onto the topographic surface derived from the survey included in *Anejo Nº3: Trabajo Topográfico*, produced by *Gecival S.L.*. Both datasets were integrated through direct georeferencing within the same coordinate system.

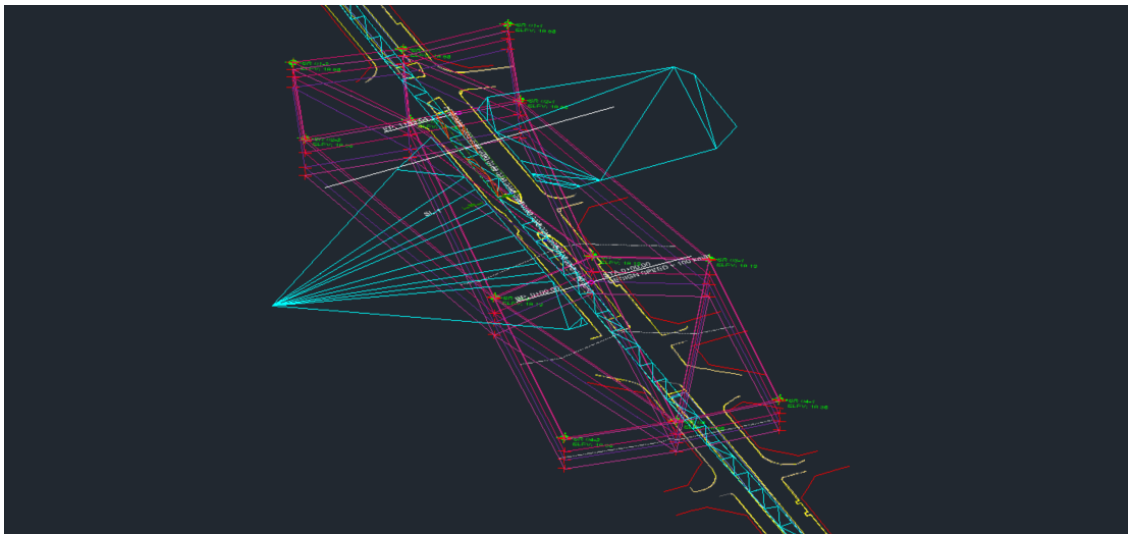

Figure 2.9. Generation of the three-dimensional stratigraphic model in Civil 3D using the Geotechnical Modeler environment.

This comparison revealed slight discrepancies between the ground elevations adopted in the preliminary geotechnical reconstruction and those obtained from the topographic survey. Since the topographic dataset was based on total station measurements and therefore considered more accurate for defining the actual urban ground surface, the stratigraphic model was subsequently reconstructed using the topographic elevations as reference values.

This correction improved the geometric consistency between the underground reconstruction and the surface morphology of the avenue, particularly for the extraction of the final tunnel sections later implemented within RS2. It is important to emphasize that no mechanical or constitutive properties were assigned to the soil layers within the Civil 3D environment itself. The three-dimensional model was used exclusively as a geometrical and stratigraphic support tool, while the actual geomechanical characterisation and numerical analyses were carried out separately in RS2.

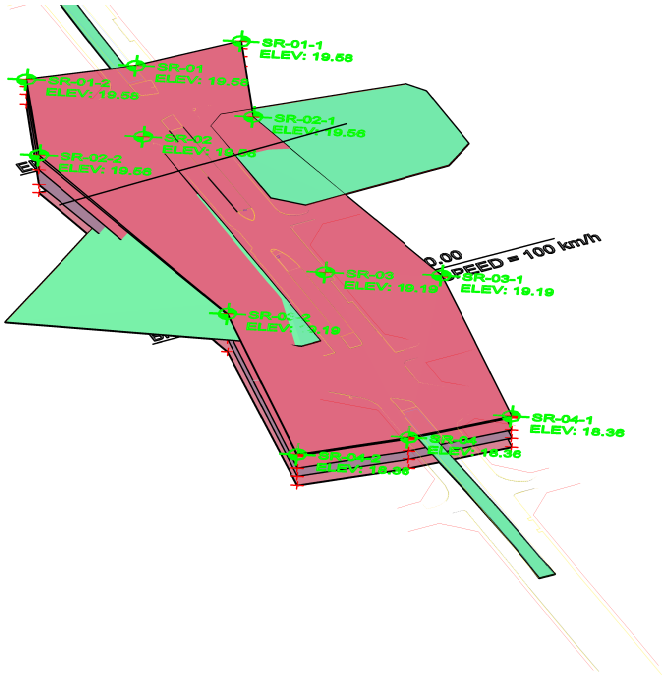

Figure 2.10. Final three-dimensional stratigraphic model generated in Civil 3D using the Geotechnical Modeler environment.

2.7 MASW survey and supporting geophysical interpretation

In parallel with the borehole investigations and laboratory testing campaign, *Geozone Asesores S.L.* developed the geophysical study *"Estudio geofísico mediante análisis multicanal de ondas superficiales 2D (MASW2D) para caracterización del subsuelo y auscultación con GPR3D en muro pantalla de paso inferior y colector en Av. Pérez Galdós (Valencia)"* [21]. Within this study, the Multichannel Analysis of Surface Waves (MASW) method was used to support the characterisation of the subsurface conditions.

Following Park et al. [30], the MASW technique is a seismic geophysical method used to estimate the distribution of shear wave velocities (V_s) within the shallow subsurface through the analysis of Rayleigh wave propagation. Since shear wave velocity is directly related to soil stiffness, the method allows an indirect characterisation of the mechanical behaviour of the ground and the identification of stiffness contrasts between different subsurface layers.

In the present study, the MASW acquisition was carried out using a PASI GEA 24-channel seismograph equipped with 4.5 Hz vertical geophones, while seismic energy was generated through mechanical hammer impacts, as reported in the original technical documentation [21]. The acquired signals were processed through dispersion analysis and inversion procedures in order to obtain two-dimensional V_s profiles along the investigated alignments.

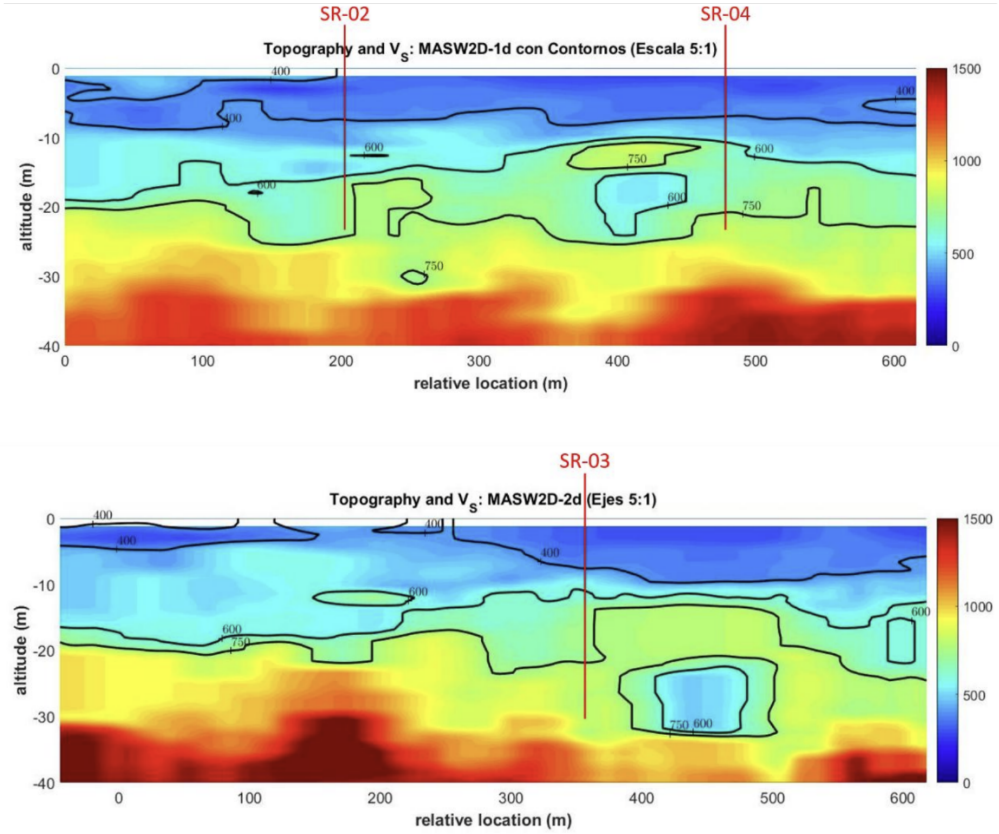

Figure 2.11. 2D shear wave velocity profiles obtained from MASW surveys performed along Avenida Pérez Galdós [21].

The obtained profiles indicate a general increase in stiffness with depth, with relatively low shear wave velocities in the superficial anthropogenic fills and progressively higher values within the deeper granular deposits. The interpreted stratification derived from the MASW sections showed a reasonably good agreement with the borehole information, particularly regarding the alternation between fine-grained horizons and denser gravelly layers.

Nevertheless, within the context of the present thesis, the MASW interpretation was used only as a secondary and supporting source of information. Since direct borehole data and laboratory results were already available, these constituted the primary basis for the geological and geotechnical characterisation of the site. Compared to boreholes, MASW represents an indirect investigation method and is therefore inherently affected by interpretation uncertainties and non-uniqueness during the inversion process.

For this reason, the geophysical results were mainly used to verify the general consistency of the stratigraphic interpretation and to qualitatively confirm the continuity and relative stiffness contrasts between the main geological units previously identified from the borehole dataset. No independent stratigraphic subdivision was derived exclusively from the MASW interpretation.

Chapter 3

Geometric and structural reconstruction of the existing underpass

3.1 Introduction and available documentation

The Pérez Galdós underpass is one of the central infrastructural elements of Avenida Pérez Galdós. As discussed in the previous chapters, it was constructed between 1968 and 1973 in response to the increasing traffic demand that developed along the corridor during the second half of the twentieth century.

The broader Pérez Galdós–Giorgeta corridor extends for approximately 2.2 km along the avenue. Within this corridor, the underpass itself has a total length of about 606 m, according to the structural assessment reported in Anejo Nº27 [20]. It should therefore not be interpreted as a conventional fully underground tunnel. Its longitudinal development includes open trench sections and covered portions, generally corresponding to road intersections and crossings at surface level. The infrastructure is better understood as an urban underpass system composed of ramps, open sections, covered portions, lateral retaining walls, and an underlying wastewater collector.

A particularly relevant feature of the system is the presence of a large wastewater collector located below the underpass. This element appears to have strongly conditioned the available space and the final configuration of the structure. The carriageway is particularly narrow, with a free width of approximately 7 m between the retaining walls, confirming the strong geometric constraints imposed by the surrounding underground infrastructure [20].

Since its construction, no detailed information is currently available regarding possible maintenance interventions, strengthening works, or local modifications carried out during the service life of the structure. Similarly, no original structural drawings, reinforcement plans, material specifications, construction calculations, or detailed as-built records were available during the development of this work. As a result, fundamental information concerning the detailed geometry of the retaining walls and deck system, the wall thicknesses, the possible presence of footing-like base enlargements, the reinforcement layout,

the concrete characteristics, and the structural connections between the different elements remains largely unknown.

This lack of documentation is particularly relevant because the underpass has been one of the central elements of the recent urban and technical debate surrounding Avenida Pérez Galdós. Initial redevelopment proposals considered the possibility of closing the tunnel and transforming its function within a broader regeneration strategy. However, the final intervention strategy progressively shifted towards maintaining the underpass in operation and preserving its role within the urban traffic system. In this context, the technical objective became the evaluation of the condition and reliability of an ageing infrastructure that is now approaching the end of its nominal service life.

The reconstruction presented in this chapter is therefore based on the integration of the technical sources already introduced in the previous chapters. For clarity, the most relevant sources for the geometric and structural reconstruction are briefly recalled here:

- *Anejo Nº27: Evaluación estructural del paso inferior*, which represented the first structured assessment of the underpass and identified the need for further investigation [20];
- *Anejo Nº3: Trabajo Topográfico*, which provided the topographic and CAD information used to extract representative geometries and elevation differences [18];
- the 2025 geotechnical investigation campaign carried out by *Intercontrol Levante S.A.*, which provided the borehole data, in situ tests and laboratory results used for the ground characterisation;
- the 2025 geophysical study carried out by *Geozone Asesores S.L.*, which included MASW2D and GPR3D investigations and provided indirect information on the retaining walls, the collector and the surrounding ground [21];
- limited historical photographic material and secondary references, which provided only qualitative support due to their scarcity and limited technical detail.

Among these sources, the GPR investigation [21] played a particularly important role because it provided indirect information on wall thicknesses, reinforcement patterns, slab geometry, and the relationship between the underpass and the collector.

The objective of this chapter is not to claim a definitive as-built reconstruction of the underpass, which is currently impossible given the available information. Rather, the aim is to develop a technically coherent geometric and structural interpretation, sufficiently reliable to support the subsequent geotechnical modelling and finite element analyses.

3.2 Ground penetrating radar investigations and survey reference system

3.2.1 GPR method

According to Daniels [31], Ground Penetrating Radar (GPR) is a non-destructive electromagnetic technique used to investigate subsurface features through the transmission

and reception of high-frequency electromagnetic waves. Its interpretation is based on the reflection of radar signals at interfaces characterised by contrasts in dielectric properties.

The propagation velocity of electromagnetic waves in a material can be approximated as:

$$v = \frac{c}{\sqrt{\varepsilon_r}}$$

where c is the speed of light in vacuum and ε_r is the relative dielectric permittivity of the material.

In the present study, GPR investigations were carried out using two systems, as described in the available technical documentation [21]. A high-frequency multi-array system, GP8100, was used for detailed inspection of shallow features, while a lower-frequency system, GS8000 operating at 270 MHz, was employed to increase penetration depth. The combined use of these instruments allowed a balance between resolution and investigation depth.

The effectiveness of GPR strongly depends on the electrical properties of the investigated materials. Conductive or water-saturated materials can cause rapid signal attenuation and reduce penetration depth [31]. For this reason, the GPR results were interpreted as indirect supporting evidence rather than as direct measurements of the structural geometry.

Figure 3.1. Instrument used for the GPR survey, Proceq GS8000 [32], and representative acquisition setup adopted in the underpass [21].

3.2.2 Survey reference axes

The GPR investigation was organised along a set of reference axes, labelled GF, distributed along the length of the underpass and the underlying collector. These axes represent the framework within which the wall thicknesses, reinforcement patterns, and collector dimensions were interpreted.

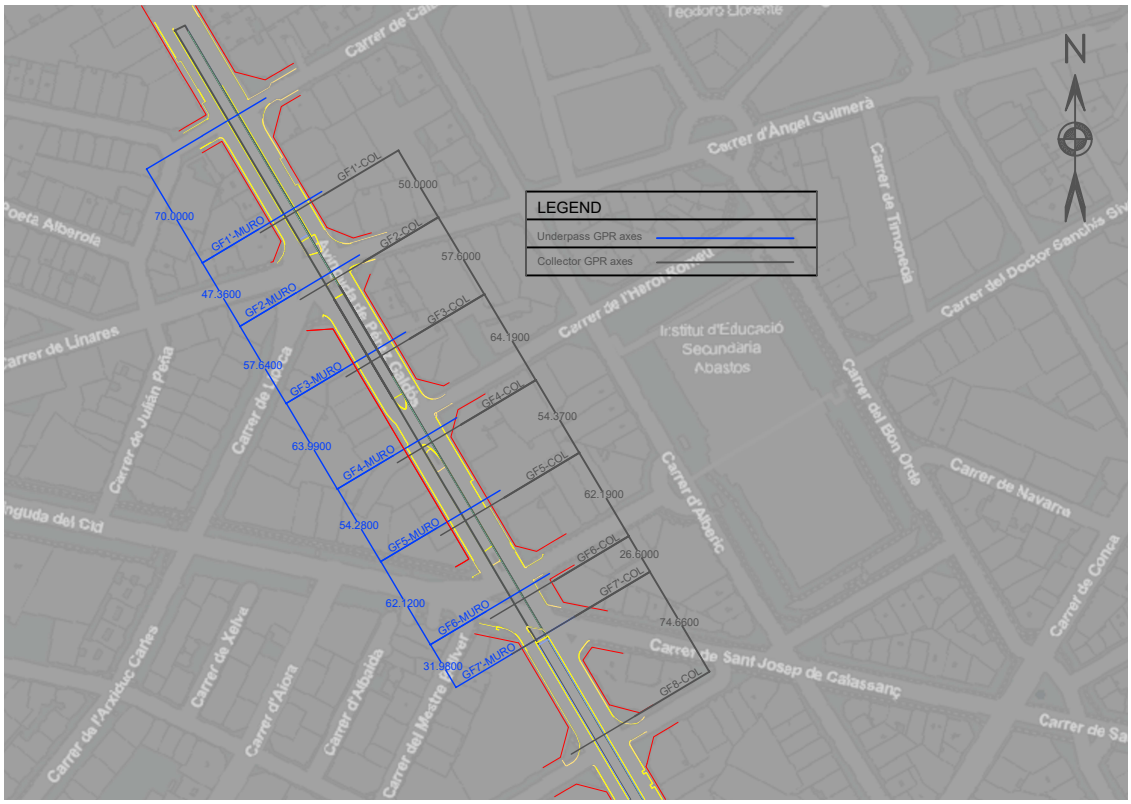

Figure 3.2. Indicative location of investigation GPR axes along the underpass and collector alignment [21].

For the retaining wall investigation, the spacing between the reference sections is summarised in Table 3.1.

Table 3.1. Spacing between GPR investigation axes for the retaining wall.

Section	Reference Axes	Distance [m]
GF1 – GF1'	GF1 (not used) to GF1'	70.00
GF1' – GF2	GF1' to GF2	47.36
GF2 – GF3	GF2 to GF3	57.64
GF3 – GF4	GF3 to GF4	63.99
GF4 – GF5	GF4 to GF5	54.28
GF5 – GF6	GF5 to GF6	62.12
GF6 – GF7'	GF6 to GF7'	31.98

For the collector, a slightly different longitudinal reference was adopted, starting from the beginning of the joists on the Cartagena side. The corresponding distances are reported in Table 3.2.

Table 3.2. Spacing between GPR investigation axes for the collector.

Section	Reference Axes	Distance [m]
GF1' – GF2	GF1' to GF2	50.00
GF2 – GF3	GF2 to GF3	57.60
GF3 – GF4	GF3 to GF4	67.19
GF4 – GF5	GF4 to GF5	54.37
GF5 – GF6	GF5 to GF6	62.19
GF6 – GF7	GF6 to GF7	26.60
GF7 – GF8	GF7 to GF8	74.66

These reference axes provide the basis for the interpretation developed in the following sections, where the retaining walls and the collector are analysed separately due to their different geometrical characteristics and investigation constraints.

A specific clarification is required for the interpretation of the beam system in the collector. In the 2025 report, the beginning of the *viguetas* (precast prestressed beams) on the C/ Cartagena side was used as a longitudinal reference. From this point, 29.7 m were measured back towards the collector entrance in order to locate GF1'.

3.3 Retaining wall geometry and reinforcement interpretation

The GPR-based interpretation indicates that the retaining wall thickness generally increases with depth. The interpreted geometry suggests a stepped structural pattern, with upper wall sections generally thinner than the lower portions near the base zone.

This trend suggests a conventional structural rationale in which the wall becomes wider toward the base in order to provide greater resistance and stability against lateral earth pressures. However, since the interpretation derives from geophysical evidence, the values must be considered approximate and subject to uncertainty.

The interpretation also suggests the presence of an orthogonal reinforcement mesh, generally characterised by vertical bars spaced at approximately 15 cm with diameters around 16 mm, and horizontal bars spacing at approximately 30 cm with diameters around 25 mm.

The depth of the first reinforcement layer appears to vary significantly depending on the investigated zone. In covered sections, reinforcement is often interpreted very close to the exposed inner face, with concrete cover generally ranging between approximately 3 and 6 cm. Conversely, in open sections, the first reinforcement layer appears significantly deeper, often at approximately 40–50 cm from the exposed inner face.

This contrast suggests that the structural arrangement may change according to the local loading conditions, with covered sections likely requiring a different reinforcement configuration due to the presence of slabs and surface loads. Nevertheless, this interpretation must be regarded as a plausible engineering hypothesis rather than as a confirmed as-built condition.

3.4 Axis-by-axis interpretation of the retaining wall

The interpretation of the individual GPR sections revealed significant variability along the longitudinal development of the underpass. The following paragraphs summarize the main observations for each investigation axis.

The GF1' section corresponds to an open setback area where the wall thickness is estimated at approximately 60 cm in the upper portion, increasing to approximately 82–90 cm near the base. Shallow reinforcement is interpreted at approximately 15 cm depth, while a second reinforcement level appears between approximately 35 and 45 cm.

The GF2 section corresponds to a covered transition zone. In this area, the wall thickness varies between approximately 50 and 61 cm in the upper portion and reaches approximately 90 cm near the base. The reinforcement arrangement appears asymmetrical between the two sides of the section, possibly suggesting the presence of construction joints or transitions between different structural panels.

The GF3 section corresponds to an open area where the upper wall thickness could not be clearly identified. Nevertheless, the lower wall thickness is estimated between approximately 71 and 76 cm. Reinforcement appears relatively deep and no shallow reinforcement layer was clearly detected.

The GF4 section corresponds to another covered transition zone. The interpreted wall thickness ranges between approximately 55 and 65 cm near the top and approximately 80–90 cm near the base. A second reinforcement level was identified at approximately 30 cm depth.

The GF5 section corresponds to an open trench area characterised by wall thicknesses around 60 cm in the upper section and approximately 80–90 cm near the base. As observed in GF3, the reinforcement appears relatively deep and no shallow reinforcement layer was clearly detected.

The GF6 section corresponds to a covered heterogeneous zone where the wall thickness appears greater than 60 cm near the top and approximately 80–90 cm near the base. The reinforcement configuration appears highly variable and may indicate the interaction of different construction typologies or phases.

Finally, the GF7' section corresponds to a heavily loaded covered zone characterised by particularly dense reinforcement. The estimated wall thickness ranges between approximately 65 and 70 cm near the top and approximately 80–90 cm near the base. The interpretation suggests the presence of double horizontal reinforcement and a second reinforcement layer located approximately 20–25 cm from the surface.

Overall, the axis-by-axis interpretation confirms that the retaining walls cannot be described by a single uniform transverse section. Rather, the structure appears characterised by local transitions and geometrical variations likely associated with different construction phases, changing load conditions, or local geometric constraints. Nevertheless, the observed variability remains compatible with the adoption of a representative transverse section for a preliminary two-dimensional finite element analysis, provided that the results are interpreted at the scale of the global soil–structure interaction rather than as a local as-built verification.

3.5 Collector geometry and structural interaction

The general geometry of the Colector Sur is described in Anejo Nº27 as a large buried concrete gallery, with an internal ovoid-like section adapted to its hydraulic function. The lower part includes a central circular channel flanked by horizontal maintenance passages, while the upper part is described as a three-centred arch [20]. Therefore, the general internal shape of the collector should not be considered completely unknown.

The 2025 Geozone report [21] complements this information by providing a recent GPR-based interpretation of the collector thicknesses and of the concrete–subsoil interfaces along the investigated axes. The system used for the collector investigation was mainly suitable for identifying geometric interfaces and thickness variations, while it did not provide a detailed reconstruction of the reinforcement layout. For this reason, the possible presence of reinforcement in the collector cannot be excluded, but it could not be explicitly characterised from the available GPR data.

The available photographic sources provided additional qualitative support for interpreting the internal geometry of the collector. Historical photographs offer limited assistance, while a photograph taken during the 2024 inspection provides a more direct confirmation of the general internal shape of the structure.

Figure 3.3. View of the collector recorded during the 2024 inspection, showing the internal geometry of the structure [20].

The collector cannot be considered a secondary infrastructure element. On the contrary, it represents a major underground structure running below the underpass and appears to have played a decisive role in constraining both the width and the structural configuration of the retaining walls.

The collector investigation was performed along axes GF1' to GF8. The interpreted

echoes generally suggest wall-related concrete–subsoil interfaces in the range of approximately 1.1–1.4 m, slab-related interfaces generally between approximately 0.9 and 1.4 m, and aerial wall echoes often around approximately 2.1 m in sections containing joists.

The interpreted data suggest collector wall thicknesses commonly around 1.1–1.3 m, while slab thicknesses are generally estimated around 1.2–1.4 m. However, significant local variability exists, and some sections are affected by overlapping real and aerial echoes.

This information is directly relevant for the present thesis because the collector must be regarded as a potentially load-bearing adjacent structure in scenarios involving tunnel closure, reuse, or backfilling. Any intervention affecting the underpass must therefore consider the possible redistribution of loads toward the collector and the geometric proximity between the two systems.

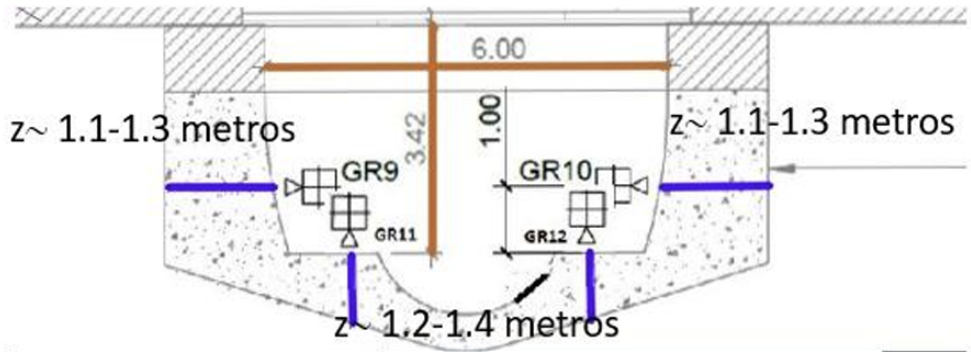

Figure 3.4. Geometry summary of the collector reported after GPR investigations [21].

3.6 Methodological reconstruction approach

The reconstruction process adopted in this thesis is based on the progressive integration of information characterised by different levels of reliability and resolution. The topographic survey provided the most reliable reference for the external geometry of the avenue, the ground surface elevations, the road levels, and the general layout of the underpass. These data were used to estimate the vertical distance between the surface roadway and the underpass level, as well as to define the position of the opposite retaining wall across the carriageway.

The GPR results provided indirect evidence regarding the internal structural configuration. In particular, they were used to interpret possible wall thicknesses, reinforcement depths, slab positions, and collector thicknesses. These results were not considered as exact measurements, but as ranges of plausible values to be integrated with the remaining available information.

The reconstruction first required the definition of representative thicknesses for both

the retaining wall and the collector. For the retaining wall, all available GPR-based measurements were considered in order to define minimum and maximum interpreted values. In the upper portion of the wall, the adopted range was approximately 48–73 cm, while in the lower portion the adopted range was approximately 70–90 cm.

Starting from these limits, two boundary lines were constructed in CAD: one corresponding to the minimum interpreted thicknesses and one corresponding to the maximum interpreted thicknesses. A median line was then traced between these two limits and adopted as the representative wall geometry for the reconstructed section. This criterion was adopted in order to account for the variability of the GPR interpretation without selecting either the minimum or the maximum extreme as the final geometry.

The same procedure was applied to the collector. The interpreted thickness ranges were approximately 1.10–1.30 m for one set of measurements and approximately 1.20–1.40 m for another. As for the retaining wall, minimum and maximum geometric envelopes were defined and a representative median line was adopted for the reconstruction.

The labels GR shown in Figure 3.5 indicate the GPR auscultation locations from which the interpreted thicknesses were obtained. For the retaining wall, these measurements correspond to the inspection grids performed at different heights along the wall, while for the collector they refer to the GPR profiles carried out from the internal surface of the concrete section.

This procedure is illustrated schematically in Figure 3.5, where the minimum and maximum GPR-based limits and the selected median reconstruction line are shown for both the retaining wall and the collector.

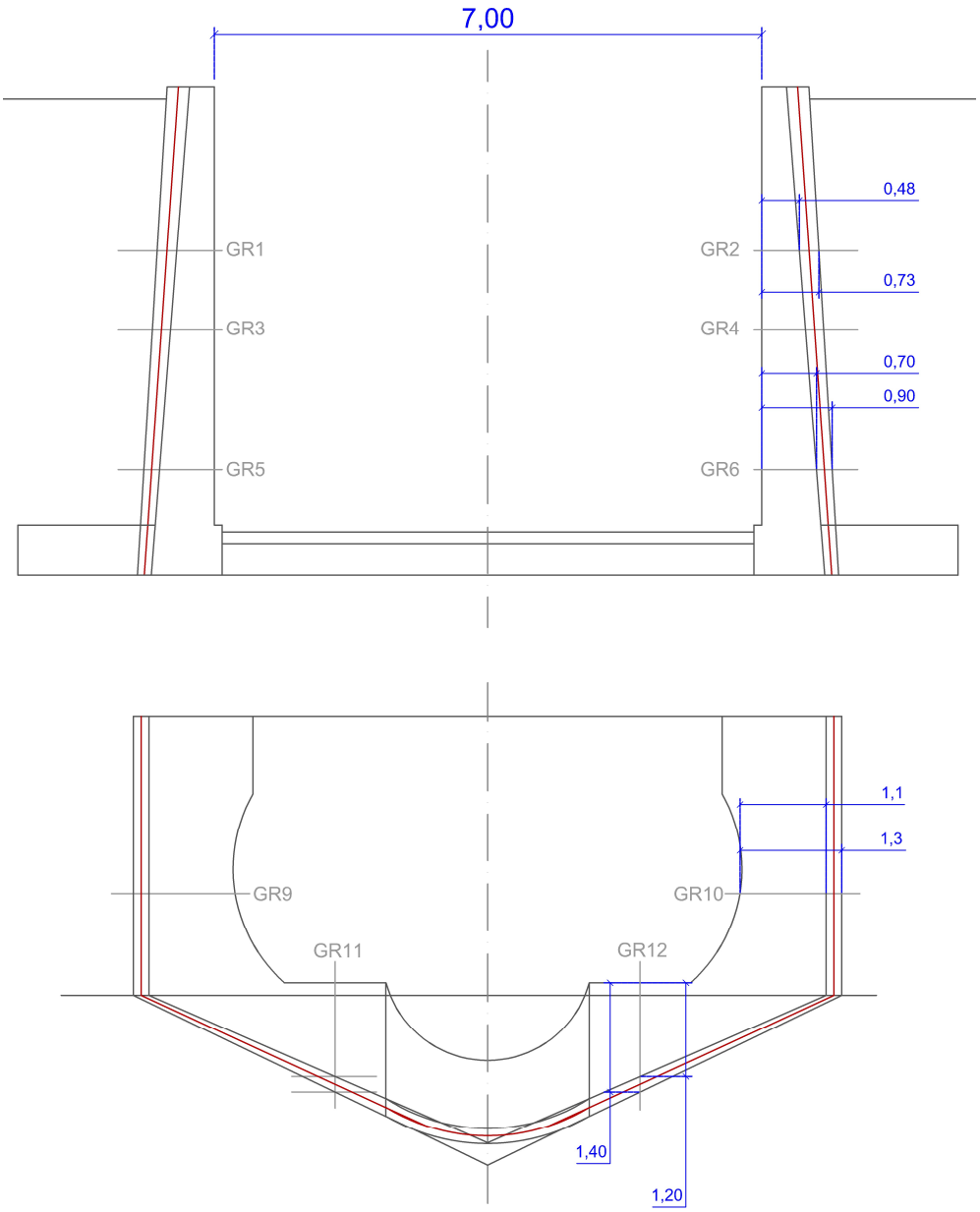

Figure 3.5. Geometric reconstruction criterion adopted for the retaining wall and collector. The figure shows the minimum and maximum GPR-based thickness limits and the red median line selected as representative geometry.

Based on these criteria, representative transverse sections were produced in CAD. The opposite retaining wall of the underpass was positioned using the distances measured from the topographic survey, while the height of the underpass section was derived from the

elevation difference between the road surface and the underpass carriageway.

This procedure allowed the definition of a geometrical section as close as possible to the expected real configuration, while explicitly acknowledging the uncertainty associated with the lack of original design data. The adopted approach is therefore interpretative and conservative: it does not eliminate uncertainty, but makes it explicit and incorporates it into the subsequent modelling strategy.

3.7 Geometric uncertainties and competing interpretations

One of the principal unresolved issues concerns the geometry of the wall base, particularly the possible existence of a footing-like base enlargement. In retaining wall systems, this element would correspond to a structural base or footing extending laterally from the wall, potentially modifying the way loads are transferred toward the surrounding ground or toward the adjacent collector.

The available GPR measurements carried out at the lowest elevations are not sufficient to determine precisely the geometry of this base zone. The main difficulty is that the investigated depth approximately coincides with the structural level of slabs and joists, where wave propagation and signal interpretation become particularly complex. Consequently, the possible presence, dimensions, and continuity of a footing-like base enlargement cannot be confirmed or excluded solely on the basis of the GPR data.

This uncertainty is also consistent with the preliminary interpretation included in Anexo II of Anejo Nº27. In that document, the possibility of a simple L-shaped retaining wall was discarded on the basis of historical photographic evidence, while a reinforced-concrete gravity wall configuration was considered the most plausible hypothesis, although the report explicitly stated that this geometry would still require verification in situ [20]. This supports the idea that the base of the wall may be more massive than a simple vertical wall, without allowing its actual geometry to be defined with certainty.

A particularly relevant result concerns two additional boreholes carried out in July 2024 close to the wall near the GF1 area, as reported in the preliminary geotechnical documentation [19]. Borehole SR-2, located approximately 1.55 m from the wall, detected structural concrete between 3.60 m and 6.60 m depth. Conversely, borehole SR-1, located approximately 2.51 m from the wall, did not detect concrete at the depths where it might have been expected if a continuous and laterally extended base enlargement had been present.

The first result suggests a wall or wall-related concrete thickness substantially greater than the one estimated exclusively through GPR interpretation, potentially more than twice the georadar estimate in that specific area. The second result, however, suggests that the possible footing-like base enlargement, if present, is likely to have a limited lateral extension. In particular, its width can reasonably be assumed to be smaller than approximately 2.50 m from the wall, since no structural concrete was encountered at that distance in the borehole where it would have been expected.

Taken together, these results indicate that the actual geometry of the wall base is uncertain and probably more complex than a single simplified transverse section would imply. The combined interpretation of GPR data, boreholes, topographic information, and

historical references suggests significant local variability, particularly in the transition zone between retaining walls, slabs, collector structures, and possible foundation enlargements.

3.8 Adopted geometric assumptions and reconstruction scenarios

Based on the available evidence, the geometric reconstruction adopted in this thesis was developed by defining plausible lower and upper bounds for the main structural dimensions. The minimum and maximum interpreted thicknesses of both the retaining wall and the collector were used to generate representative transverse sections. This approach was adopted in order to account for uncertainty without introducing unsupported geometric detail.

Through this procedure, a representative section of the underpass and collector system was obtained. The section does not represent a verified as-built drawing, but rather a technically consistent interpretation based on the best available information.

Two main geometric scenarios were then adopted for the subsequent analyses. The first scenario considers the presence of a retaining wall with a footing-like base enlargement resting above or close to the collector system. In this case, the geometry of the base enlargement was not defined arbitrarily, but was constrained using the information obtained from the two boreholes carried out near the wall in the GF1 area.

In particular, the borehole located approximately 1.55 m from the wall detected structural concrete at the relevant depth, while the borehole located approximately 2.51 m from the wall did not encounter structural concrete. These two distances were therefore interpreted as geometric bounds for the possible lateral extension of the footing-like base enlargement. For the reconstructed scenario with a base enlargement, an intermediate line was adopted between these two limits, corresponding to an approximate representative extension of 2.03 m from the wall.

This assumption is illustrated in Figure 3.6, where the two borehole-based limits and the adopted intermediate reconstruction line are shown.

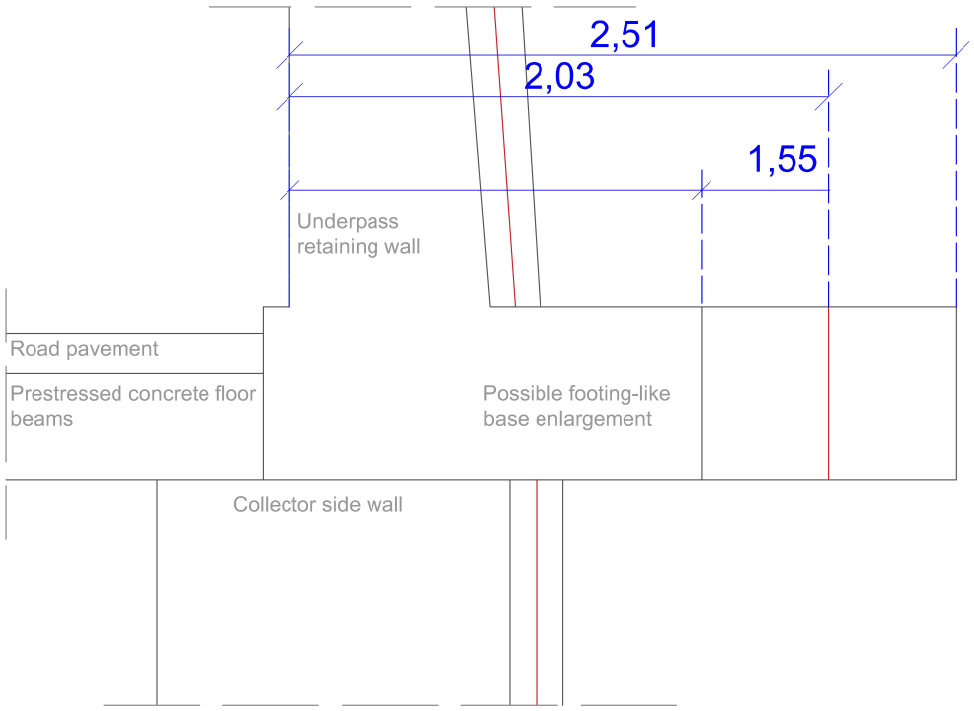

Figure 3.6. Geometric criterion adopted for the footing-like base enlargement. The adopted extension was defined as an intermediate value between the borehole that detected structural concrete at 1.55 m from the wall and the borehole that did not detect concrete at 2.51 m from the wall.

This scenario represents the possibility that the retaining wall behaves as a wall with a local base element, although the actual geometry and continuity of this element remain uncertain.

The second scenario considers a simpler vertical wall configuration without a footing-like base enlargement. In this case, the wall is not interpreted as resting on an independent footing-like element, but as a more direct vertical structural body connected to the underlying collector. This assumption was adopted to represent the alternative possibility that the wall and the collector-side structural elements behave as a continuous or effectively connected system in the analysed transverse section. This alternative was introduced because the available investigations do not provide sufficient evidence to confirm the presence of a continuous footing-like element along the entire alignment.

These two scenarios were selected because they represent the two most relevant structural interpretations compatible with the available evidence: a wall with a limited base enlargement and a simpler vertical wall configuration.

The adoption of these two scenarios allows the numerical analysis to account for the main geometric uncertainty affecting the structural reconstruction. Rather than selecting a single unverified configuration, the thesis considers two plausible alternatives and evaluates

their implications in the subsequent modelling phase.

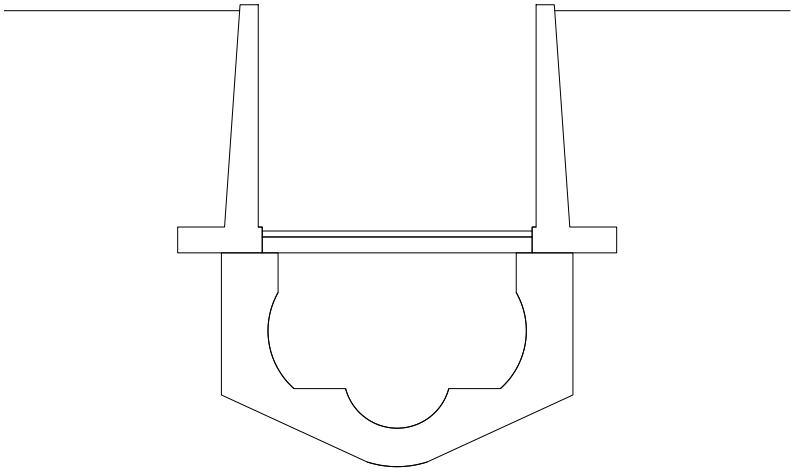

Figure 3.7. Reconstructed transverse section of the underpass and collector system considering the presence of a footing-like base enlargement.

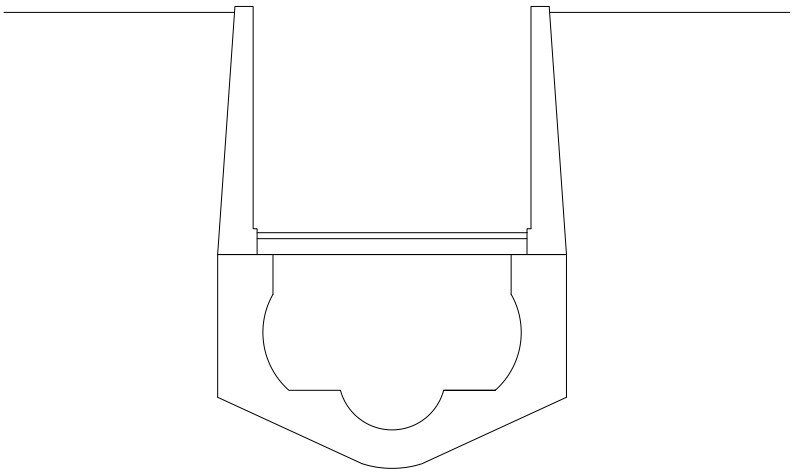

Figure 3.8. Reconstructed transverse section of the underpass and collector system considering a vertical wall configuration without footing-like base enlargement.

3.9 Selection of the representative section for numerical modelling

The reconstruction of the underpass geometry represents only the first step toward the finite element analysis. In order to develop a two-dimensional numerical model, it was necessary to select a representative transverse section where the interaction between the structure and the surrounding ground could be studied in a meaningful way.

The selected section corresponds to a location considered critical within the longitudinal development of the underpass. It is positioned in an open trench portion approximately midway between two covered intersections. This choice was made because, in this area, the retaining walls are not directly constrained by an immediately adjacent covered slab, and the section is therefore representative of the open configuration of the underpass.

Once the critical section was selected, the corresponding stratigraphic profile was extracted from the three-dimensional ground model described in the previous chapter. The reconstructed structural section was then superimposed onto the local soil stratigraphy, producing the complete geometrical basis for the subsequent RS2 numerical model.

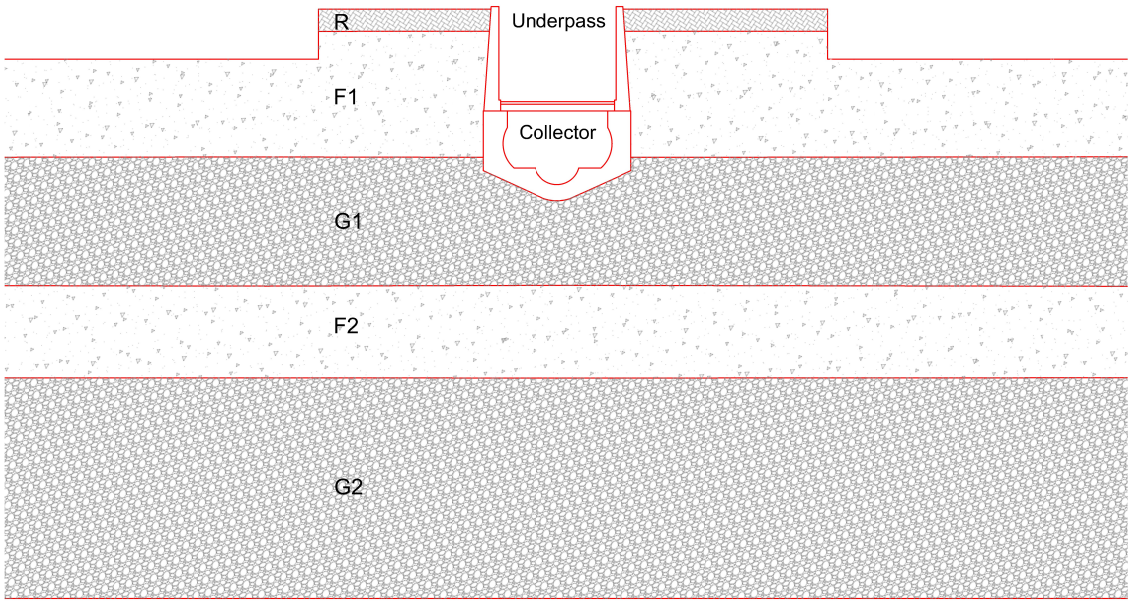

Figure 3.9. Representative transverse section selected for numerical modelling, showing the reconstructed underpass and collector geometry superimposed onto the local stratigraphic profile.

This combined section represents the transition between the geometric reconstruction

developed in the present chapter and the finite element modelling phase discussed in the following chapter. The detailed procedure adopted to prepare the CAD geometry for RS2 import, including the simplification of the section, removal of overlapping lines, creation of closed polylines, definition of material boundaries, excavation regions, structural elements, and construction stages, is presented in the finite element analysis chapter.

3.10 Summary of identified knowledge gaps

The reconstruction carried out in this chapter highlights several unresolved issues that remain central to the interpretation of the existing infrastructure. The exact geometry of the wall base zone remains uncertain, particularly with respect to the possible presence and extension of a footing-like base enlargement. The degree to which the wall geometry changes between different construction phases also remains only partially understood. Similarly, the precise structural interaction between the retaining wall and the collector system cannot be fully defined with the currently available information.

Another relevant uncertainty concerns the actual reinforcement continuity and detailing of the covered sections. Although GPR interpretation provides useful indications regarding reinforcement position and spacing, it does not allow a complete reconstruction of bar continuity, anchorage conditions, or structural connections.

These uncertainties do not invalidate the present study. On the contrary, they define its technical framework and justify the adoption of a modelling strategy based on explicitly stated assumptions, engineering interpretation, sensitivity evaluation, and careful integration of heterogeneous sources of information. This interpretation is also consistent with the caution expressed in the Geozone report, where geophysical methods are described as indirect tools that provide approximate models of reality rather than exact reconstructions [21].

Chapter 4

Finite element analysis

4.1 Introduction and objectives of the numerical analysis

The finite element analysis was carried out in order to evaluate the mechanical behaviour of the existing underpass–collector system under the adopted geometrical and geotechnical assumptions. The numerical model was developed in RS2 using the reconstructed transverse section described in the previous chapter, combined with the stratigraphic model obtained from the geological and geotechnical interpretation.

The analysis does not aim to reproduce the original construction process with absolute accuracy, since the original construction sequence and design documentation are not available. An additional uncertainty concerns the relationship between the underpass and the underlying collector. The available documentation does not clarify whether the two structures were built together or whether one was later adapted to the other. For this reason, the RS2 stages should be interpreted only as a simplified numerical sequence aimed at obtaining a plausible present-day stress state, not as a reconstruction of the real construction process.

The main objectives of the numerical analysis are:

- to evaluate the global soil–structure interaction between the underpass, the collector and the surrounding ground;
- to assess the deformation pattern induced by excavation, backfilling and operational loads;
- to identify the main zones of stress concentration and plasticization;
- to compare two possible geometrical interpretations of the buried structural system;
- to evaluate whether the presence or absence of a footing-like base enlargement significantly affects the numerical response.

Two geometrical scenarios were analysed:
Scenario 1: retaining wall with a footing-like base enlargement;
Scenario 2: retaining wall without footing-like base enlargement, with the wall and collector-side concrete elements modelled as a continuous structural body.

The comparison between these two scenarios is particularly relevant because the presence of the base enlargement cannot be confirmed directly from the available documentation. The finite element analysis was therefore used as an additional interpretative tool to assess the mechanical plausibility of the alternative reconstructed configurations.

4.2 Overview of the RS2 modelling environment

RS2 is a two-dimensional finite element software used for geotechnical and underground engineering analyses. It allows the mechanical behaviour of soil and structural elements to be evaluated under different loading conditions, excavation stages, groundwater conditions and support configurations.

In the present thesis, RS2 was used to perform a plane strain analysis of the reconstructed underpass–collector section. This assumption is consistent with the longitudinal development of the infrastructure, where the geometry can be locally represented by a representative transverse section. Nevertheless, the limitations associated with the two-dimensional simplification must be considered when interpreting the results, especially because local three-dimensional effects, longitudinal discontinuities and construction details are not explicitly represented.

The analyses were carried out using metric units, with stresses expressed in MPa. The adopted solver was Gaussian elimination, with automatic load stepping and a comprehensive convergence criterion. In the final models, the maximum number of iterations was set to 500 and the convergence tolerance to 0.001. The analyses were performed as plastic analyses for the soil domain, using the Mohr–Coulomb constitutive model.

4.3 Preparation of the geometrical model for RS2

4.3.1 Selection of the representative section

As discussed in the previous chapter, the representative section selected for the numerical analysis corresponds to the open trench portion located approximately midway between two covered intersections. This section was considered particularly significant because the retaining walls are not directly constrained by an adjacent roof slab, allowing the interaction between the wall, the surrounding ground and the collector to be evaluated in a relatively clear two-dimensional configuration.

The selected section therefore represents a suitable location for assessing the mechanical response of the open underpass configuration and for comparing the two reconstructed geometrical scenarios.

Figure 4.1. Location of the representative section selected for the RS2 numerical analysis.

4.3.2 CAD processing and DXF preparation

Before importing the geometries into RS2, the reconstructed sections were prepared in AutoCAD. This step was necessary because the geometry obtained from the combination of the structural reconstruction and the stratigraphic model contained several elements that were not directly suitable for finite element modelling.

The CAD preparation included the simplification of the sections, the removal of unnecessary or overlapping lines, and the creation of closed polylines corresponding to the main regions of the model. Particular attention was paid to the distinction between:

- **material boundaries**, used to separate different soil units or structural materials;
- **excavation boundaries**, used to delimit regions that are removed during the staged excavation sequence;
- **structural boundaries**, used to define concrete regions and contact surfaces.

Joint elements were not defined during the AutoCAD preparation phase. They were introduced later directly in RS2, where selected structural contacts were modelled as simple bearing or frictional contact surfaces rather than as monolithic connections.

The distinction between material and excavation boundaries was essential because, in RS2, a material boundary only separates two regions with different properties, whereas an excavation boundary allows the enclosed material to be deactivated at a given stage. Therefore, the geometry had to be constructed so that the future concrete regions and the excavated soil regions were both clearly defined and numerically recognizable.

The final geometries were exported from AutoCAD in DXF format and subsequently imported into RS2. After the import, the geometry was checked and locally adjusted in RS2 in order to close regions, avoid small gaps or overlapping lines, and ensure that all materials could be correctly assigned.

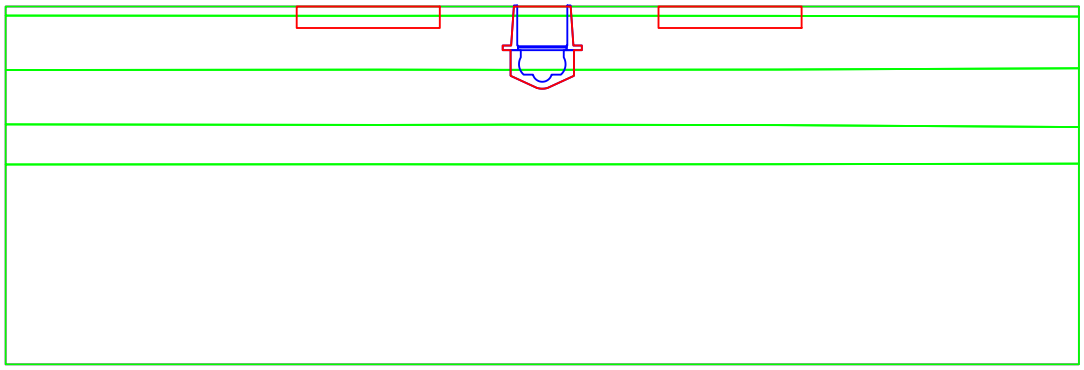

Figure 4.2. Preparation of the DXF geometry for Scenario 1, including the footing-like base enlargement.

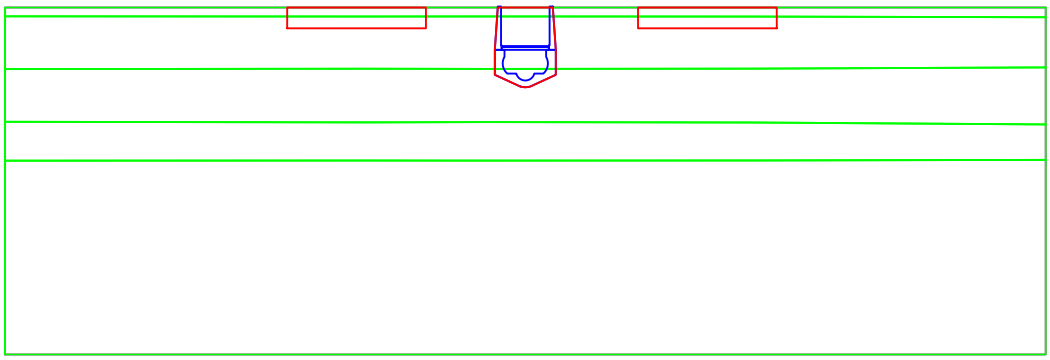

Figure 4.3. Preparation of the DXF geometry for Scenario 2, without the footing-like base enlargement.

In Figures 4.2 and 4.3, the red rectangular regions located on both sides of the underpass represent the simplified excavation volumes associated with adjacent building foundations considered in the numerical reconstruction. These regions were introduced

to reproduce, in a simplified way, the effect of nearby excavations and urban structural constraints before the application of the corresponding equivalent surcharge in the staged RS2 model.

4.4 Geometry of the numerical model

The numerical model includes the reconstructed underpass retaining walls, the lower collector and the surrounding stratified ground. The geometry was derived from the CAD reconstruction described in the previous chapter and from the local stratigraphic section extracted from the Civil 3D geotechnical model.

Two geometrical configurations were analysed. The first considers the possible presence of a footing-like base enlargement at the base of the retaining wall. The second considers a configuration without such enlargement, in which the retaining wall and the concrete elements adjacent to the collector were represented as a continuous structural body. These two cases represent the main geometrical and structural uncertainty affecting the reconstruction of the existing system.

In both cases, the external numerical domain was extended sufficiently far from the underpass in order to reduce boundary effects in the area of interest. The total model width is approximately 150 m and the model depth is approximately 50 m.

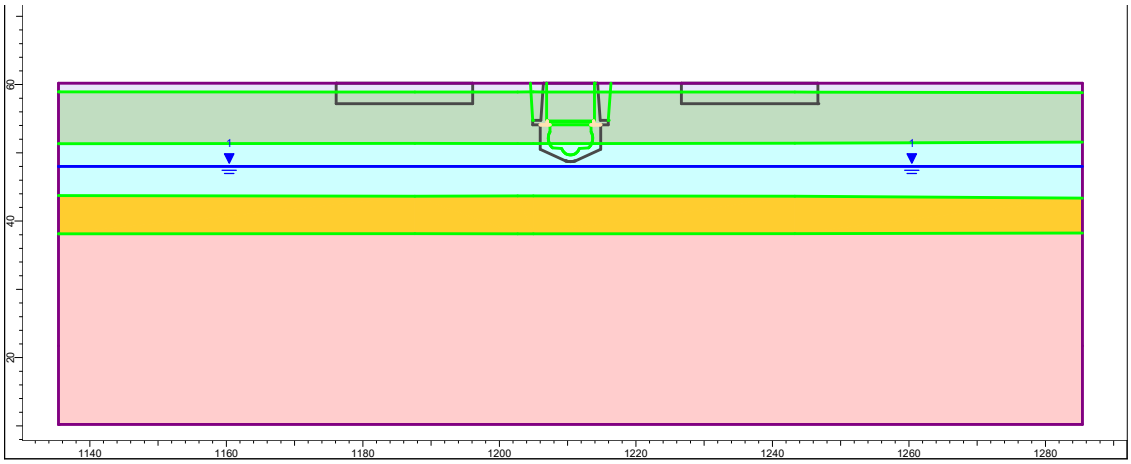

Figure 4.4. Numerical model geometry for Scenario 1, considering the presence of a footing-like base enlargement at the base of the retaining wall.

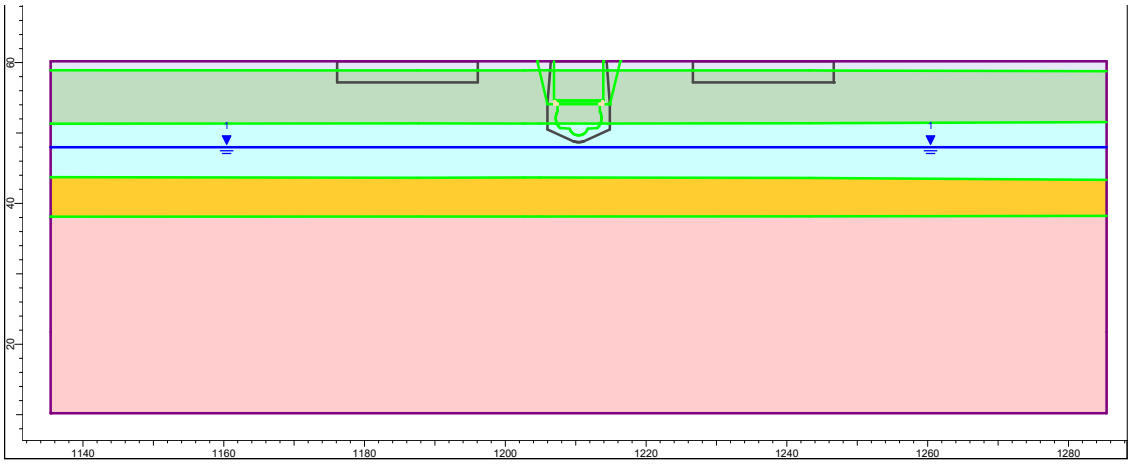

Figure 4.5. Numerical model geometry for Scenario 2, considering a continuous structural configuration without footing-like base enlargement.

4.5 Material properties

4.5.1 Soil materials

The soil materials adopted in the numerical model correspond to the representative geotechnical units defined in the geological and geotechnical framework chapter. Each layer was assigned mechanical parameters derived from the available borehole data, laboratory tests, geophysical interpretation and empirical correlations.

The soil behaviour was modelled using the Mohr–Coulomb constitutive model. This choice provides a simplified but widely adopted representation of shear strength behaviour and is appropriate for a preliminary finite element assessment of the underpass–collector system. The Mohr–Coulomb model was also considered suitable because it is commonly adopted in geotechnical modelling of Valencia soils, where the urban subsoil is mainly composed of alluvial deposits with alternating fine-grained and granular layers.

All soil materials were modelled as elastoplastic materials. The residual strength parameters were assumed equal to the peak values, consistently with an elastic-perfectly plastic interpretation and with the absence of specific post-peak laboratory data. A zero dilation angle was adopted for all soil layers in order to avoid overestimating volumetric expansion during shear.

The adopted parameters are summarised in Table 4.1. The values are expressed in the unit system used by RS2, where stresses are given in MPa.

Table 4.1. Final soil parameters adopted in the RS2 finite element analyses.

Material	γ	n	E	ν	c'	ϕ'	**Water condition**
	[MN/m^3]	**[-]**	**[MPa]**	**[-]**	**[MPa]**	**[°]**	
R	0.02000	0.30	20.00	0.30	0.0130	27	Dry
F1	0.02080	0.28	21.29	0.35	0.0130	27	Dry
G1	0.02078	0.32	146.70	0.28	0.0000	36	Piezometric line
F2	0.02090	0.29	13.405	0.28	0.0274	34	Piezometric line
G2	0.02590	0.28	225.00	0.35	0.0000	38	Piezometric line

Note: The values reported in the table correspond to the final operational parameters adopted in RS2.

The granular layers G1 and G2 were treated as essentially frictional materials, with zero effective cohesion. This choice was adopted because no direct effective cohesion data were available for these layers and because their geotechnical interpretation indicates a predominantly granular composition. Their shear strength was therefore represented mainly through the friction angle.

4.5.2 Concrete and structural materials

The concrete elements of the underpass and collector were modelled using an equivalent isotropic concrete material. The objective was to reproduce the global stiffness contribution of the existing reinforced concrete structure rather than the local cracking or nonlinear behaviour of reinforced concrete.

The adopted parameters are summarised in Table 4.2.

Table 4.2. Concrete parameters adopted in the RS2 finite element analyses.

Parameter	**Adopted value**
Unit weight, γ	0.024 MN/m^3
Young's modulus, E	25 000 MPa
Poisson's ratio, ν	0.20
Material behaviour	Elastic
Reference tensile strength	1.5 MPa
Reference cohesion	5 MPa
Reference friction angle	35°

The adopted elastic modulus and reference strength parameters were selected as cautious representative values for an old reinforced concrete structure. Since the underpass was constructed several decades ago and detailed information on concrete class, reinforcement continuity, cracking, corrosion and previous deterioration is not available, excessively high stiffness and strength values were avoided.

Although a Mohr–Coulomb strength envelope was included in the material definition, the concrete was treated as elastic in the final analyses. This choice was considered more

appropriate for the objectives of the model. The analysis aims to evaluate the global soil–structure interaction and the influence of the two geometrical scenarios, rather than to simulate the local nonlinear behaviour or failure of reinforced concrete members.

A plastic model for concrete would have required reliable information on the location of cracks, reinforcement continuity, concrete degradation, corrosion effects and local member thicknesses. Since these data are not available, assigning elastoplastic strength and residual parameters to the concrete would have introduced an apparent level of precision not supported by the investigation data. Therefore, the concrete was modelled as an equivalent elastic material, while the possible limitations of this simplification are discussed in the final part of the chapter.

The reference strength parameters adopted in RS2 correspond approximately to a tensile strength of 1.5 MPa and to an equivalent uniaxial compressive strength of about 19 MPa, obtained from the Mohr–Coulomb parameters $c = 5$ MPa and $\phi = 35°$. However, since the concrete was modelled as elastic, these values were not used to simulate local concrete failure. They are only reference material properties within the RS2 material definition.

Steel reinforcement was not explicitly modelled. Consequently, tensile stress results in the elastic concrete continuum should be interpreted only as indicators of zones where cracking or reinforcement demand may become relevant, and not as a complete reinforced concrete verification.

4.5.3 Joints and contact conditions

In Scenario 1, the retaining wall was interpreted as being simply supported on the lower structural system rather than fully monolithically connected to it. Joint elements were therefore introduced along selected contact boundaries in RS2. This modelling choice was made to represent the possibility that the upper wall and the lower concrete elements were not cast as a single continuous body, but rather behave as adjacent parts in compression contact.

The adopted joint model used a Mohr–Coulomb slip criterion with zero cohesion and zero tensile strength. In this way, the contact surfaces can transfer compression and frictional shear resistance, but they cannot transfer tensile stresses as if they were bonded.

Table 4.3. Joint parameters adopted to represent simple contact between structural elements.

Parameter	**Adopted value**
Slip criterion	Mohr–Coulomb
Normal stiffness, k_n	100 000 MPa/m
Shear stiffness, k_s	10 000 MPa/m
Tensile strength	0 MPa
Cohesion, c	0 MPa
Friction angle, ϕ	30°
Dilation	Not included
Initial deformation	Yes
Pore pressure in joint	Applied

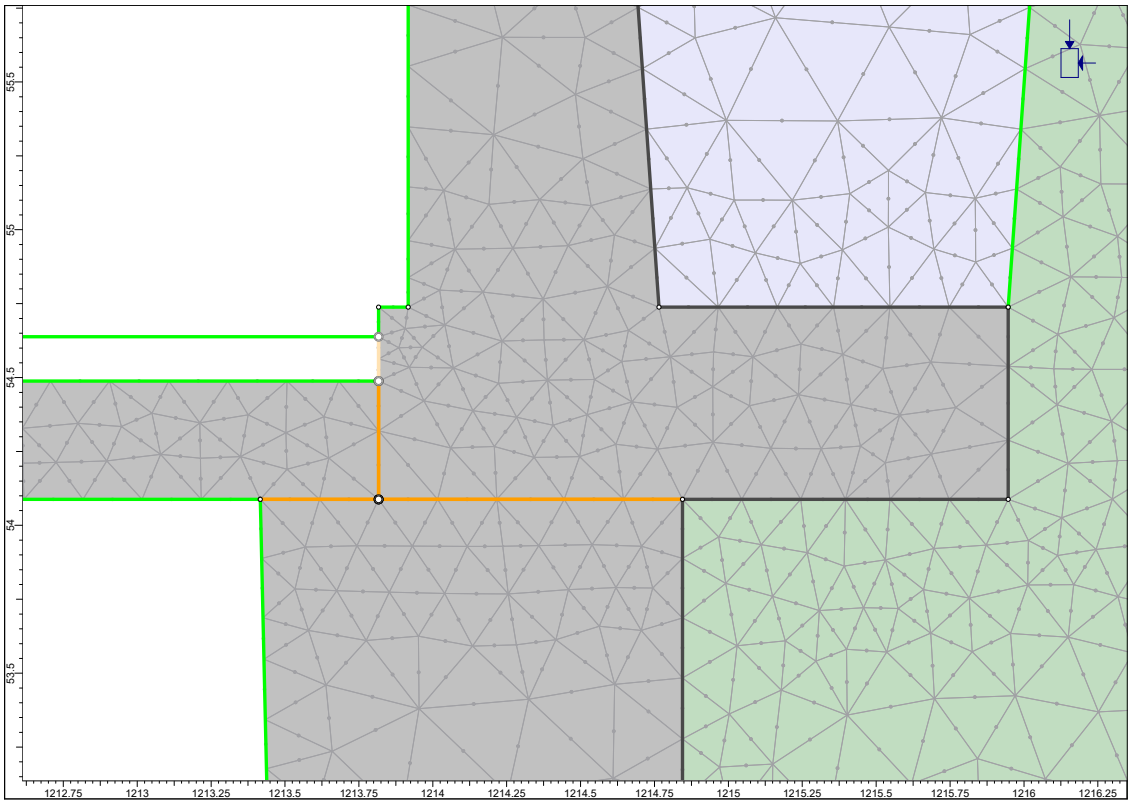

Figure 4.6. Joint elements introduced to simulate simple contact between adjacent structural components in Scenario 1.

In Scenario 2, the footing-like base enlargement was removed and the wall was modelled as connected to the collector-side concrete structure. Therefore, the structural system was represented in a more continuous way. This difference must be considered when comparing the two scenarios, as it affects both the structural load transfer mechanism and the local stress redistribution.

4.6 Boundary conditions and initial stress state

The external boundaries of the numerical model were defined in order to reduce boundary effects in the area of interest. The lateral boundaries were restrained in the horizontal direction, while the bottom boundary was restrained in the vertical direction. The ground surface was left free. The corner nodes of the external boundary were restrained in both directions in order to ensure global stability of the model.

The initial stress state was generated through gravity loading using the actual ground surface. The coefficient of earth pressure at rest was set equal to:

$$K_0 = 0.60 \tag{4.1}$$

for both the in-plane and out-of-plane effective stress ratios.

This value was selected starting from the K_0 values previously estimated in the geotechnical characterisation chapter. As discussed there, the values obtained from empirical correlations are affected by uncertainty because the investigated ground includes anthropogenic fill, natural alluvial deposits and soils located close to existing retaining structures. The adopted value is slightly higher than some of the preliminary estimates, and was therefore considered a cautious representative value while remaining within the same order of magnitude.

Groundwater was modelled through a static groundwater analysis. The phreatic surface intersects the G1 layer and is located below the main structural system. For this reason, groundwater does not play a dominant role in the global response of the underpass in the analysed section. The upper materials R and F1 were treated as dry, while the deeper materials G1, F2 and G2 were associated with the piezometric line.

The groundwater level in the surrounding soil and the water level inside the collector were treated as two distinct hydraulic conditions. The former defines the pore pressure regime in the ground, while the latter was introduced only as a distributed hydrostatic load acting on the internal wetted boundary of the collector. The water inside the collector was therefore not modelled as seepage through the ground or through the concrete structure.

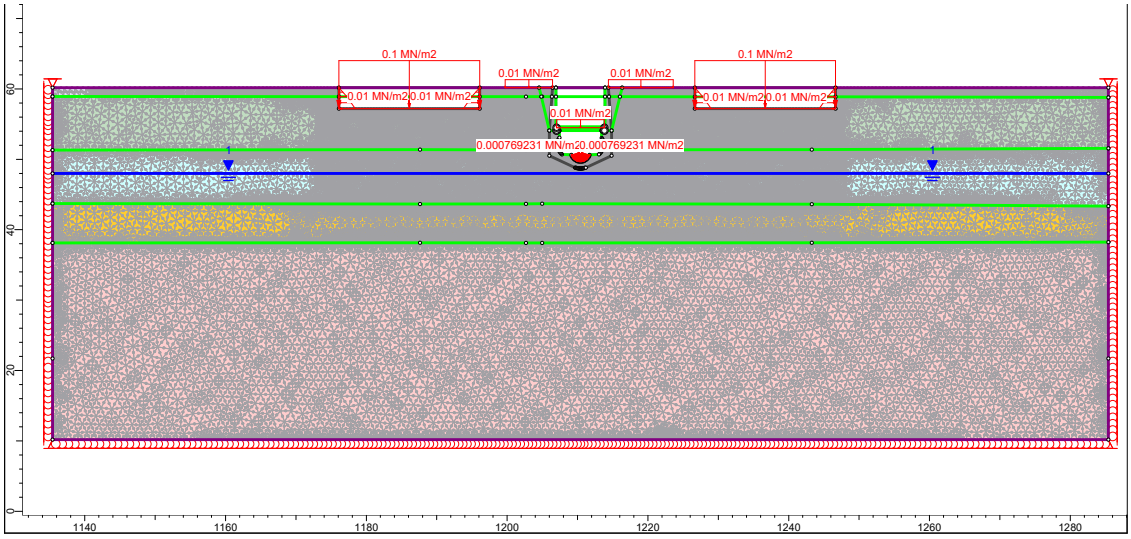

Figure 4.7. Boundary conditions, groundwater level and main loading scheme adopted in the RS2 model.

4.7 Construction stages and loading sequence

4.7.1 General approach

The numerical analysis was carried out through staged construction. Since the real historical construction sequence is unknown, the adopted staging should be interpreted as an engineering reconstruction rather than as a documented as-built construction process.

The purpose of the staged modelling was not to reproduce every construction phase

exactly, but to reach a mechanically plausible current stress state after excavation, concrete installation, backfilling and operational loading. For this reason, temporary support pressures were applied during excavation stages to represent the stabilising effect of construction support systems that were not explicitly modelled.

This point is important because the actual underpass has existed for many years and the main objective of the analysis is to evaluate the present condition, not the short-term unsupported stability of an excavation during construction.

4.7.2 Main stages

The main stages adopted in the model are summarised in Table 4.4.

Table 4.4. Main interpreted construction stages adopted in the RS2 analysis.

Stage	Description
1	Initial stress state
2	Adjacent buildings excavation
3	Application of equivalent adjacent urban surcharge
4	Main excavation of the underpass
5	Excavation of the collector
6	Installation of concrete structural elements
7	Backfilling
8	Application of upper traffic load and hydraulic loading in the collector
9	Application of internal traffic load / final operational condition

4.7.3 Equivalent temporary support pressures

During the excavation stages, equivalent distributed pressures were applied along selected excavation boundaries. These pressures were introduced to represent the stabilising effect of temporary support systems, such as excavation bracing, retaining elements or other construction measures that would have prevented the soil from freely deforming into the excavation.

The values were estimated using a simplified earth pressure approach:

$$\sigma_h = K\gamma z \tag{4.2}$$

where K is a representative earth pressure coefficient, γ is the soil unit weight and z is the depth measured from the relevant excavation level.

For the upper excavation, the maximum equivalent support pressure was of the order of:

$$q_{\max} \approx 0.07 \text{ MN/m}^2 \tag{4.3}$$

For the lower collector excavation, the equivalent pressure was generally in the range:

$$q \approx 0.03 - 0.04 \text{ MN/m}^2 \tag{4.4}$$

depending on the local depth and geometry.

These pressures should not be interpreted as exact in situ earth pressures acting on the final structure. They are numerical support pressures introduced to simulate temporary construction support and to avoid an unrealistic unsupported excavation condition.

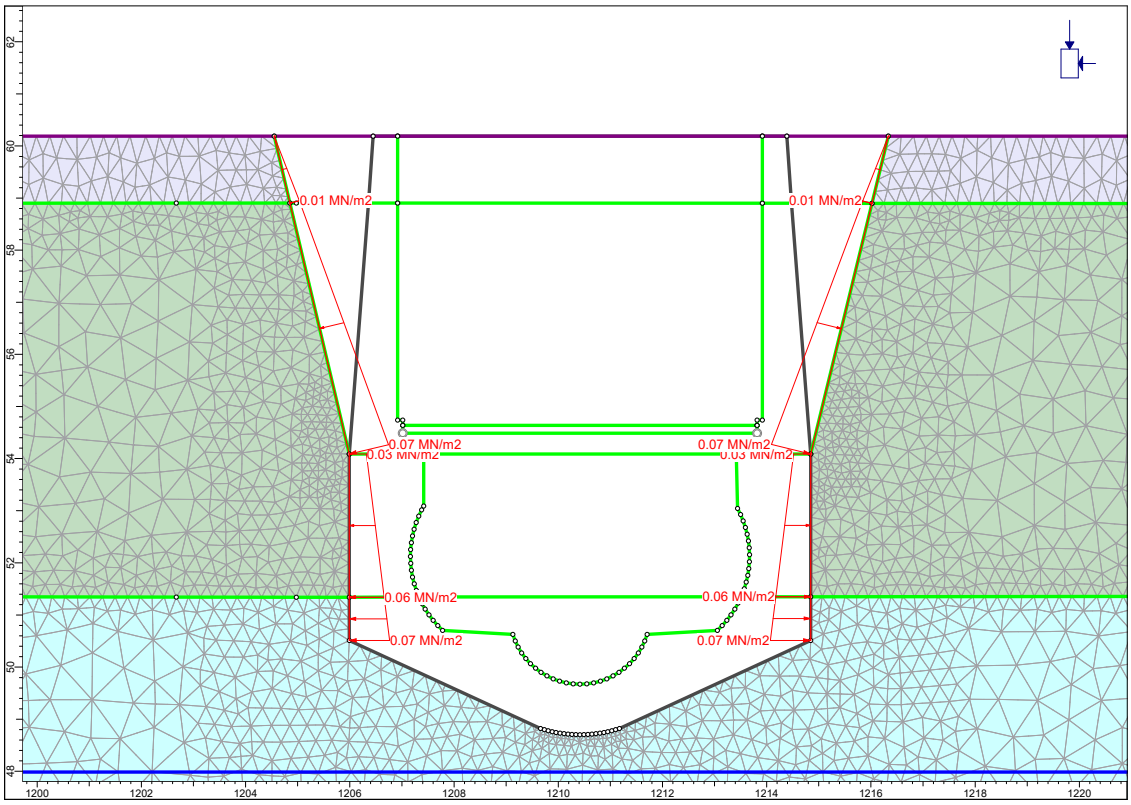

Figure 4.8. Equivalent temporary support pressures applied along the excavation boundaries during the staged analysis.

4.7.4 Hydrostatic pressure inside the collector

In addition to groundwater in the surrounding soil, internal water pressure was applied in the lower curved portion of the collector. This was introduced to simulate the presence of water inside the collector during the operational condition.

The water pressure was modelled as a hydrostatic pressure acting normal to the wetted internal boundary. Assuming approximately 1 m of water height, the maximum pressure was approximated as:

$$p_{\max} \approx 0.01 \text{ MN/m}^2 \tag{4.5}$$

The pressure distribution was applied as an increasing pressure with depth along the wetted curved surface.

4.8 Mesh generation and numerical settings

The finite element mesh was generated using a graded mesh with 6-noded triangular elements. Mesh refinement was concentrated around the underpass walls, the lower collector, the excavation boundaries and the contact zones where higher stress and displacement gradients were expected.

For Scenario 1, the final stages contained 23 242 elements and 47 286 nodes. For Scenario 2, the final stages contained 25 635 elements and 52 197 nodes. The slightly higher number of elements and nodes in Scenario 2 is related to the different geometry and to the absence of the footing-like base enlargement, which required a local discretization able to capture the geometry and stress gradients around the collector. In both models, the RS2 mesh quality report indicated that all elements were of good quality.

The two meshes can therefore be considered comparable for the purpose of this engineering-level assessment. The comparison between the scenarios is interpreted mainly in terms of global response, deformation pattern and order of magnitude.

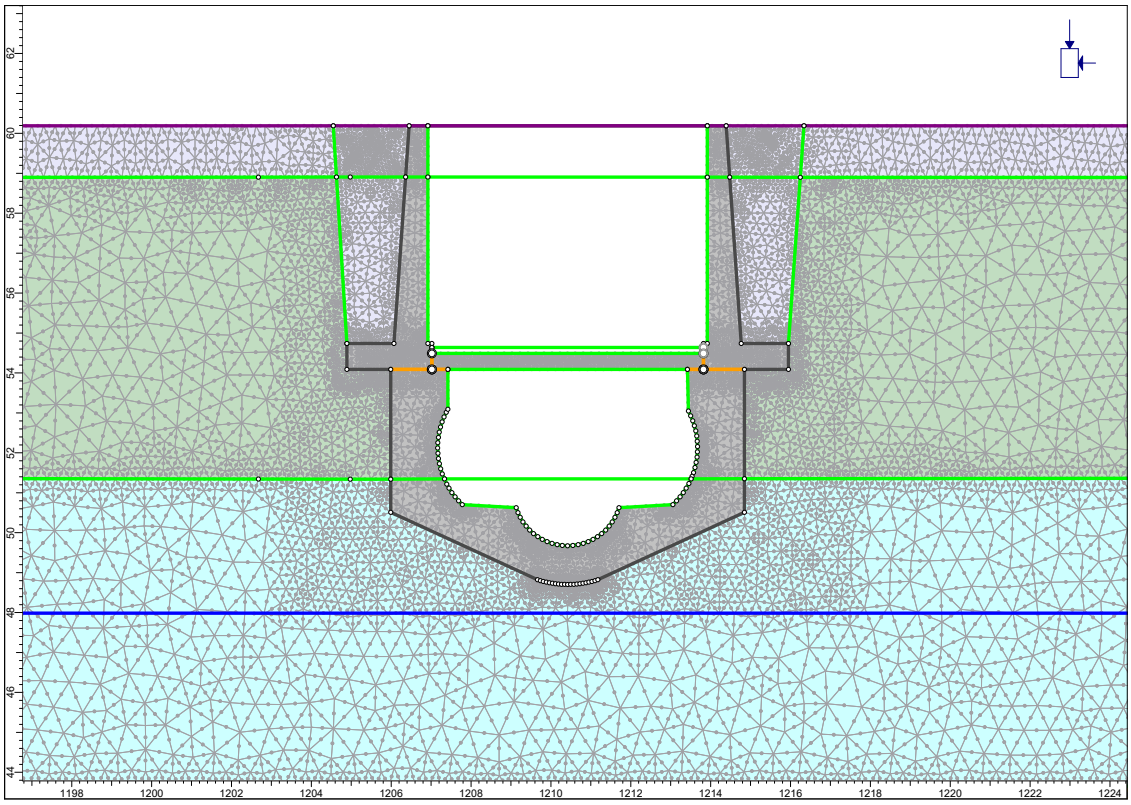

Figure 4.9. Finite element mesh adopted for Scenario 1, showing local refinement around the underpass and collector.

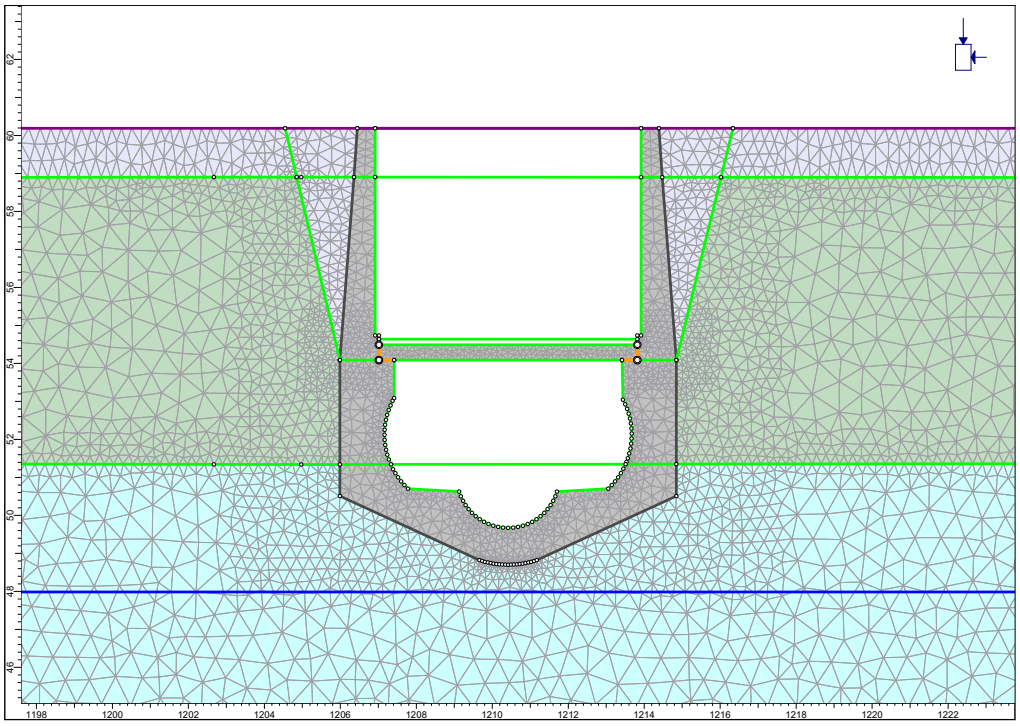

Figure 4.10. Finite element mesh adopted for Scenario 2, showing the refined discretization around the collector and excavation boundaries.

4.9 Analysis cases

4.9.1 Scenario 1: wall with footing-like base enlargement

Scenario 1 considers the presence of a footing-like base enlargement at the base of the retaining wall. This configuration represents the hypothesis that the wall includes a local base element extending laterally, which contributes to distributing the load and stabilising the excavation around the collector.

In this scenario, the wall was interpreted as resting on the lower structural system through contact surfaces rather than being fully monolithically connected. This configuration was considered mechanically plausible because a local base enlargement could modify the load transfer mechanism between the wall, the collector and the surrounding soil. However, its actual effect on the global response must be evaluated through the comparison with the alternative scenario, since the numerical results do not allow this geometry to be considered automatically more favourable.

4.9.2 Scenario 2: wall without footing-like base enlargement

Scenario 2 considers a retaining wall without a footing-like base enlargement. In this case, the structural system is represented by a more direct vertical configuration, without

the lateral widening at the wall base. Differently from Scenario 1, the wall and the collector-side concrete elements were modelled as a continuous structural body.

The comparison between the two scenarios must therefore be interpreted carefully. It reflects not only the geometrical difference between the two reconstructed configurations, but also the different structural contact assumptions adopted in the two models.

4.10 Results of Scenario 1: wall with footing-like base enlargement

The final results of Scenario 1 show a generally plausible deformation pattern. The largest displacements are mainly vertical and are concentrated around the underpass–collector system. The plastic zones remain localised near the lower structural discontinuities and around the collector.

The maximum values obtained in the final operational stage are summarised in Table 4.5.

Table 4.5. Main results obtained for Scenario 1 in the final operational stage.

Quantity	**Maximum value**
Absolute horizontal displacement	3.53×10^{-3} m
Absolute vertical displacement	9.97×10^{-3} m
Total displacement	1.03×10^{-2} m
Maximum shear strain	5.30×10^{-3}
Maximum shear plastic strain	5.83×10^{-3}
Maximum σ_1	3.67 MPa
Minimum σ_3	-4.14 MPa

The total displacement in the final operational condition is therefore approximately 1 cm. The maximum shear plastic strain remains localised and does not indicate the development of a global failure mechanism.

The stress results show local concentrations near the sharp corners of the footing-like enlargement, at the contact surfaces and close to the collector. These concentrations are expected in finite element models where abrupt geometrical changes and stiffness contrasts are present. Some local tensile stress peaks exceed the reference tensile strength of the concrete, but they remain concentrated near corners and contact zones.

For the purpose of the present study, the response of Scenario 1 is therefore considered acceptable at the global scale. The model does not indicate a generalised instability mechanism, and the stress peaks are interpreted as local effects associated with geometry, contact and modelling assumptions.

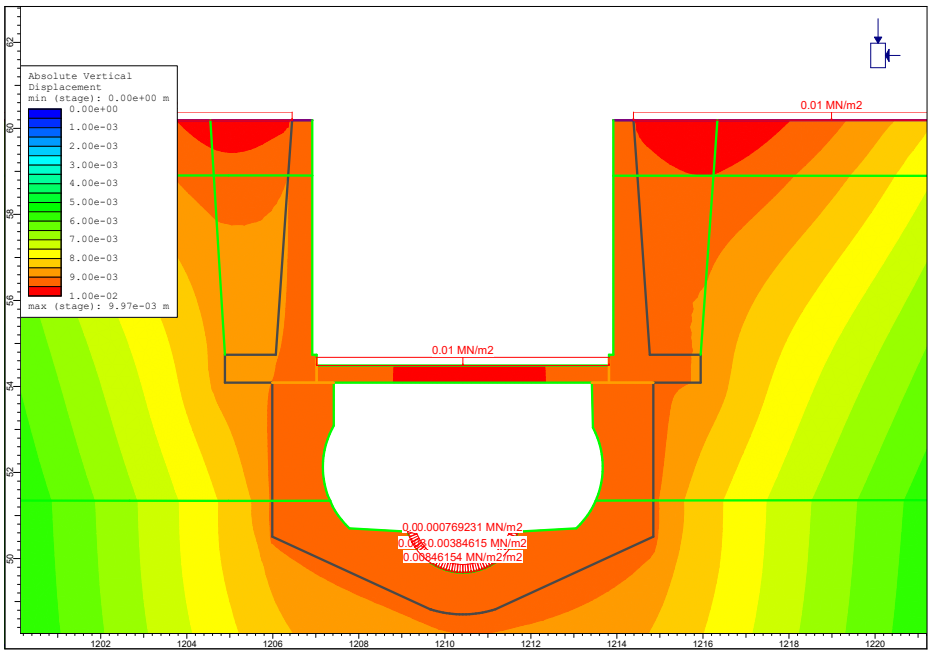

Figure 4.11. Absolute vertical displacement contours in the final operational stage of Scenario 1.

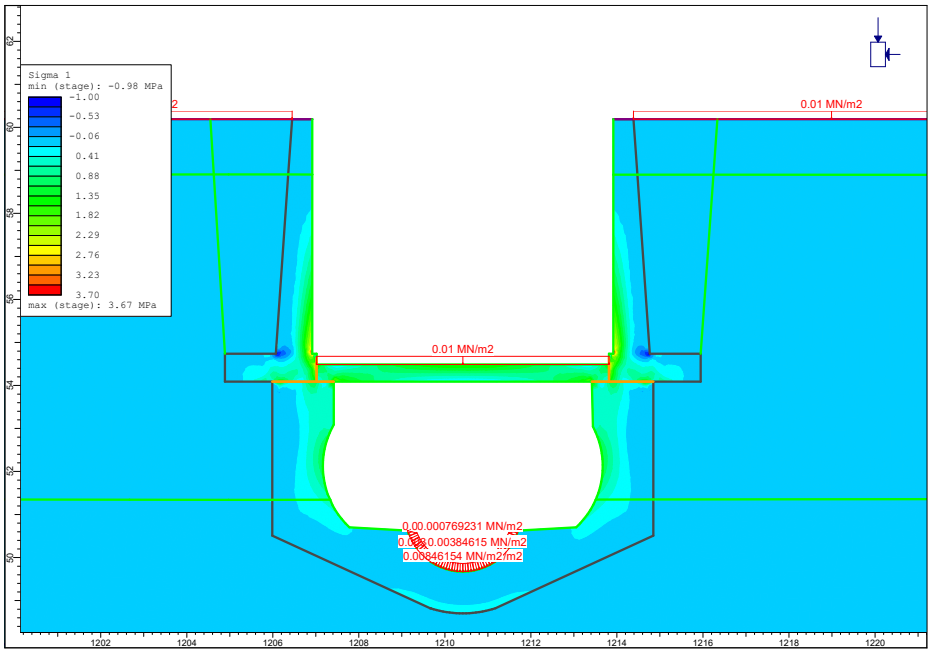

Figure 4.12. Major principal stress, σ_1, contours in the final operational stage of Scenario 1.

4.11 Results of Scenario 2: wall without footing-like base enlargement

The model without footing-like base enlargement reached convergence for the full staged analysis. The final deformation pattern is similar in terms of global shape, but the magnitude and localization of the results differ from Scenario 1.

The maximum values obtained in the final operational stage are summarised in Table 4.6.

Table 4.6. Main results obtained for Scenario 2 in the final operational stage.

Quantity	**Maximum value**
Absolute horizontal displacement	3.09×10^{-3} m
Absolute vertical displacement	7.46×10^{-3} m
Total displacement	7.66×10^{-3} m
Maximum shear plastic strain	6.46×10^{-3}
Maximum σ_1	3.47 MPa
Minimum σ_3	−2.05 MPa

The maximum displacement values are lower than those obtained in Scenario 1. However, the maximum shear plastic strain is slightly higher, indicating a more localised plastic response around the lower excavation zones.

The principal stress results show negative values of σ_3 in both scenarios, mainly in correspondence with geometrical discontinuities, stiffness contrasts and contact regions of the structural system. In Scenario 2, the minimum value of σ_3 is lower in absolute value than in Scenario 1, while the overall contour pattern remains broadly comparable to that obtained in the model with footing-like base enlargement.

Therefore, the absence of the footing-like base enlargement does not appear to produce a clearly more critical tensile stress condition at the scale of the global model. The differences between the two scenarios should rather be interpreted as local variations in stress redistribution caused by the different geometry and contact assumptions adopted in the models.

As for Scenario 1, the negative σ_3 zones should be interpreted mainly as indicators of possible local cracking or reinforcement demand, without invalidating the global soil–structure interaction assessment.

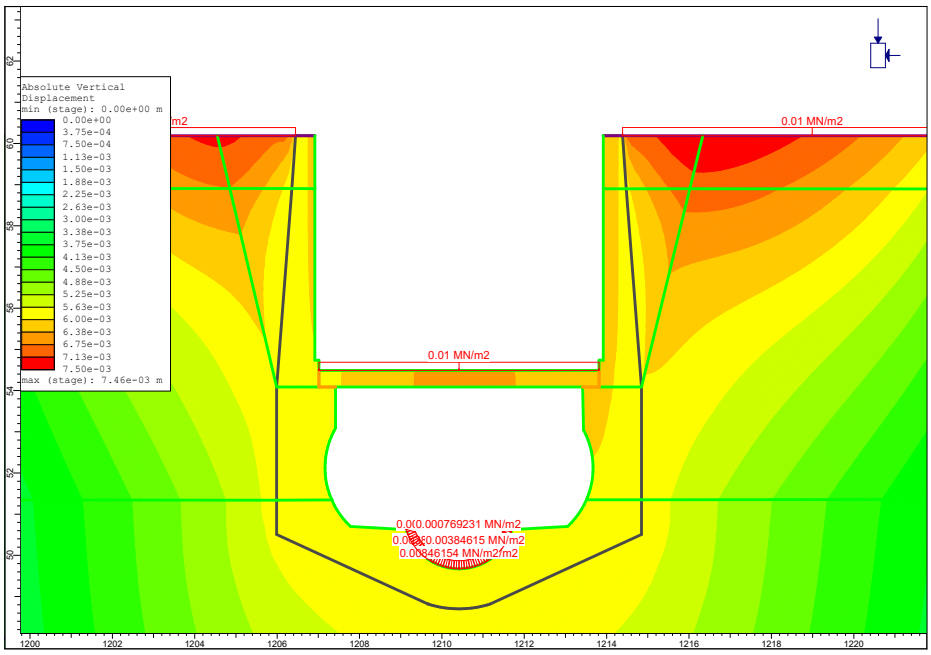

Figure 4.13. Absolute vertical displacement contours in the final operational stage of Scenario 2.

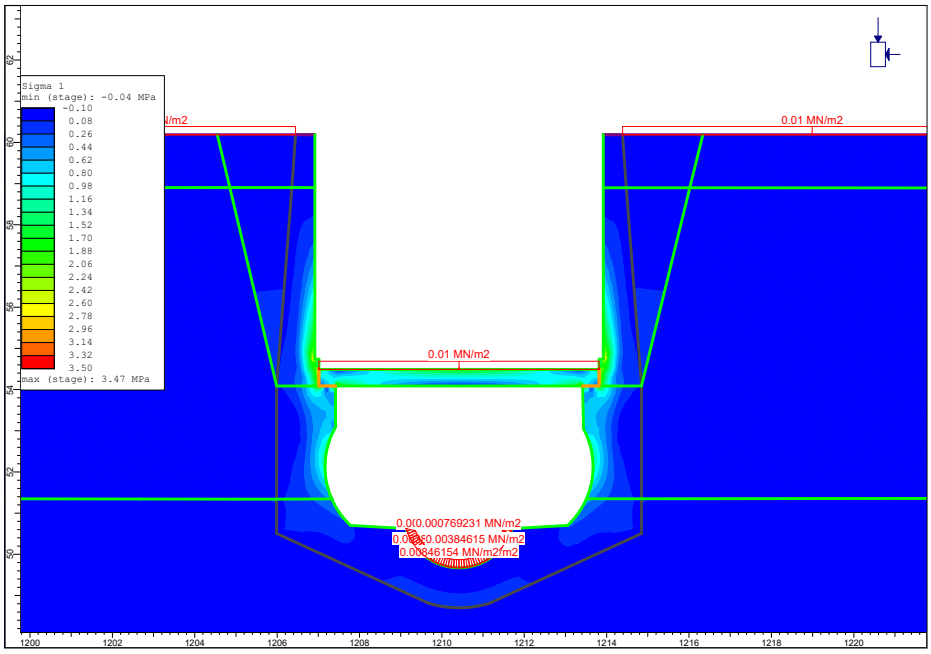

Figure 4.14. Major principal stress, σ_1, contours in the final operational stage of Scenario 2.

4.12 Comparison and interpretation of the analysed scenarios

The comparison between the two analysed scenarios is summarised in Table 4.7. The results show that both models reach a stable numerical solution and that the computed displacements remain within the same order of magnitude. However, the two configurations present different deformation and stress redistribution patterns.

Table 4.7. Comparison between the final operational results of Scenario 1 and Scenario 2.

Quantity	**Scen. 1**	**Scen. 2**	**Interpretation**
Absolute horizontal displacement	3.53×10^{-3} m	3.09×10^{-3} m	Similar order of magnitude
Absolute vertical displacement	9.97×10^{-3} m	7.46×10^{-3} m	Higher in Scen. 1
Total displacement	1.03×10^{-2} m	7.66×10^{-3} m	Higher in Scen. 1
Maximum shear plastic strain	5.83×10^{-3}	6.46×10^{-3}	Slightly higher in Scen. 2
Maximum σ_1	3.67 MPa	3.47 MPa	Similar compressive stress level
Minimum σ_3	-4.14 MPa	-2.05 MPa	Higher numerical tensile peak in Scen. 1; no clear global worsening in Scen. 2
Final mesh elements	23 242	25 635	Comparable mesh density

Scenario 1, which includes the footing-like base enlargement, produces slightly larger total and vertical displacements. This is consistent with the final displacement contours, where the deformation field around the lower structural system appears somewhat more pronounced in the model with footing-like enlargement. The presence of the base element therefore does not reduce the maximum displacement in the adopted model; rather, it modifies the way deformation is redistributed around the wall base and the collector.

Scenario 2, without footing-like base enlargement, produces lower maximum displacements but a slightly higher maximum shear plastic strain. This indicates that the absence of the base enlargement affects the local plastic response of the soil around the lower structural and excavation zones, although the overall deformation pattern remains of the same order of magnitude as Scenario 1.

The principal stress contours also suggest that the two scenarios are more similar than initially assumed. In RS2, σ_1 and σ_3 represent the major and minor principal stresses,

respectively. Negative values of σ_3 indicate local tensile stress states. The minimum numerical value of σ_3 is more severe in Scenario 1, where it reaches approximately -4.14 MPa, while Scenario 2 reaches approximately -2.05 MPa. The contour comparison does not indicate a clear worsening of the tensile stress distribution in the model without footing-like enlargement.

These tensile stress zones do not by themselves demonstrate a global instability mechanism. Since the concrete was modelled as an equivalent elastic continuum, the negative σ_3 values mainly identify areas where more detailed reinforced concrete checks should be concentrated.

From an engineering point of view, both scenarios remain mechanically plausible within the adopted modelling assumptions. The footing-like enlargement cannot be considered clearly beneficial or clearly detrimental based only on the present numerical comparison. It produces slightly higher displacements and higher local tensile peaks, while the model without footing-like enlargement remains globally stable and shows a comparable stress pattern. Therefore, the comparison should be interpreted as a sensitivity analysis on geometric uncertainty rather than as evidence that one configuration is structurally safer than the other.

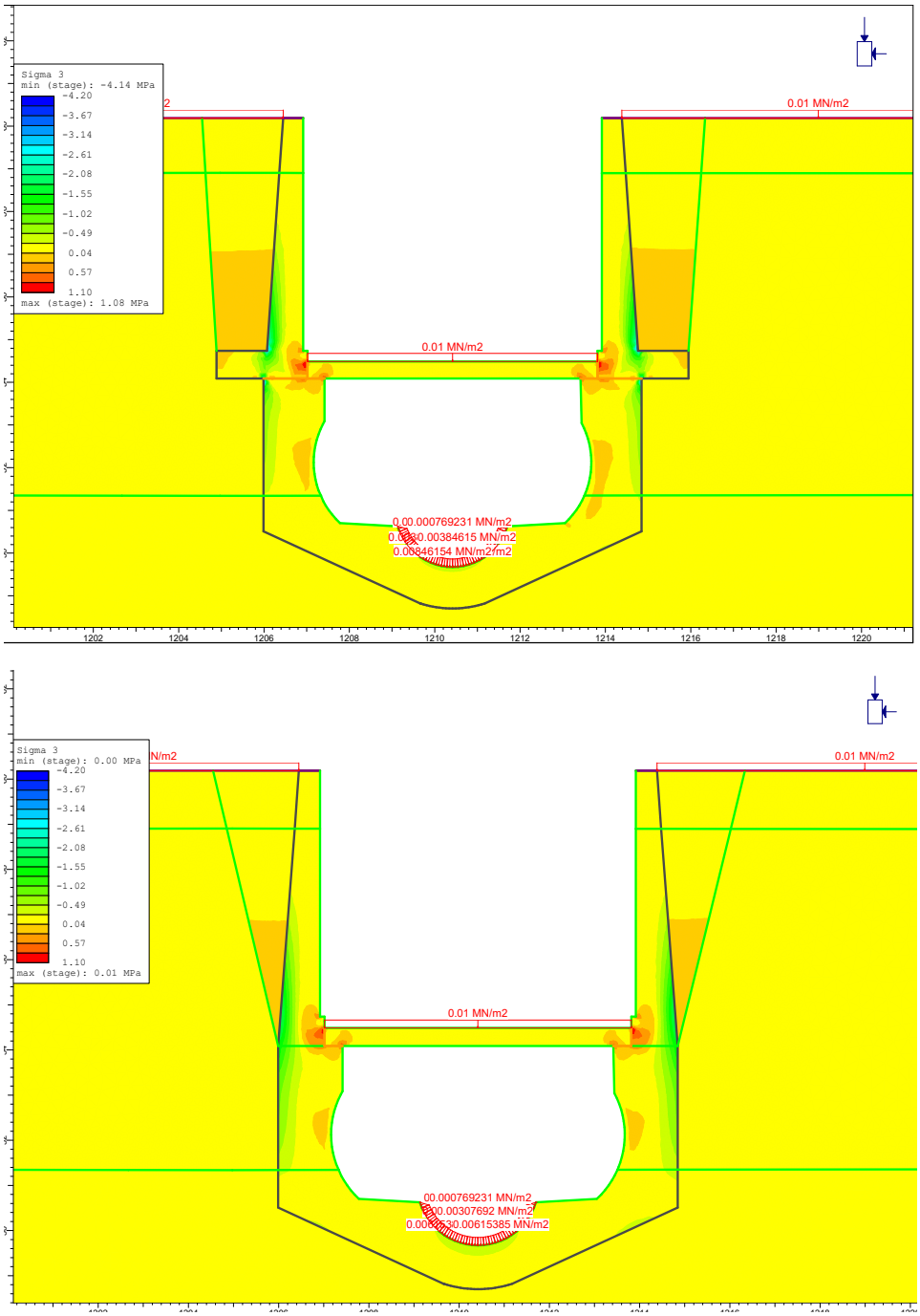

Figure 4.15. Comparison of minor principal stress σ_3 contours in the final operational stage. The same colour scale was adopted for both scenarios in order to improve the visual comparison. The results show that the tensile stress distribution is broadly comparable in the two scenarios, while the highest local tensile peak is obtained in Scenario 1.

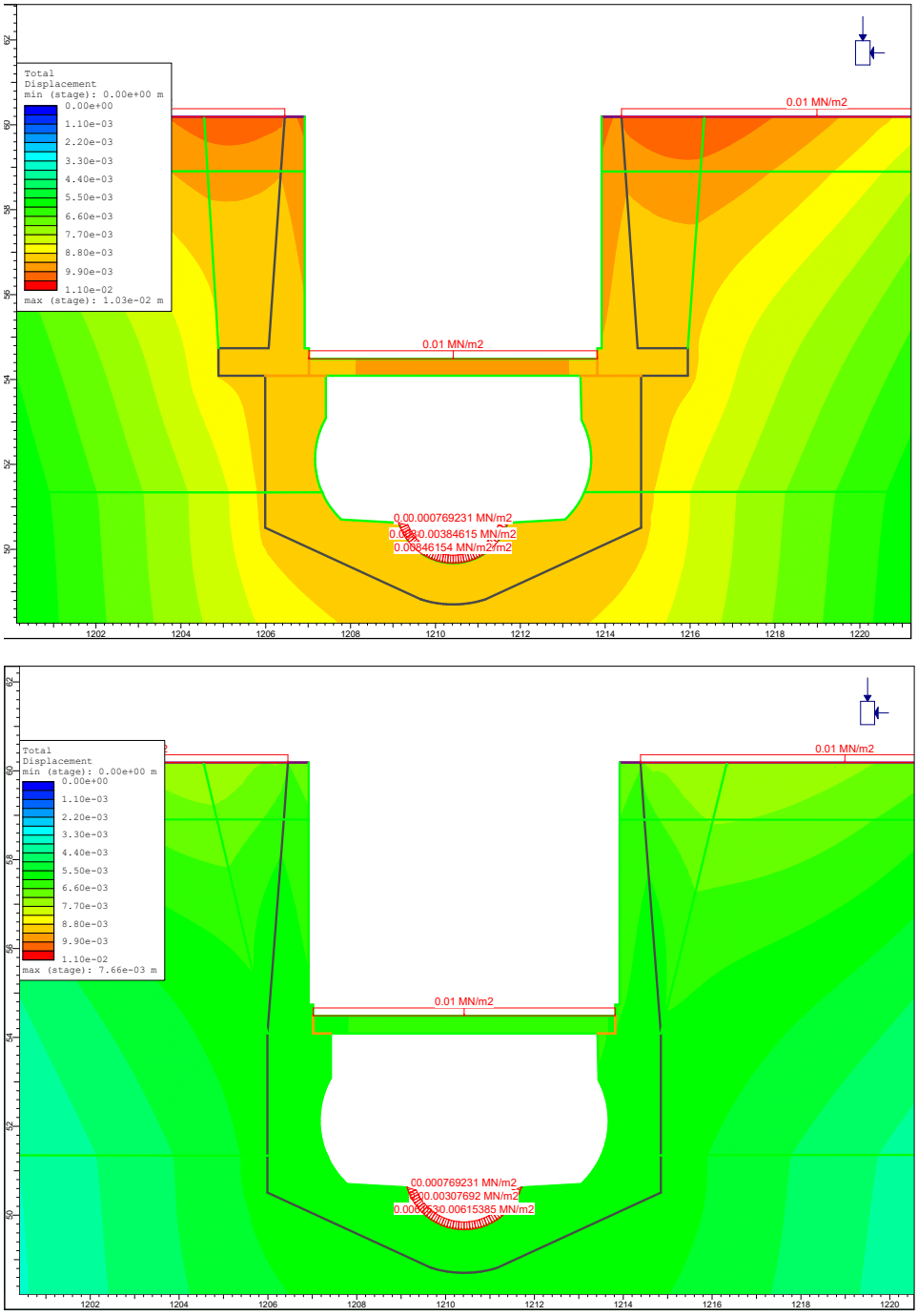

Figure 4.16. Comparison of total displacement contours in the final operational stage. The same colour scale was adopted for both scenarios in order to improve the visual comparison. Scenario 1 shows slightly higher maximum total displacement, while both scenarios remain within the same order of magnitude.

4.13 Limitations of the numerical model

Several limitations must be considered when interpreting the numerical results.

First, the model is two-dimensional and based on a plane strain assumption. This is appropriate for a representative transverse section, but it cannot reproduce longitudinal discontinuities, local three-dimensional effects or variations along the alignment.

Second, the geometry of the buried structural elements is uncertain. In particular, the presence and extension of the footing-like base enlargement are interpretative assumptions based on indirect information.

Third, the construction sequence is not known. The staged analysis therefore represents an engineering reconstruction rather than a documented construction process. Its main role is to obtain a plausible present-day stress state and to compare the two geometrical hypotheses.

Fourth, the soil behaviour was represented using the Mohr–Coulomb model. This provides a reasonable first-order approximation, but it does not account for stress-dependent stiffness, strain softening or advanced nonlinear soil behaviour.

Fifth, the concrete structure was modelled as an equivalent elastic material. This approach is suitable for global soil–structure interaction analysis, but it does not reproduce cracking, reinforcement corrosion or local deterioration of the concrete. The steel reinforcement identified through GPR interpretation was not explicitly modelled. This simplification is conservative with respect to tensile behaviour, but it prevents the analysis from being used as a direct reinforced concrete verification.

Finally, temporary excavation support was represented through equivalent distributed pressures. These loads should be interpreted as modelling assumptions introduced to represent construction support effects that are not explicitly included in the model, rather than as exact measured earth pressures.

4.14 Summary of the finite element analysis

The finite element analysis was developed in RS2 to assess the mechanical response of the reconstructed underpass–collector system. Two geometrical scenarios were considered: one including a possible footing-like base enlargement and one without such enlargement.

Both models reached numerical stability and the computed displacements remained limited when compared with the overall dimensions of the structure. This suggests that, under the adopted assumptions, the underpass–collector system does not exhibit a relevant global deformation or collapse mechanism.

Both geometrical scenarios reached numerical stability and produced responses of the same order of magnitude. Scenario 1 resulted in slightly higher total and vertical displacements, as well as a higher local tensile peak in terms of minimum σ_3. Scenario 2 produced lower displacements but a slightly higher maximum shear plastic strain in soil. Overall, the comparison does not indicate a clearly more critical behaviour of the model without footing-like enlargement; rather, it shows that the main geometric uncertainty modifies the local redistribution of stresses and plastic strains without changing the global stability assessment.

The stress contours showed local tensile and compressive concentrations near corners, joints and contact zones. These results should be interpreted as indicators of potentially critical local areas rather than as direct evidence of structural failure. Since the concrete was modelled as an equivalent elastic material and the reinforcement was not explicitly represented, a detailed reinforced concrete verification would be required to assess cracking, reinforcement demand and degradation effects.

Overall, the finite element results provide a coherent interpretation of the global soil–structure interaction of the underpass–collector system. They do not indicate an immediate global instability of the current configuration, but they highlight the importance of local structural checks and of a careful interpretation of the main geometric uncertainties.

Chapter 5

Evaluation of intervention alternatives

5.1 Introduction

The previous chapters showed that the Pérez Galdós underpass is an ageing urban infrastructure affected by geometric, material and structural uncertainties. At the same time, the finite element analyses suggest that, within the assumptions of the adopted model, the underpass–collector system does not exhibit a global instability mechanism under the analysed operational conditions.

The purpose of this chapter is therefore to compare possible intervention strategies at a preliminary level. The aim is not to define a final design solution, but to evaluate how different choices could affect the existing soil–structure–collector system and the future role of the underpass within the urban transformation of Avenida Pérez Galdós.

Four main alternatives are considered:

- **Alternative 0**: preservation of the existing underpass in service;
- **Alternative 1**: structural rehabilitation or replacement of the deteriorated floor beam system;
- **Alternative 2**: closure and controlled backfilling of the underpass;
- **Alternative 3**: adaptive reuse of the abandoned underpass as an underground functional volume.

These alternatives are not necessarily mutually exclusive. Inspection and monitoring remain common requirements in all cases, either during continued operation, during temporary construction phases, or after any major intervention. This is especially relevant because the surface regeneration works currently being carried out along Avenida Pérez Galdós may affect the mechanical and service conditions of the underlying structure.

A fundamental aspect common to all alternatives is the strategic role of the underpass within the mobility system of Valencia. The corridor historically carried traffic volumes of the order of 50,000 vehicles per day, and its sudden closure could generate significant

disruption, especially during the ongoing surface regeneration works. Therefore, any intervention should be evaluated not only from a structural point of view, but also considering traffic management, construction phasing and urban resilience.

5.2 Common requirement: inspection and monitoring

Inspection and monitoring should be considered as a common requirement for all the intervention scenarios discussed in this chapter. This need is justified by the age of the reinforced concrete structure, the absence of original design documentation, the deterioration reported during previous inspections [20], and the presence of surface works that may modify loads, drainage paths, vibrations and accessibility conditions around the underpass.

A complete monitoring plan is outside the scope of this thesis. Nevertheless, a reasonable strategy should combine periodic visual inspections, photographic documentation, topographic control points on the retaining walls and surface pavement, crack gauges or displacement targets in selected critical zones, and more advanced sensors only where continuous strain or displacement monitoring is justified by the risk level.

The monitoring system should be associated with threshold values and response actions. These thresholds should consider both absolute values and rates of change over time. A slow and stable displacement trend may be acceptable, whereas sudden changes in wall convergence, crack opening or vertical displacement should trigger additional inspection, traffic restrictions or temporary structural measures. In this sense, monitoring would not replace structural verification, but would provide measured evidence to support the management of an existing structure affected by incomplete information.

5.3 Common light urban interventions

Some minor interventions could be considered independently of the structural alternative selected. These measures would not solve the main structural uncertainties of the underpass, but they could reduce some of the urban impacts associated with its current configuration. Two possible light interventions are considered here: the installation of acoustic barriers and the partial covering of selected open trench sections.

5.3.1 Noise barriers

Avenida Pérez Galdós has long been perceived by local residents as a problematic corridor in terms of traffic noise. This perception is consistent with the broader acoustic diagnosis of Valencia. The 2022 Strategic Noise Map of Valencia includes road traffic-generated noise as one of the main sources to be represented [33]. It classifies traffic noise using Lden ranges up to 75 dBA and higher [34].

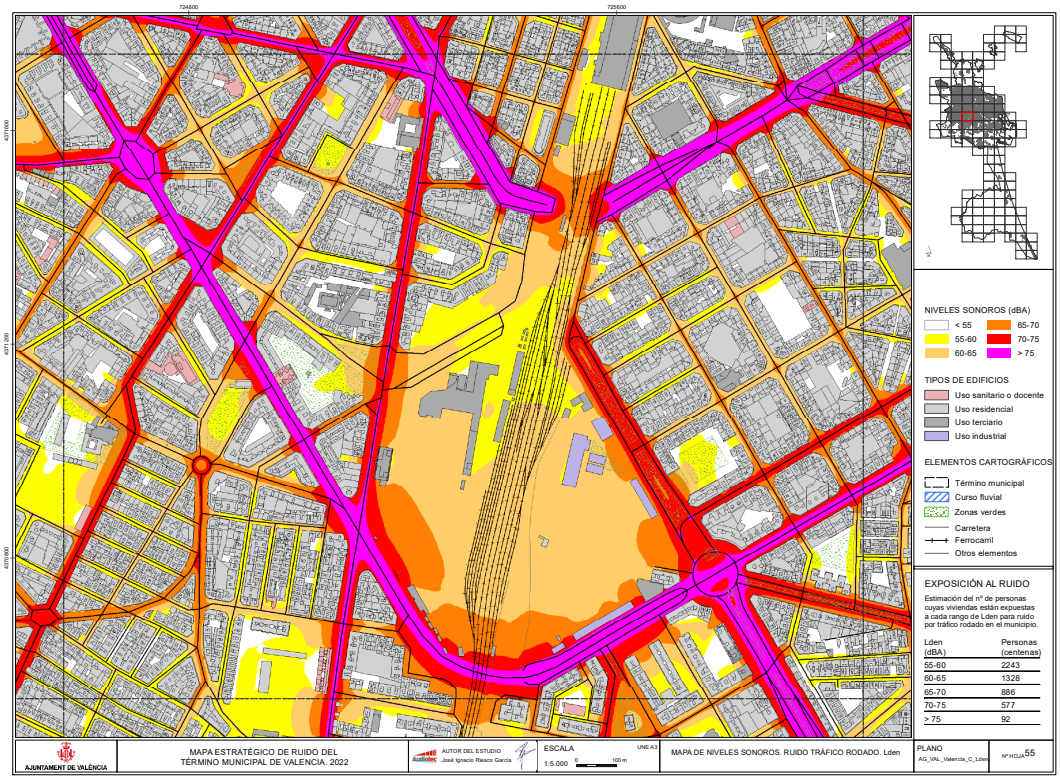

Figure 5.1. Extract of the 2022 Strategic Noise Map of Valencia for road traffic noise, highlighting the acoustic exposure of the Pérez Galdós–Giorgeta corridor.

In the case of the underpass, the acoustic problem is not only related to traffic volume. The geometry of the open trench can favour the propagation and reflection of traffic noise, while the absence of traffic lights along a relatively long section may encourage higher speeds than those observed on surface streets. Above approximately 30 km/h, tyre–road noise generally becomes increasingly important compared with engine noise, especially for light vehicles. Therefore, speed control and pavement characteristics can significantly influence the emitted noise level as shown by Sandberg and Ejsmont [35].

Noise barriers could be considered along the underpass walls or along the upper edges of the trench. In practical applications, road traffic noise barriers can provide reductions of several decibels when properly designed. The CEDR report by Bendtsen et al. [36] indicates average real-world reductions commonly of the order of 5–10 dB, depending on the configuration. For the Pérez Galdós underpass, absorbent panels could be more appropriate than purely reflective barriers, because reflective surfaces may contribute to repeated sound reflections within the trench.

5.3.2 Partial covering of open trench sections

A second possible light intervention is the partial covering of selected open trench sections. The underpass currently acts as a physical barrier between the two sides of the avenue,

limiting pedestrian crossings over long stretches. A partial covering would not necessarily imply complete closure or backfilling, but could consist of localized structural decks or pedestrian platforms placed above selected open sections.

Such a solution could improve transversal connectivity, provide additional surface space and contribute to reducing the propagation of traffic noise from the trench. Depending on the size and location of the covering elements, the surface space could be partially reconceived through pedestrian areas, cycling connections or small green areas.

However, this intervention would require careful structural verification. Any new deck or covering element would introduce additional loads on the retaining walls or on independent foundations. It would also modify ventilation, lighting and emergency accessibility within the trench. Therefore, partial covering should be considered only after verifying its compatibility with the existing structure, the collector below, the required clearances and operational safety requirements.

5.4 Alternative 0: preservation of the existing underpass in service

The first alternative consists of maintaining the underpass in operation and preserving its current traffic function. This solution represents the least invasive option and is broadly consistent with the current urban regeneration strategy, which maintains the underpass in service while transforming the surface level of Avenida Pérez Galdós.

From an urban point of view, this alternative preserves the existing traffic capacity of the corridor and reduces the risk of severe traffic redistribution toward neighbouring streets. From a structural point of view, the finite element analysis does not indicate a global instability mechanism under the analysed assumptions.

For this reason, Alternative 0 should be interpreted as active preservation rather than as a passive "do nothing" strategy. Its feasibility depends on periodic inspection, monitoring, maintenance and, where necessary, localized repairs of the deteriorated elements. The main limitation of this option is that it preserves the existing function of the underpass without directly solving the long-term ageing of the structure.

Table 5.1. Preliminary assessment of Alternative 0.

Aspect	**Preliminary assessment**
Main objective	Maintain the underpass in service while controlling its condition through inspection, maintenance and monitoring.
Structural impact	Low direct intervention, but local deterioration must be verified.
Mobility impact	Favourable, because the existing traffic function is preserved.
Main advantage	Lowest immediate disruption and compatibility with the current surface regeneration strategy.
Main limitation	Does not solve long-term ageing and deterioration by itself.
Required condition	Continuous management of the structure through inspection, monitoring and targeted maintenance.

5.5 Alternative 1: structural rehabilitation or replacement of the floor beams

5.5.1 General description

The second alternative consists of repairing, strengthening, or replacing the deteriorated floor beam system of the underpass. This system corresponds to the prefabricated prestressed concrete beams of the *tablero* described in Anejo Nº27, which are reported to have a constant depth of approximately 0.40 m, a span arrangement with a free length of about 6.0 m, and a reinforced concrete slab above them [20].

This option is directly related to the structural deficiencies reported during previous inspections. Anejo Nº27 identifies the beams as one of the most deteriorated elements of the system, with widespread surface degradation, spalling, loss of concrete cover and exposed reinforcement in several areas. The deterioration is reported to become more severe towards the southern part of the underpass, with particularly critical conditions in the sector below Avenida del Cid [20].

This alternative is more invasive than simple preservation, but it represents a targeted structural intervention. The floor beams, referred to in the Spanish documentation as *vigas*, contribute to maintaining the relative distance between the lateral retaining walls and to transferring loads within the structural system. Their deterioration is therefore not only a local durability issue, but may also affect the global mechanical response of the underpass–collector system.

5.5.2 Numerical simulation of beam removal

In order to evaluate the influence of the floor beams on the global behaviour of the section, an additional RS2 simulation was carried out starting from the configuration without footing-like base enlargement. A final stage was introduced in which the floor beam system was removed. This stage was not intended to reproduce a realistic demolition sequence, but to perform a sensitivity analysis on the loss of transverse restraint.

The results show a significant increase in displacements after beam removal. In the previous final operational condition of the same scenario, the maximum total displacement was approximately:

$$u_{tot,max} = 7.66 \times 10^{-3} \text{ m} \tag{5.1}$$

whereas after removal of the beam system it increased to:

$$u_{tot,max} = 1.87 \times 10^{-2} \text{ m} \tag{5.2}$$

corresponding to approximately 1.9 cm. The maximum horizontal displacement also increased significantly, reaching:

$$u_{x,max} = 1.78 \times 10^{-2} \text{ m} \tag{5.3}$$

This result indicates that the beams provide an important transverse restraining effect between the lateral walls. Their removal allows a greater tendency of the walls to move laterally, with a possible convergence mechanism of the underpass section.

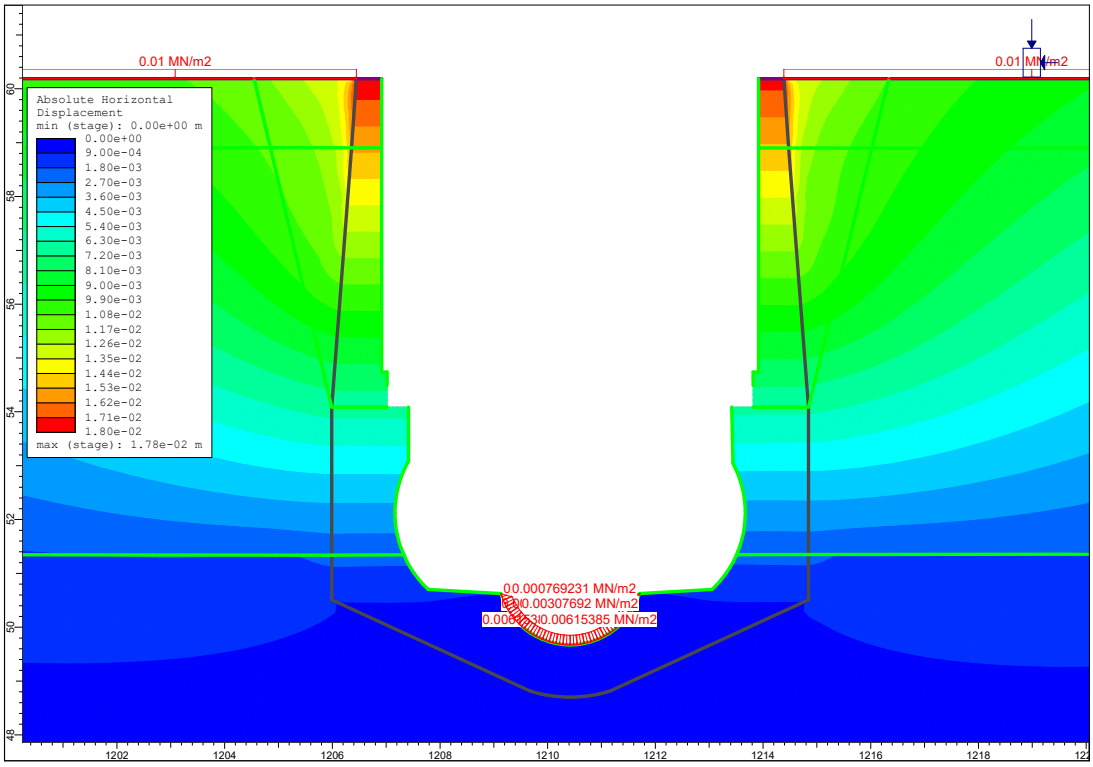

Figure 5.2. Absolute horizontal displacement contours after removal of the floor beam system.

The stress results also show a relevant redistribution within the lower structural system. After beam removal, the maximum major principal stress increases to approximately:

$$\sigma_{1,max} = 9.39 \text{ MPa} \tag{5.4}$$

while the minimum minor principal stress reaches:

$$\sigma_{3,min} = -4.84 \text{ MPa} \tag{5.5}$$

The maximum shear plastic strain also increases from approximately 6.44×10^{-3} in the operational stage to approximately:

$$\varepsilon_{s,p,max} = 3.20 \times 10^{-2} \tag{5.6}$$

These results should not be interpreted as a direct collapse prediction, because the model does not include reinforcement explicitly, does not simulate cracking and does not

reproduce the real construction sequence of beam removal. Nevertheless, they clearly indicate that the beams cannot be considered secondary or negligible elements.

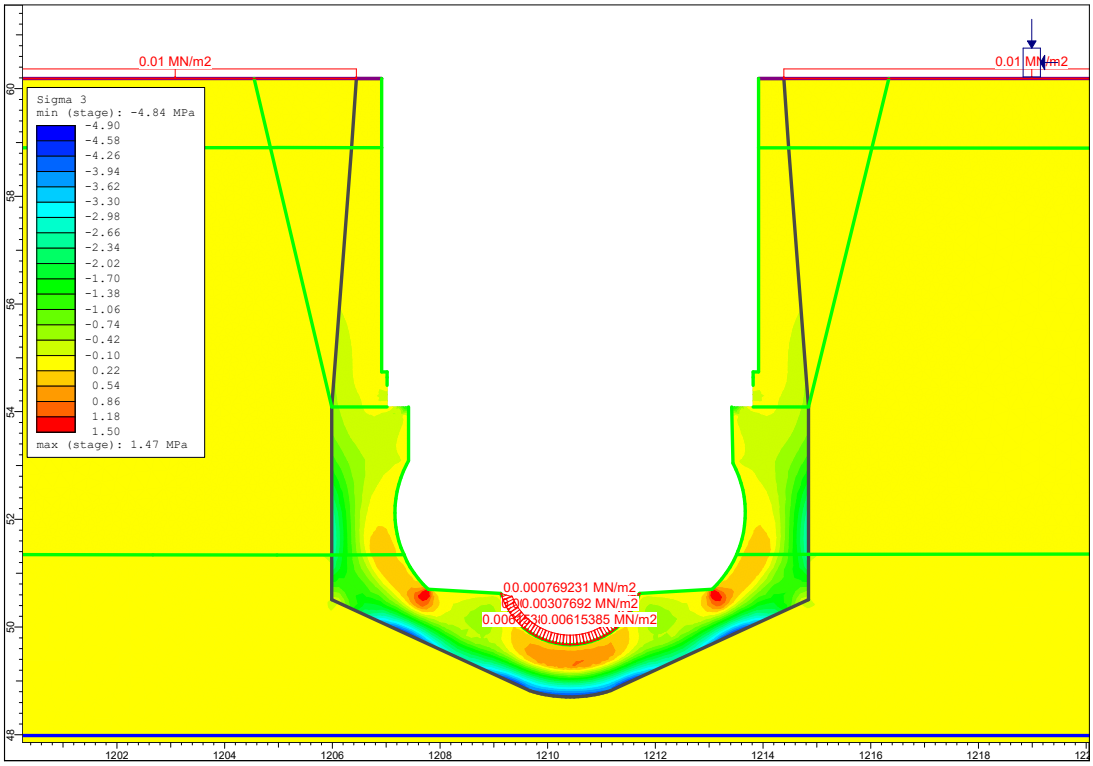

Figure 5.3. Minor principal stress σ_3 after removal of the floor beam system.

5.5.3 Construction implications and preliminary assessment

If the beams were found to require replacement, their removal should not be carried out simultaneously along the entire section. A staged construction procedure would be necessary, maintaining sufficient transverse restraint at every phase. Temporary supports, bracing elements or provisional steel frames could be installed before removing the deteriorated beams, in order to prevent excessive convergence of the retaining walls.

Monitoring requirements would be higher during construction than during ordinary operation, because temporary removal of transverse restraint may directly affect wall convergence and stress redistribution.

Table 5.2. Comparison between the operational stage and the beam-removal stage in the RS2 model without footing-like base enlargement.

Quantity	Operational stage	After beam removal	Interpretation
Absolute horizontal displacement	3.09×10^{-3} m	1.78×10^{-2} m	Strong increase in lateral wall movement
Absolute vertical displacement	7.46×10^{-3} m	1.02×10^{-2} m	Moderate increase
Total displacement	7.66×10^{-3} m	1.87×10^{-2} m	Significant increase, up to approximately 1.9 cm
Maximum shear plastic strain	6.44×10^{-3}	3.20×10^{-2}	Strong increase in localized plastic response
Maximum σ_1	3.47 MPa	9.39 MPa	Significant increase in compressive stress concentration
Minimum σ_3	−2.05 MPa	−4.84 MPa	Higher tensile stress concentration in the structural system

Alternative 1 appears technically meaningful because it directly addresses one of the most critical deterioration issues identified in the existing structure. The RS2 simulation confirms the structural relevance of the beams within the transverse behaviour of the underpass. Before implementation, however, the real geometry, reinforcement layout, residual capacity, deterioration state and connection details of the beams would need to be determined.

Table 5.3. Preliminary assessment of Alternative 1.

Aspect	Preliminary assessment
Main objective	Repair, strengthen, or replace deteriorated floor beams while preserving the underpass function.
Structural relevance	High, because the beams contribute to the transverse restraint of the retaining walls.
RS2 indication	Beam removal increases the maximum total displacement from approximately 7.7 mm to approximately 18.7 mm and strongly increases horizontal wall displacement.
Stress redistribution	The maximum σ_1 increases to approximately 9.39 MPa, while σ_3 reaches approximately -4.84 MPa.
Construction requirement	Sequential removal and replacement, with temporary support.
Main uncertainty	Real residual capacity, reinforcement condition and deterioration state of the existing reinforced concrete beams.

5.6 Alternative 2: closure and controlled backfilling of the underpass

5.6.1 General description

The third alternative consists of closing the underpass to traffic and filling the internal volume with controlled backfill material. This option is closely related to the initial urban regeneration proposals for Avenida Pérez Galdós, which considered the possibility of suppressing or transforming the existing underpass in order to improve surface continuity and public space quality.

This alternative was later abandoned in the official development of the project, mainly because traffic studies confirmed the strategic role of the underpass within the urban mobility system. Nevertheless, it remains relevant as a possible long-term scenario if the underpass were eventually removed from traffic service due to structural, safety, political or urban planning reasons.

5.6.2 Technical concept and numerical modelling

The alternative would transform the underpass from an open traffic void into a buried filled volume. The choice of backfill material is important because it directly controls the additional permanent load transmitted to the structural system. A lightweight material could reduce the loads acting on the lower collector and on the floor beam system, while a conventional granular fill would be simpler and cheaper but would generate higher vertical stresses.

In the RS2 model, this alternative was analysed starting from the geometrical configuration without footing-like base enlargement. Two additional stages were introduced after the operational condition: filling of the internal volume and subsequent application of the final surface load.

The adopted filling material was modelled as a drained Mohr–Coulomb material with zero cohesion, zero tensile strength, friction angle equal to 34°, Young's modulus equal to 40 MPa and unit weight equal to 0.020 MN/m^3.

Table 5.4. RS2 parameters adopted for the filling material.

Parameter	**Adopted value**
Material name	Filling material
Unit weight, γ	0.020 MN/m^3
Porosity, n	0.30
Young's modulus, E	40 MPa
Poisson's ratio, ν	0.30
Failure criterion	Mohr–Coulomb
Material type	Plastic
Peak cohesion, c'	0 MPa
Peak friction angle, ϕ'	34°
Dilation angle, ψ	0°
Tensile strength	0 MPa
Material behaviour	Drained
Static water mode	Dry

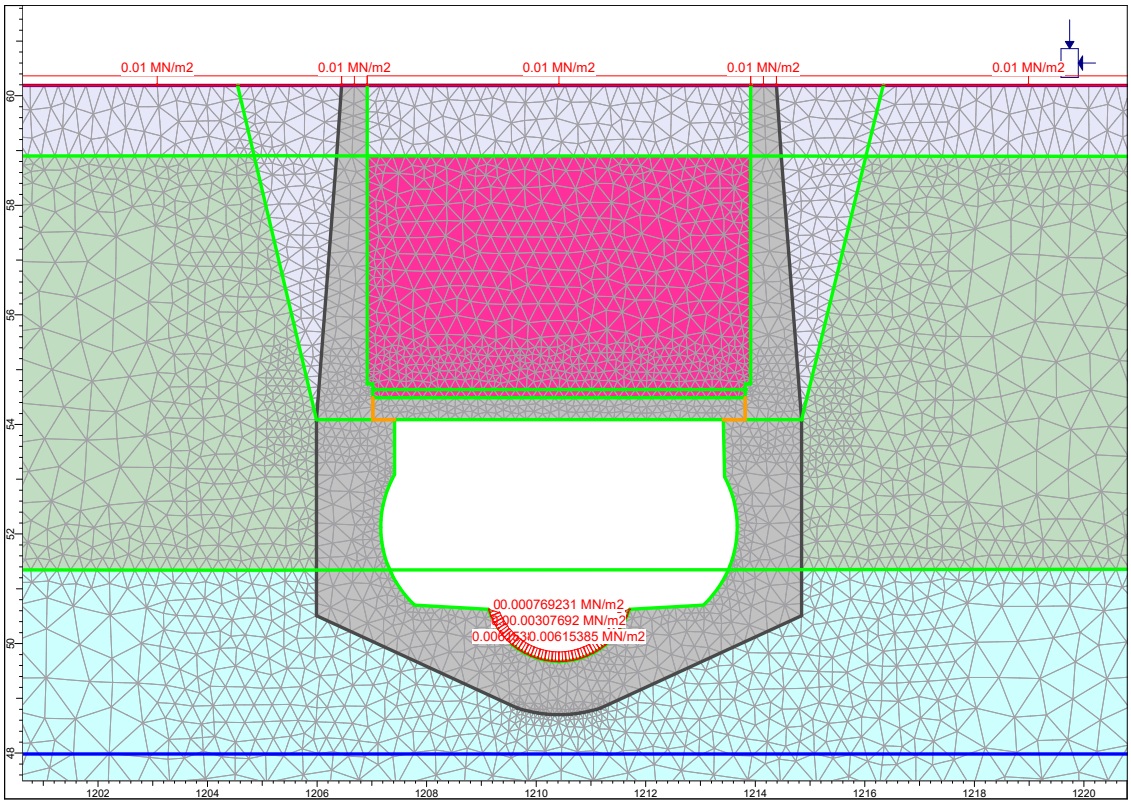

Figure 5.4. Numerical configuration adopted for the controlled backfilling alternative.

5.6.3 Numerical results and interpretation

The RS2 results show that the controlled backfilling alternative does not produce a clear global instability mechanism in the model. The maximum shear plastic strain remains essentially unchanged with respect to the operational stage, indicating that the filling does not generate a new relevant plastic mechanism in the surrounding soil.

However, the filling introduces a significant increase in vertical displacement and in the principal stresses of the lower structural system. The comparison with the operational stage is summarized in Table 5.5.

Table 5.5. Comparison between the operational stage and the backfilling stages in the RS2 model without footing-like base enlargement.

Quantity	Operational stage	After filling	Filling + surface load
Absolute horizontal displacement	3.09×10^{-3} m	5.23×10^{-3} m	5.56×10^{-3} m
Absolute vertical displacement	7.46×10^{-3} m	2.22×10^{-2} m	2.37×10^{-2} m
Total displacement	7.66×10^{-3} m	2.22×10^{-2} m	2.37×10^{-2} m
Maximum shear plastic strain	6.44×10^{-3}	6.44×10^{-3}	6.44×10^{-3}
Maximum σ_1	3.47 MPa	11.31 MPa	11.82 MPa
Minimum σ_3	−2.05 MPa	−7.14 MPa	−7.76 MPa

The maximum total displacement increases from approximately 7.7 mm in the operational condition to approximately 22.2 mm after filling, and to approximately 23.7 mm after the final surface load. This increase is mainly vertical, while the horizontal displacement remains more limited.

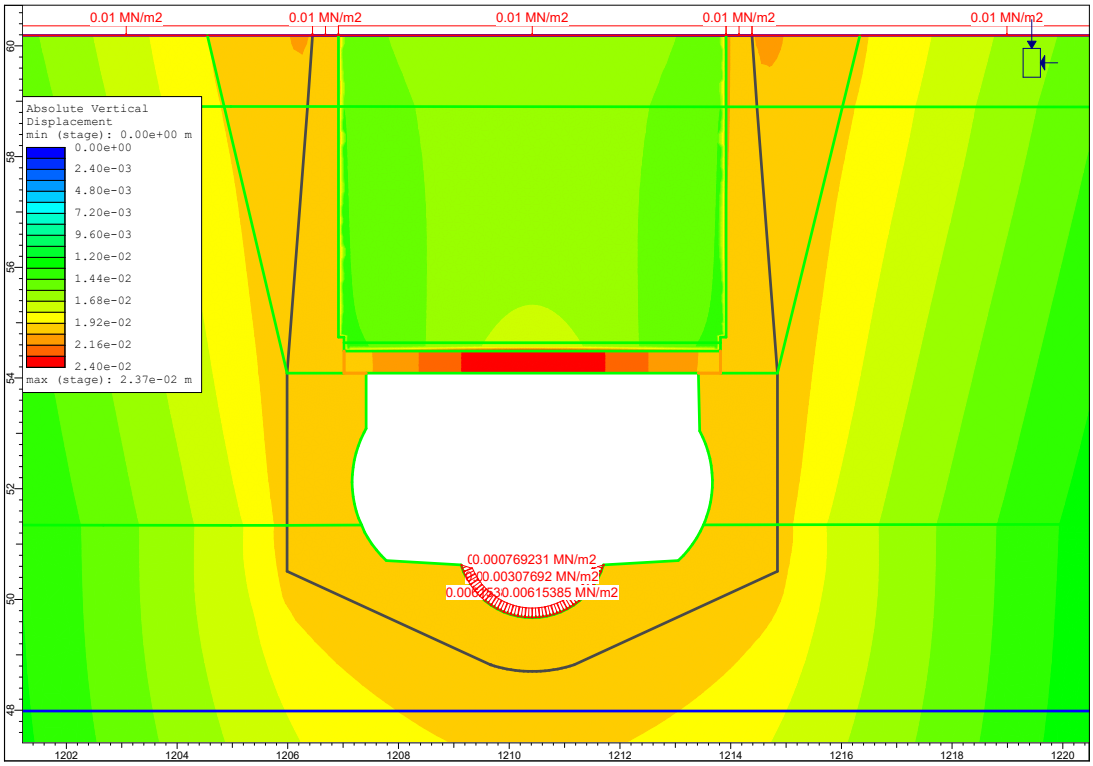

Figure 5.5. Vertical displacement contours obtained for the controlled backfilling alternative after filling and surface loading.

The most critical effect is the increase in principal stresses. The maximum major principal stress increases from approximately 3.47 MPa in the operational stage to approximately 11.82 MPa in the final backfilled condition, while the minimum minor principal stress decreases from approximately −2.05 MPa to approximately −7.76 MPa.

These values indicate a significant increase in local compressive and tensile stress concentrations, especially in the lower structural system close to the collector. Since the concrete was modelled as an equivalent elastic material and the reinforcement was not explicitly represented, these tensile stresses should not be interpreted as a direct reinforced concrete failure verification. Nevertheless, they show that the backfilling alternative would substantially increase the structural demand on the lower concrete elements and on the collector.

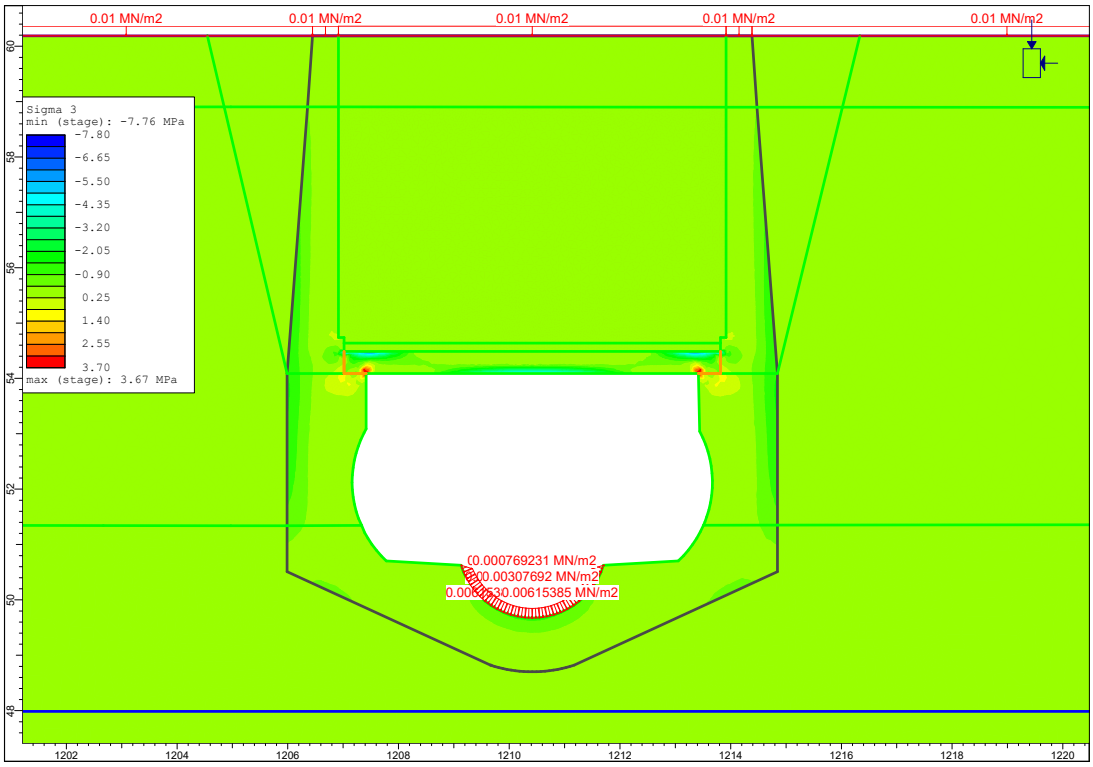

Figure 5.6. Minor principal stress σ_3 contours for the controlled backfilling alternative.

The backfilling alternative therefore produces a different type of response compared with beam removal. Beam removal mainly affects horizontal displacement and transverse restraint, whereas backfilling mainly increases vertical displacement and stress level in the lower structural system. For this reason, the alternative cannot be considered a simple urban infill operation. It would require a detailed structural verification of the lower concrete elements, the collector and the existing beams.

The use of a lighter filling material could be beneficial. Since the main negative effect

of this alternative is the increase in permanent vertical loading, a lightweight engineered fill could reduce the stress transmitted to the lower structural system.

5.6.4 Preliminary assessment

Alternative 2 is technically and urbanistically relevant, but more complex than it may appear at first sight. The RS2 results suggest that it does not generate a clear global instability mechanism and does not significantly increase the maximum shear plastic strain. However, it produces a marked increase in vertical displacement and principal stress concentrations.

Table 5.6. Preliminary assessment of Alternative 2.

Aspect	Preliminary assessment
Main objective	Close the underpass and transform it into a buried filled volume.
Urban effect	High potential for surface continuity and public space improvement.
Structural effect	Significant increase in vertical displacement and local principal stresses in the lower structural system.
RS2 indication	No clear global instability mechanism and no relevant increase in maximum shear plastic strain, but strong increase in σ_1 and tensile σ_3 concentrations.
Construction requirement	Controlled placement and compaction of backfill, preferably considering lightweight materials to reduce permanent loading.
Main limitation	Significant mobility impact and increased structural demand on the collector.
Main uncertainty	Residual capacity of the existing floor beams, collector and lower structural elements under increased permanent load.

5.7 Alternative 3: adaptive reuse of the abandoned underpass

5.7.1 General concept

A further possible alternative, in the event that the underpass is no longer used for traffic, is its functional reconversion as an underground service volume. Unlike Alternatives 1 and 2, this option was not analysed through finite element modelling. It is introduced as a conceptual long-term scenario, relevant only if the underpass were permanently abandoned for traffic use due to structural, safety-related, political or urban planning reasons.

The basic idea is to interpret the existing underground space not only as an obsolete transport infrastructure to be demolished or filled, but also as a potential urban asset. In this perspective, the abandoned underpass could be reused for functions compatible with its geometry, accessibility, hydraulic conditions and structural capacity. Two possible directions are considered here: energy reuse and temporary stormwater storage.

5.7.2 Energy reuse as an underground storage system

The concept is related to the broader field of energy tunnels and energy geostructures, where underground structures are used not only for their primary civil engineering function, but also as assets for heat exchange, thermal storage or energy recovery. With reference to existing or abandoned tunnels, Barla and Insana [37] highlight that these infrastructures can be retrofitted for energy purposes and transformed into underground energy storage systems. The authors refer to Underground Thermal Energy Storage (UTES), Tank Thermal Energy Storage (TTES), and other storage options based on pressurised air, sand or water [37].

In this perspective, the Pérez Galdós underpass could be interpreted not only as an obsolete or redundant transport infrastructure, but also as a potential underground volume to be reused within a broader urban energy strategy. Such a solution would be consistent with the principles of circular reuse of existing infrastructure and with the objectives of reducing demolition and reusing existing urban assets.

However, in the present case, this option should be considered only as a preliminary and conceptual alternative. The underpass is a very shallow structure, and the efficiency of any thermal exchange with the surrounding ground would need to be specifically assessed. Moreover, if the upper open trench were closed and covered with a concrete slab, the new configuration could affect the thermal behaviour of the system.

It is also important to distinguish this reuse scenario from the more common concept of thermally activated tunnel linings. In newly constructed energy tunnels, heat exchanger pipes can be embedded directly into the lining during construction. In the case of the Pérez Galdós underpass, however, the structure already exists and the walls are not expected to be demolished or rebuilt. The most realistic energy reuse hypothesis would therefore be based on the exploitation of the existing underground cavity as a storage volume, rather than on the thermal activation of a newly constructed lining.

5.7.3 Stormwater retention and temporary water storage

A second possible reuse of the abandoned underpass could be related to temporary stormwater retention. In this scenario, the underground volume would be studied as a temporary storage basin during intense rainfall events, with the aim of reducing peak discharge into the drainage network or providing additional hydraulic buffering capacity in a dense urban area.

This possibility may be relevant in a city such as Valencia, where extreme rainfall events and urban drainage capacity represent important issues for climate adaptation and urban resilience. The underpass is already located below the surrounding street level and is physically connected to an area affected by major drainage infrastructure. For this reason, its possible hydraulic reuse could deserve preliminary consideration if the traffic function were permanently abandoned.

Nevertheless, this option would require a dedicated hydraulic and structural study. Its feasibility would depend on the available storage volume, hydraulic connections with the drainage network, water quality, sedimentation, cleaning and maintenance requirements, safety during operation, ventilation, access, waterproofing, and the resistance of the

existing structure to hydrostatic and uplift pressures. The presence of the collector below the underpass would also be a central constraint, since any hydraulic reuse should avoid negative interactions with the existing sewer system.

Therefore, the stormwater storage option should not be interpreted as a developed design proposal, but as a possible direction for future research. Together with energy reuse, it shows that the abandoned underpass could potentially be reconsidered as an underground urban service volume rather than simply as a void to be removed or filled.

5.7.4 Preliminary assessment

Alternative 3 has a different nature compared with the previous alternatives. While Alternatives 0, 1 and 2 are directly related to the structural and urban management of the underpass, the adaptive reuse option represents a functional reconversion scenario. It would only become relevant if the underpass were permanently removed from traffic service.

The main advantage of this alternative is that it proposes a circular reuse of an existing underground volume, avoiding demolition and giving the infrastructure a new function. However, the technical feasibility is currently uncertain. Dedicated energy, hydraulic, mechanical, structural and safety studies would be required before any of these options could be considered realistic.

Table 5.7. Preliminary assessment of Alternative 3.

Aspect	**Preliminary assessment**
Main objective	Reuse the abandoned underpass as an underground functional volume rather than demolishing or backfilling it.
Possible functions	Energy storage, thermal storage, temporary stormwater retention or other urban service functions.
Applicability	Only relevant if the underpass is permanently removed from traffic service.
Main advantage	Circular reuse of existing infrastructure and potential contribution to local energy, hydraulic or resilience strategies.
Technical limitation	Requires dedicated thermal, hydraulic, mechanical, structural and safety studies.
Structural implication	Depends on whether the cavity is left accessible, partially modified, filled with water or adapted with internal systems.
Level of maturity	Preliminary and conceptual.

5.8 Comparative assessment of the alternatives

The four alternatives do not have the same technical maturity or the same time horizon. Alternatives 0, 1 and 2 are directly related to the current structural and geotechnical behaviour of the underpass and are supported, at least in part, by the numerical analyses

carried out in RS2. Alternative 3, instead, is a conceptual long-term reuse scenario and would require independent multidisciplinary studies.

The comparison is summarised in Table 5.8. The table is intended to highlight the main engineering implications of each option rather than to provide a final decision framework.

Table 5.8. Comparative assessment of the intervention alternatives.

Alternative	Main role	Main benefit	Main constraint
Alternative 0			
Preservation in service	Short-term management of the existing underpass	Preserves traffic function and requires limited direct intervention	Does not solve ageing or deterioration without inspection, monitoring and maintenance
Alternative 1			
Beam rehabilitation or replacement	Targeted structural intervention on deteriorated elements	Addresses a critical component of the transverse restraint system	Requires staged execution, temporary support and verification of residual capacity
Alternative 2			
Controlled backfilling	Radical transformation if traffic use is removed	Improves surface continuity and supports full urban reconversion	Increases permanent loading and stress demand on the lower structural system and collector
Alternative 3			
Adaptive reuse	Conceptual long-term reuse of the abandoned volume	Reuses an existing underground space for possible service functions	Not supported by FEM in this thesis; requires dedicated energy, hydraulic, structural and safety studies

Note: Alternatives 0, 1 and 2 are linked to the structural and geotechnical assessment developed in this thesis. Alternative 3 is included only as a conceptual long-term scenario.

5.9 Discussion

The comparison indicates that the underpass does not appear to require immediate removal on the basis of global geomechanical instability alone. Under the adopted assumptions, the current configuration remains globally stable in the finite element model. However, the numerical analyses also show that the system is sensitive to interventions that modify the existing load path or remove structural restraint.

From an engineering point of view, the most coherent short-term strategy is therefore active preservation: maintaining the underpass in service while implementing inspection, monitoring and targeted maintenance. If deterioration of the floor beam system is confirmed, Alternative 1 represents the most direct structural intervention, but it should be carried out through staged replacement or strengthening, with temporary support and

deformation control.

Alternative 2 and Alternative 3 belong to a different decision level. Controlled backfilling may become relevant only if the traffic function is permanently removed, and it would require detailed verification of the collector and lower structural elements due to the increase in permanent load. Adaptive reuse is even more preliminary and should be considered only as a long-term research direction, not as a design solution supported by the present FEM analyses.

Overall, the chapter confirms that the future of the Pérez Galdós underpass cannot be decided only from a traffic or urban design perspective. The structure is embedded within a complex soil–structure–collector system, and each alternative modifies this system in a different way. Any final decision should therefore be supported by structural inspection, monitoring and additional analyses focused on the selected intervention.

Chapter 6

Conclusions and future work

6.1 Main findings

This thesis investigated the Pérez Galdós underpass as an existing urban infrastructure for which original construction drawings, structural calculations and complete as-built documentation are not available. The work therefore combined historical sources, topographic data, geotechnical investigations, geophysical surveys and engineering interpretation in order to reconstruct a coherent technical model of the underpass–collector system.

The finite element analyses carried out in RS2 did not indicate a global instability mechanism for the current configuration under the adopted assumptions. The computed displacements remained limited when compared with the overall dimensions of the structure, and the plastic strain zones in the surrounding soil were generally localised. At the scale of the two-dimensional geomechanical model, the system therefore does not appear to behave as a globally unsafe or collapsing structure.

This result must not be interpreted as a complete structural safety verification. The numerical model also identified local stress concentrations, especially near geometrical discontinuities, contact zones and the lower structural system close to the collector. Since the concrete was modelled as an equivalent elastic material and reinforcement was not explicitly represented, these stress peaks should be interpreted as indicators of possible cracking or reinforcement demand, not as direct proof of local failure.

The overall conclusion is therefore deliberately balanced. The model provides a positive indication regarding global stability, but the ageing condition of the underpass, the uncertainty of its real geometry and the lack of detailed information on reinforcement and concrete properties require further inspection, monitoring and local reinforced concrete verification before any major intervention is undertaken.

6.2 Geotechnical and geometrical interpretation

The geological and geotechnical interpretation confirmed the heterogeneous nature of the urban subsoil beneath Avenida Pérez Galdós. The available boreholes showed a complex alternation of anthropogenic fills, fine-grained soils and gravelly layers. In order to develop a usable engineering model, this variability was simplified into five representative

geotechnical layers, later adopted in both the Civil 3D stratigraphic model and the RS2 finite element analyses.

The MASW survey supported the interpretation by confirming the general increase in stiffness with depth and the presence of deeper, stiffer granular horizons. Nevertheless, the boreholes remained the primary source for defining the stratigraphic sequence and the geotechnical parameters, while the geophysical data were used mainly as a consistency check.

From the geometrical point of view, the most relevant unresolved issue concerned the real configuration of the retaining wall base. The available evidence did not allow the presence of a footing-like base enlargement to be confirmed or excluded with certainty. For this reason, two geometrical scenarios were analysed: one including a possible footing-like enlargement and one without it. This choice made it possible to evaluate how the main geometrical uncertainty affects the mechanical response of the system, instead of relying on a single unverified reconstruction.

The GPR interpretation also showed that the structure varies along the longitudinal development of the underpass. This confirms that a single transverse section cannot represent all local configurations, but can still provide useful insight into the behaviour of a representative and potentially critical portion of the system.

6.3 Finite element modelling results

The finite element model was developed as a two-dimensional plane strain representation of a selected transverse section of the underpass. The analysed section corresponds to an open trench portion located approximately midway between covered intersections, where the retaining walls are not directly constrained by an upper road crossing. This configuration was considered suitable for studying a potentially vulnerable portion of the system.

Both analysed geometrical scenarios reached numerical stability. The computed total displacements remained limited when compared with the overall dimensions of the structure, suggesting that the underpass–collector system does not exhibit a relevant global deformation mechanism under the adopted assumptions. Although the two scenarios produced slightly different displacement patterns, their overall response was comparable.

The presence of a footing-like base enlargement appears mechanically plausible, since it provides a wider load transfer mechanism and a more distributed response. However, the model without such enlargement was also stable. Therefore, the finite element analysis cannot prove the existence of this element, but it clarifies the influence of this geometrical assumption on the system response.

The local stress concentrations observed in both scenarios should be interpreted as indicators of potentially critical zones rather than as direct evidence of failure. Since reinforcement, cracking, corrosion, bond behaviour and local degradation were not explicitly modelled, these results mainly indicate where more detailed reinforced concrete checks should be concentrated.

The analyses of the intervention alternatives confirmed the structural importance of the existing beam system. The hypothetical removal of the beams caused a significant

increase in horizontal displacement and plastic strain, showing their contribution to the transverse restraint of the retaining walls. Similarly, controlled backfilling did not generate a new global plastic mechanism in the soil, but increased vertical displacements and stresses in the lower structural system. For this reason, both beam replacement and backfilling would require staged execution, monitoring and specific verification of the residual capacity of the existing structural elements.

6.4 Assessment of intervention alternatives

The assessment of the intervention alternatives led to a clear hierarchy. Maintaining the underpass in service, combined with inspection and monitoring, appears to be the most realistic short-term strategy, because it preserves the current mobility function and is consistent with the absence of global instability in the numerical model. However, this option should be understood as active preservation, not as a passive absence of intervention.

If the deterioration of the floor beam system is confirmed, rehabilitation or staged replacement of these elements represents the most directly justified structural intervention. The numerical simulation of beam removal showed that the beams contribute significantly to the transverse restraint of the retaining walls; therefore, their replacement would require temporary support, staged execution and deformation monitoring.

The closure and controlled backfilling of the underpass would represent a more radical urban transformation. Although the RS2 model did not show a new global instability mechanism in the soil, the alternative produced higher vertical displacements and stress demand in the lower structural system and collector. Adaptive reuse, finally, should remain a conceptual long-term possibility, relevant only if the underpass is permanently abandoned for traffic use and supported by dedicated multidisciplinary studies.

6.5 Limitations of the study

The main limitations of this work are linked to the nature of the available information and to the complexity of the existing structure. The model developed in this thesis is not a complete reproduction of reality, but a simplified representation aimed at understanding the main geomechanical mechanisms of the underpass–collector system.

The first limitation concerns the use of a two-dimensional plane strain model. A three-dimensional analysis could represent the longitudinal variability of the structure more accurately, including transitions between covered and uncovered sections, local joints and changes in geometry. However, the uncertainty affecting the real geometry and structural details of the underpass was too high to justify the apparent precision of a full three-dimensional model. For the objectives of this thesis, a two-dimensional model of a representative critical section was therefore considered more appropriate.

The second limitation concerns the geometry of the structure. The exact configuration of the retaining walls, the possible footing-like base enlargement, the connections between structural elements and the detailed geometry of the collector could not be fully verified.

The adoption of two geometrical scenarios was used to address this uncertainty in a transparent way.

The third limitation concerns material properties. The mechanical properties of the concrete and reinforcement are not known with sufficient precision. Reinforcement was not explicitly included in the RS2 model, and the concrete was represented as an equivalent elastic material. This approach is suitable for evaluating the global soil–structure interaction, but it cannot replace a detailed reinforced concrete verification.

Further simplifications were introduced in the stratigraphic model, in the selection of representative geotechnical parameters and in the reconstruction of construction stages. These assumptions were necessary to make the problem numerically manageable and consistent with the available data.

These limitations define the correct field of application of the study. The results provide an engineering-level interpretation of the global behaviour of the system, not a final structural design or a definitive safety certification.

6.6 Engineering perspective and broader relevance

The Pérez Galdós underpass is representative of a broader challenge faced by many European cities: the assessment and management of mid-twentieth-century infrastructure with limited documentation and increasing functional, environmental and political pressure. In such contexts, engineering is not only concerned with designing new structures, but also with understanding existing ones and making their uncertainties explicit.

The case study shows the importance of combining indirect investigation, numerical modelling, inspection and critical interpretation. The purpose of the analysis is not to replace detailed structural verification, but to provide a technically grounded basis for deciding where further investigation and monitoring should be concentrated.

This perspective is particularly relevant for urban regeneration projects, where decisions about infrastructure are often linked to mobility, public space and social expectations. The contribution of engineering is to clarify the physical constraints and consequences of each alternative, so that future decisions can be based on evidence rather than on assumptions alone.

6.7 Recommendations for future work

Future work should first focus on reducing the main uncertainties identified in this thesis. A detailed structural investigation should be carried out to determine the real geometry of the retaining walls, the collector and the beam system. This should include direct inspections, concrete core extraction, characterisation of concrete strength and durability, identification of the reinforcement layout and evaluation of corrosion. Without this information, any local structural verification remains necessarily incomplete.

A monitoring plan should also be implemented for any future intervention. Topographic targets, crack gauges, convergence measurements, vibration control and periodic inspection of the beams and retaining walls should be associated with predefined threshold values.

Monitoring would be particularly important during beam replacement, partial covering, backfilling or any intervention modifying the current load path.

Further analyses should then be focused on the selected intervention. In the case of beam rehabilitation, the priority would be the residual capacity and connection detail of the existing beam system. In the case of controlled backfilling, the priority would be the verification of the collector and lower concrete elements under increased permanent load, including the possible use of lightweight filling materials.

Lighter urban interventions, such as acoustic barriers or partial covering of selected open trench sections, could also be studied. These solutions may improve noise conditions and pedestrian continuity without necessarily suppressing the traffic function of the underpass. However, partial covering would require specific checks on structural loads, ventilation, lighting and operational safety.

Long-term reuse scenarios, including energy-related or hydraulic uses of the underground volume, should be considered only if the underpass is permanently removed from traffic service. These options are not directly supported by the FEM results developed in this thesis and would require dedicated energy, hydraulic, structural and safety studies.

Finally, the case highlights the importance of maintainability in infrastructure design. Future structures should be conceived not only for their initial function, but also for inspection, repair, monitoring and adaptation. Designing accessible and maintainable structures can reduce uncertainty, extend service life and improve the quality of future engineering decisions.

The Pérez Galdós underpass therefore represents not only a local engineering problem, but also an example of how ageing urban infrastructure can be assessed in a context of incomplete information and changing urban priorities. The work developed in this thesis provides a technical basis for this discussion and shows how engineering assessment can help transform uncertainty into informed decision-making.

Bibliography

[1] Sixto D. Lozano Esteban. Análisis de la ciudad de valencia, 2010. Master en Jardinería y Paisaje.

[2] Army Map Service (U.S.). Orthophotos of the american flight (series b, 1956–1957), 1956. Flight carried out between January 1956 and November 1957 over mainland Spain and the Balearic Islands. URL: https://www.geamap.com/en/orthophoto-comparator-spain135.

[3] Ayuntamiento de Valencia. Plan general de ordenación urbana de valencia: Memoria informativa i, 1988.

[4] Censos de población anuales, 2025. URL: https://pegv.gva.es/auto/produccion/web/CPA/Mapas/Mapas_com_cas.html.

[5] Radio Valencia / Cadena SER. La avenida de pérez galdós, 2020. Accessed April 17, 2026. URL: https://cadenaser.com/emisora/2020/01/08/radio_valencia/1578486760_498963.html.

[6] Alfredo Faus Prieto. Al servicio de una ciudad en expansión. casimiro meseguer bonet, director de caminos del ayuntamiento de valencia (1874–1914). *Investigaciones Geográficas*, (76):141–161, 2021. doi:10.14198/INGEO.17616.

[7] Open street map database. URL: https://www.openstreetmap.org/#map=15/39.46923/-0.38135.

[8] Las Provincias. Las obras odiadas que fueron bendición. Las Provincias, 10 April 2016. URL: https://www.lasprovincias.es/valencia-ciudad/201604/11/obras-odiadas-fueron-bendicion-20160411004459-v.html.

[9] Las Provincias. Pérez galdós causa atascos pese a haber menos coches. Las Provincias, 21 November 2025. URL: https://www.lasprovincias.es/valencia-ciudad/perez-galdos-causa-atascos-pese-coches-valencia-20251121004558-nt.html.

[10] Miguel Ángel Montesinos. Traffic and construction works on avenida pérez galdós. Photograph, 2025. Published in Levante-EMV.

[11] Francisco Calabuig and Josephine Burgos. Comienzan las obras del segundo tramo de pérez galdós entre la crítica y la resignación. URL: https://www.levante-emv.com.

[12] Moisés Domínguez. Las obras de pérez galdós congestionan todo el suroeste de la ciudad. URL: https://www.levante-emv.com.

[13] Europa Press. Vecinos cortan el túnel de pérez galdós para exigir su eliminación. URL: https://www.europapress.es.

[14] Ajuntament de València. La junta de gobierno abrirá el proceso de licitación de las obras de giorgeta y pérez galdós. URL: https://www.valencia.es.

[15] Ayuntamiento de Valencia. Reurbanización definitiva de las avenidas pérez galdós y giorgeta, n.d. Accessed: 2026-04-27. URL: https://www.valencia.es/cas/urbanismo/proyectos-urbanos/-/content/reurbanizacion_definitiva_de_las_avenidas_perez_galdos_y_giorgeta.

[16] Ajuntament de València. El ayuntamiento adjudica a la ute de pavasal y grupo bertolín la regeneración de pérez galdós y giorgeta por 24 millones. Press release. URL: https://www.valencia.es.

[17] Vicente Bellvis. El 30 de junio empiezan las obras de pérez galdós con el corte al tráfico. URL: https://www.valenciaciudad.es.

[18] Gecival S.L. Topographic survey data for avenida pérez galdós (València), 2024. Digital CAD files provided by Gecival S.L. within the framework of the urban regeneration project. Unpublished technical material.

[19] Francisco José Pericás Sancho. Campaña Geotécnica para Reurbanización Avda. Pérez Galdós, Valencia. Informe Técnico EG-5689/24, C2C Servicios Técnicos de Inspección, S.L., Ribarroja de Túria, Valencia, July 2024. Peticionario: GECIVAL, S.L. (Obra 28999).

[20] Ayuntamiento de València, Julián Alcalá González, and Víctor Martínez Ibáñez. Regeneración urbana y renaturalización de las avenidas pérez galdós y giorgeta (valència). anejo no. 27: Evaluación estructural del paso inferior, March 2024. Technical annex, uploaded project documentation.

[21] Geozone Asesores S.L. Estudio geotécnico para el proyecto de regeneración urbana y renaturalización de las avenidas pérez galdós y giorgeta (valència). Technical report, Geozone Asesores S.L., Bétera, Spain, 2025. Geotechnical report including MASW, GPR surveys, boreholes, and laboratory testing.

[22] Instituto Geológico y Minero de España. *Mapa Geológico de España. Hoja 722 – Valencia.* IGME, Madrid, 1974. Escala 1:50,000 (MAGNA Series). URL: https://info.igme.es/cartografiadigital/datos/magna50/jpgs/d7_G50/Editado_MAGNA50_722.jpg.

[23] Instituto Geológico y Minero de España (IGME). Mapa geológico de españa. hoja 722 – valencia. memoria. Technical report, Instituto Geológico y Minero de España, Madrid, Spain, 1974. Scale 1:50,000 (MAGNA Series). URL: https://info.igme.es/cartografiadigital/datos/magna50/memorias/MMagna0722.pdf.

[24] Instituto Geológico y Minero de España (IGME). Estudio hidrogeológico de la plana de valencia. Technical report, IGME, Madrid, Spain, 1990. Accessed March 2026. URL: https://info.igme.es/SidPDF/139000/868/139868_0000012.pdf.

[25] Archivo Histórico del Ayuntamiento de Valencia. Flood of the turia river in valencia, october 1957, 1957. Historical photographic archive.

[26] Ángela Salerno. Plan sur: graphic illustration, 2026. Exposition for the 160th year of Las Provincia's Journal. URL: https://www.lasprovincias.es/valencia-ciudad/desafios-eternos-valencia-160-anos-despues-20260110121910-nt.html.

[27] Aventuras Geológicas. Hidrogeología urbana: los ríos perdidos de valencia, 2016. Accessed March 2026. URL: https://www.aventurasgeologicas.com/2016/02/hidrogeologia-urbana-los-rios-perdidos.html.

[28] Josef Jaky. The coefficient of earth pressure at rest. *Journal of the Society of Hungarian Architects and Engineers*, 78:355–358, 1944.

[29] Joseph E. Bowles. *Foundation Analysis and Design*. McGraw-Hill, 5th edition, 1996.

[30] C.B. Park, R.D. Miller, and J. Xia. Multichannel analysis of surface waves. *Geophysics*, 64(3):800–808, 1999.

[31] D.J. Daniels. *Ground Penetrating Radar*. IET, 2004.

[32] Screening Eagle Technologies. Proceq gs8000 ground penetrating radar. URL: `https://www.screeningeagle.com/es/products/proceq-gs8000`.

[33] Ajuntament de València and Audiotec. *Actualización del Mapa Estratégico de Ruido de València 2022. Memoria Resumen*. Ajuntament de València, València, 2022. Strategic Noise Map of the municipality of València.

[34] Ajuntament de València. *Mapa Estratégico de Ruido del Término Municipal de València 2022. Mapa de Niveles Sonoros: Ruido Tráfico Rodado, Lden*. Ajuntament de València, València, 2022. Noise level maps for road traffic noise, Lden indicator.

[35] Ulf Sandberg and Jerzy A. Ejsmont. *Tyre/Road Noise Reference Book*. Informex, Kisa, Sweden, 2002.

[36] Hans Bendtsen et al. State of the art in managing road traffic noise: Summary report. Technical Report CEDR Report 2017-03, Conference of European Directors of Roads, 2017.

[37] Marco Barla and Alessandra Insana. Energy tunnels for a sustainable future. *GeoEnergy Communications*, 2(4), 2026. `doi:10.1007/s44421-026-00016-7`.